A Multi-Disciplinary University Research Initiative
Grant No. F49602-01-1-0352

Final Report

Reporting Period: 9/1/05 to 9/1/06

The Development of an Environmentally Compliant, Multi-Functional Aerospace Coating Using Molecular- and Nano-Engineering Methods

Submitted by:

S.R. Taylor
University of Mississippi Medical Center

G.J. Shiflet and J.R. Scully
University of Virginia

R.G. Buchheit
The Ohio State University

W.J. van Ooij
University of Cincinnati

K. Sieradzki and R.E. Diaz
Arizona State University

C.J. Brinker
University of New Mexico

A.L. Moran
U.S. Naval Academy

Submitted to:
Major Jennifer Gresham, Ph.D.
AFOSR/NL
4015 Wilson Blvd.
Arlington, VA 22203-1954

REPORT DOCUMENTATION PAGE

Form Approved
OMB No. 0704-0188

1. REPORT DATE *(DD-MM-YYYY)*	2. REPORT TYPE	3. DATES COVERED *(From - To)*
02-10-2006	Final	05/01/01 - 08/31/06

4. TITLE AND SUBTITLE
The Development of an Environmentally Compliant, Multi-Functional Aerospace Coating Using Molecular- and Nano-Engineering Methods

5a. CONTRACT NUMBER
N/A

5b. GRANT NUMBER F49620 - [redacted]2-01-1-0352

5c. PROGRAM ELEMENT NUMBER
N/A

6. AUTHOR(S)
S.R. Taylor, G.J. Shiflet, J.R. Scully, R.G. Buchheit, W.J. van Ooij, K. Sieradzki, R.E. Diaz, C.J. Brinker, and A.L. Moran

5d. PROJECT NUMBER
N/A

5e. TASK NUMBER
N/A

5f. WORK UNIT NUMBER
N/A

7. PERFORMING ORGANIZATION NAME(S) AND ADDRESS(ES)
University of Virginia
Office of Sponsored Programs
P. O. Box 400195
Charlottesville, Virginia
22904-4195

8. PERFORMING ORGANIZATION REPORT NUMBER
113339-101-GG10306-31340
(FAS #5-25897)

9. SPONSORING / MONITORING AGENCY NAME(S) AND ADDRESS(ES)
AFOSR
875 N. Randolph St., Rm. 3112
Arlington, Virginia 22203
Jennifer Gresham/NL

10. SPONSOR/MONITOR'S ACRONYM(S)
N/A

11. SPONSOR/MONITOR'S REPORT NUMBER(S)

12. DISTRIBUTION / AVAILABILITY STATEMENT
Approved for public release, distribution unlimited.

AFRL-SR-AR-TR-06-0436

13. SUPPLEMENTARY NOTES
N/A

14. ABSTRACT

The coating system presently used on military aircraft is constrained in function (e.g., static color, low glint) and limited to the use of toxic, chromate-based compounds for the mitigation of corrosion. This report summarizes a MURI that was tasked to establish the scientific foundation for a military aerospace coating with expanded functionality and environmental compliance. By implementing advances in molecular and nano-engineered materials, an academic team has identified the enabling science for a multi-functional coating system with the ability to provide: (1) corrosion protection using environmentally compliant materials, (2) sensing of corrosion and mechanical damage of the aircraft skin, (3) mitigating responses to sensed chemical and physical damage, (4) color-on-demand, (5) optimal adhesion using environmentally compliant materials, (6) fatigue resistance and mechanical integrity of the fuselage, (7) self-cleaning and water rejection character. The enhanced functionality of this advanced coating system is achieved through the research and development of now tangible technologies. These components include: (1)a field-replaceable, nano-engineered aluminum alloy cladding, (2) new approaches for the identification, encapsulation, and intelligent delivery of environmentally compliant corrosion inhibitors for paint, (3) colloidal crystals, and photonic antenna for sensing and color-change-on-demand, (4) optimization of organic coating adhesion to the aluminum alloy substrate through the use of an environmentally compatible surface treatment., (5) development of self-assembled biomimetic surfaces for superhydrophobicity The research from this MURI has resulted in tangible coatings, coating additives, and technologies with very promising and realizable benefit to the Air Force mission.

15. SUBJECT TERMS
mitigation, corrosion, aluminum alloy, colbidal crystals

16. SECURITY CLASSIFICATION OF:			17. LIMITATION OF ABSTRACT	18. NUMBER OF PAGES	19a. NAME OF RESPONSIBLE PERSON
a. REPORT	b. ABSTRACT	c. THIS PAGE			Dr. G. J. Shiflet
Unclassified	Unclassified	Unclassified	UL	142	19b. TELEPHONE NUMBER *(include area code)* 434-982-5653

TABLE OF CONTENTS

	Page
PREFACE	2
SUMMARY OF MURI FINDINGS	3
SUMMARY OF MURI PUBLICATIONS & PATENTS	9
SUMMARY OF MRI GRA's AND PDRAs	22
ANNUAL REPORT	24
MURI PROGRAM OVERVIEW	24
I. PROGRAM OBJECTIVES	24
II. SUMMARY OF ACTIVITIES	25
PROJECT PERFORMANCE	
NANO-ENGINEERED METALLIC CLADDING J.R. Scully, G.J. Shiflet, A.L. Moran	26
IDENTIFICATION OF ENVIRONMENTALLY COMPLIANT INHIBITORS S.R. Taylor	82
INHIBITOR ENCAPSULATION AND DELIVERY STRATEGIES C.J. Brinker, R.G. Buchheit, S.R. Taylor. W.J. van Ooij	91
STRATEGIES FOR ADDEDED COATING FUNCTIONALITY K. Sieradzki and R.E. Diaz	116
ENHANCED ADHESION USING NANO-ENGINEERED MATERIALS W.J. van Ooij	133
SYSTEM PERFORMANCE S.R. Taylor	138

PREFACE

This is the 5th and final report for the Multi-disciplinary University Research Initiative (MURI) on "The Development of an Environmentally Compliant, Multi-Functional Aerospace Coating Using Molecular- and Nano-Engineering Methods". The research findings of this highly productive and multi-faceted MURI team have established the scientific foundation for a future generation of multi-functional aerospace coatings that:

(1) Provide corrosion protection using environmentally compliant materials
(2) Sense corrosion and mechanical damage of the aircraft skin
(3) Initiate coating repair responses to sensed chemical and physical damage
(4) Provide color change-on-demand
(5) Achieve optimal adhesion using environmentally compliant materials
(6) Improve the fatigue resistance and mechanical integrity of the fuselage
(7) Provide self-cleaning, water-rejection, and icephobicity via super hydrophobicity

This report is divided into three sections. The first section will summarize the major findings of this MURI. The second section will summarize the publications and presentations. The third section will provide the annual report for the 5th year.

As the Principal Investigator of this MURI, I would like to express my most sincere gratitude to my co-investigators: Gary Shiflet, John Scully, Rudy Buchheit, Wim van Ooij, Jeff Brinker, Karl Sieradzki, Rudy Diaz, and Angela Moran. It has been an honor to be associated with such talented people. I am forever appreciative of their friendship and collegiality.

Many of the coating and surface treatment technologies developed within this MURI are intellectual properties that could be translated into marketable products. The actual assembly of the various technical components of this MURI into a multi-functional coating will require further developmental effort. Any reader that is interested in a particular technology or the further development of a multi-functional coating system is encouraged to contact the relevant individual investigator, or myself.

On behalf of the entire MURI team, I would like to express our most sincere thanks to the Air Force Office of Scientific Research, the Air Force Research Laboratories, the Department of Defense, and the AFOSR program managers, Lt. Col Paul Trulove (retired) and Major Jennifer Gresham for their support and oversight of this research effort. In light of current events, the sacrifices made by these agencies and individuals in support of the academic mission has been heroic. Thank you.

S. Ray Taylor
MURI Program Director

SUMMARY OF MAJOR MURI FINDINGS

Methods have been identified for the production of an amorphous aluminum cladding. The mechanism of formation, thermodynamic stability, and corrosion protection have been determined.

- Amorphous Al-Co-Ce alloys were invented. These alloys will provide a multi-functional base layer for subsequent organic layers. These materials were investigated from the standpoint of thermodynamic stability, corrosion resistance, and field application.

- The Glass Formation Range (GFR) was experimentally mapped for the Al-Co-Ce system. Databases for binary Al-Ce and ternary Al-Co-Ce were created and optimized.

- The Al-Sm system was obtained and verified as an amorphous metal that crystallizes with no long-range diffusion (polymorphic). This material will allow the definitive delineation of structure versus chemistry with regards to the corrosion properties of amorphous alloys.

- A new approach to the thermodynamics of phase equilibria was outlined which coupled experiments, first principles and optimization.

- The Al-rich Al-Ce-Co system was thermodynamically optimized for the first time. The enthalpies of formation for the ternary compounds obtained from CALPHAD modeling are comparable to those from FP calculations.

- The newly developed Al-Co-Ce alloys were found to have excellent corrosion resistance and high potential for multi-function as sacrificial anodes and as a reservoir for inhibitor release. Tunable intrinsic barrier properties and sacrificial cathodic protection capabilities of Al-Co-Ce alloys, combined with inhibitor release capability create a metal coating that exhibits all strategies in one coating.

- Critical inhibitor concentration for Co(III), Ce(III) and Mo(VI) of AA2024-T3 were defined as a function of chloride concentration. A protocol was perfected for rapid determination of critical inhibitor concentration for Cu rich Al precipitation age hardened alloys used in aerospace.

- Mechanisms for the inhibition of the oxygen reduction reaction on AA2024-T3 by Ce(III), Co(II), and Mo(VI) were elucidated based on concepts of cathode site blocking via homogeneous chemical precipitation and direct electrochemical reduction. A model explained both the charge and mass transport controlled

oxygen reduction reaction rates on a heterogeneous electrode such as 2024-T3 as a function of Cu coverage with and without inhibitors. Additionally, the heterogeneous electrode and membrane models were adapted and developed to explain the effect of inhibitors that block reactive Cu rich sites on heterogeneous electrodes.

- The mechanistic explanation for the effects of alloy composition on repassivation potential and open circuit potential were elucidated through diagnostic electrochemical and surface science studies. A regression type model optimized for alloy composition was developed to enable prediction of pitting, repassivation potential and open circuit potential for solid solution glass alloys. The model enables prediction of the effects of alloying content on these properties. The concept of tunable cathodic protection using a sacrificial anode coating was demonstrated through experiment and modeling.

- The chemical throwing power of an Al-Co-Ce coating galvanically coupled to a AA2024-T3 scratch was successfully modeled and studied as a function of initial pH, release rates, electrolyte thickness and Cl^- concentration. The materials, geometric, chemical, and electrochemical attributes that maximize or minimize scratch protection were defined. Based on the model and experiments, generic methods have been developed to assess protection of aerospace alloys at exposed sites such as scratches. These methods have generic applicability to aerospace materials regardless of exact corrosion protection or inhibitor type.

- Pulsed Thermal Spray (PTS), Cold Spray, and HVOF spray deposits have been investigated for barrier corrosion properties. PTS materials can be amorphized and display excellent barrier corrosion properties in Cl^- solutions. Intrinsic barrier corrosion properties of the deposited materials was successfully isolated and distinguished from the corrosion properties of the coating. It has been discovered that the intrinsic corrosion resistance of Al-Co-Ce coating materials independent of 2024-T3 is better than as a coating on 2024-T3. The difference is tentatively attributed to defects in the coatings such as cracks and porosity.

- Laser surface treatments were applied to a Al-Co-Ce alloy ingot as well as powders. A major finding was that homogenization of cast Al-Co-Ce alloys is required prior to laser surface treatment to produce amorphous layers. Secondly, good barrier corrosion resistance is governed by physical defects such as cracks in the highly corrosion resistant amorphous layer.

- A method has been developed to distinguish the intrinsic corrosion properties of various spray deposited alloys from their properties as coatings on 2024-T3.

- Two STTR projects have been launched through DOD funding at SAIC/Enig-matics and at SWRI/Plasma Tech. aimed at advancing the commercialization of Al-Co-Ce coatings. Both STTR projects are being conducted in collaboration with the Univ. of Virginia SEAS.

Cr-free inhibitor chemistries with inhibitor performance that exceeds chromate on AA2024-T3 have been identified.

- Cr-free corrosion inhibition of AA2024-T3 that exceeds the performance of chromate has been established through the discovery of synergistic combinations of rare earth cations (e.g., Ce^{3+}, La^{3+}, Y^{3+}) and oxoanions (MoO_4^{2-}, WO_4-$3WO_3^{1-}$, etc.).

- The experimental discovery of inhibitor synergies was accelerated through the development of high throughput screening (HTS) methods for AA2024-T3 that increased the rate of experimental throughput by a factor of over 1000.

- Three HTS assays were developed for AA2024-T3: current during 100 mV polarization, cyclic voltammetric determination of surface Cu, and fluorometric quantification of Al^{3+}.

- Chemical systems with broad synergy (La-MoO_4) and broad antagonism (Ce-VO_3)were investigated in detail using electrochemical, chemical, and surface analysis techniques. The behavior of these systems is a function of polyoxometallate (POM) reaction kinetics.

- The Cr-free inhibitor chemistries identified within this MURI are now being examined within an aerospace coating through a partnership with NASA-KSC.

A number of methods were developed to contain and intelligently deliver these new Cr-free chemistries when incorporated within a paint.

- Evaporation-induced self-assembly (EISA) was used to prepare porous silica core/hydrogel-silica shell particles as controlled release nanocapsules for supply of corrosion inhibitors or repair agents. Several approaches for controlled release were developed and examined.

- pH-switchable poly(methacrylate) hydrogel/silica lamellar nanocomposites were synthesized that showed a reversible expansion/contraction (~75%) of the lattice parameter by changing the pH from 4 to 9.

- EISA was used to prepare the first hydrogel/silica nanocomposites showing reversible temperature-induced swelling and de-swelling of interest for thermally mediated controlled release.

- A self-assembly approach was developed to prepare optically switchable mesoporous silicas by incorporating azobenzene ligands. These materials demonstrated optically-mediated control of mass transport. This property is very useful for the development of optically-activated controlled release gates.

- Monodisperse $CeCl_3$/silica, NaCl/silica core/shell particles, mesoporous Na_2MoO_4/silica, and mesoporous V(O)(OPri)$(OPy)_2$/silica were synthesized. Their release behaviors were characterized, and the effective diffusion coefficients were obtained based on mathematical models developed for diffusion. The effects of pore size and pore surface chemistry on the release rate were investigated.

- Azobenzene-functionalized NaCl/silica model gated particles were synthesized, and their optically-stimulated release behaviors were measured.

- In order to quantify ion transport through self-assembled silica nanopores, 'patch clamp' electronic techniques, developed for probing ion transport in membrane-bound ion channel proteins were adapted. This initial work led to an NIH Nano-Medicine Center grant on nano-transporters.

- Hydrotalcites (HT) were developed as an intelligent delivery system for Cr-inhibitors. A Zn-Al-decavanadate hydrotalcite (HT-V) pigment was developed for organic coatings. This pigment released vanadates and Zn cations and takes up Na^+ and Cl^- ions . The extent of inhibitor release, the release kinetics and extent of corrosion protection due to released inhibitors was characterized.

- Coatings containing a HT-V pigment were shown to provide active corrosion protection to a bare surface in close proximity and sharing a common aggressive electrolyte and to a scribed AA2024-T3 panel subjected to 1000 h salt spray..

- The memory effect associated with calcined hydrotalcite compounds was demonstrated and exploited to detect water uptake in organic coatings using remote x-ray diffraction techniques. Water uptake could be remotely detected in a Li-Al-CO_3-pigmented epoxy coating.

- A predictive model was developed that could estimate coating water content and the onset of substrate corrosion damage based upon changes in the x-ray diffraction pattern.

- Another method that was developed to control the solubility and release of water soluble inhibitor compounds was that of plasma polymerization-wrapping. These wrapping chemistries could be controlled so that wrapped compounds could be mixed into water=based or solvent-based paints.

A silane-based, single coat inhibited coating system was developed that can be applied directly to AA2024-T3.

- A completely chromate-free coating system consisting of a silane-based pretreatment, a chromate-free primer and a topcoat was developed which

performed as well as the conventional chromate-containing system on AA2024-T3 for1000 hrs in ASTM B-117.

- A room temperature-cured superprimer system comprised of a water-dispersed resin and a water-insoluble silane was developed. This system has outstanding corrosion protection on AA2024-T3. The basic recipe consists of an acrylic resin dispersion, an epoxy resin dispersion, an isocyanate based crosslinker and a hydrophobic bis-sulfur silane.

- The acrylate-epoxy based superprimer was optimized and loaded with high levels of chromate-free corrosion inhibitors (e.g., 30 wt.% $Zn_3(PO_4)_2$, cerium silicate). The performance was found to be equal to a chromate-containing primer.

- The acrylate-epoxy based superprimer was found to be a self-assembled three-layer coating. The three layers in the coating consist of a silane-rich layer at the metal-primer interface, a silane-rich hydrophilic acrylate layer containing the inhibitor, and a hydrophobic epoxy layer as the third and topmost layer.

- The optimized superprimer was found to be packable into a two-pack system, the performance of the resulting coatings was found to be good and the packs are stable for more than 4 months.

Enhanced coating functions including sensing, color change-on-demand, and low permeability were developed.

- Colloidal crystals grown directly onto a substrate can be used as a strain sensor. Photonic crystals used as strain sensors were able to measure the mechanical properties (Young's modulus and Poisson's ratio) of colloidal crystal assemblies.

- Langmuir-Blodgett self-assembly methods were successfully used for the production of inverse opals that had remarkable strain sensitivity. Deformation of these structures was easily interrogated using optical diffraction methods.

- The signal-to-noise ratio was increased for these photonic crystals through the development of polymer encapsulated, nano-gold particle strain sensors. The nano-dimensioned gold provided signal amplification via plasmon resonance.

- Two pathways were examined for the development of color-on-demand: (1) an amplified galvanic electrochromic element, and (2) a MEMS-based metachromic pigment particle.

- For the electrochromic element, a process for the production of TiO_2 crystalline anatase nanospheres below 60 nm was developed at the University of Vigo. These viologen-coated TiO_2 nanospheres successfully demonstrate intense coloration change in an electrochromic cell. Color amplification is demonstrated by the

incorporation of gold nanospheres (1-7 nm) in the immediate proximity of quantum dots

- For the metachromic pigment, numerical simulation demonstrated that the scattering wavelength of proximity-coupled photonic antennas can be tuned across the entire optical range. Realistic photonic antennas were proposed and their operation confirmed using a full-physics model that incorporated the free electron plasma behavior of noble metals (Ag).

- Quantum Mechanical transition rate phenomena were included into a computational electromagnetics code (partially funded by NSF) to calculate realistic amplification effects of photonic antennas on nearby fluorescent or absorbing molecules.

A room-temperature cured superhydrophobic topcoat was developed that is self-cleaning, water-rejecting, and icephobic.

- A novel aerogel self-assembly approach was used to develop surfaces with superhydrophobic properties. In fluidic architectures these films exclude water and may profoundly influence corrosion behavior.

- Neutron reflectivity investigations of water penetration in superhydrophobic films and aluminum corrosion inhibition was performed using superhydrophobic coatings as water permeation barriers.

- Multifunctional hydrophobic coatings with dispersions of $CeCl_3$/silica particles have been studied for corrosion protection of aluminum and aluminum alloy. This concept has been transferred to Luna Corp. in a Phase 1 STTR which has now been extended to a Phase 2 STTR.

- The gas barrier properties of self-assembled nanocomposite thin films was examined. Gas transport in S-A silica/polymer nanocomposite films was determined to be 500x lower in permeability compared to the parent polymer. This work was incorporated into a Phase 1 DARPA grant (with Nanosolar) on flexible, large scale PV manufacturing.

A 4-day laboratory test was developed to quantify self-healing in coating systems and predict 3000 hour salt spray performance.

- A low cell-volume Damage Tolerance Test was developed to detect and quantify the phenomenon of self-healing in inhibited coatings systems on AA2024-T3. This test can be performed in 4 days and are 100% reliable for conventional coating systems that employ chromate conversion coatings. There is a 0.89 correlation between the new EIS test and salt spray data.

SUMMARY OF MURI PUBLICATIONS & PATENTS

a. Refereed Publications

1. A Zhu,; SJ Poon,; GJ Shiflet, "On glass formability of Al-Gd-Ni (Fe)", *Scripta Materialia*, **50** (2004) pp. 1451-1455.
2. A Zhu, GJ Shiflet, and D Miracle, "Glass Froming Ranges of Al-rare Earth Metal Alloys: Thermodynamics and Kinetic Analysis", *Scripta Materialia*, **50** (2004) pp. 987-991.
3. MC Gao, N Unlü, and GJ Shiflet, M Mihalkovic, M Widom,"Re-assessment of Al-Ce and Al-Nd Binary Systems Supported By Critical Experiments and First-Principles Energy Calculations", *Metallurgical Transactions*, **36A** (2005) pp. 3269-3279. Winner of APDIC Award for best thermodynamic paper published in 2005.
4. MC Gao,.GJ Shiflet, "Devitrification sequence map in the glass forming Al-Ni-Gd system", Scripta Materialia, **53** (2005) pp. 1129-1134.
5. MC Gao, N Unlu, GJ Shiflet,; M Mihalkovic, M Widom,"Reassessment of Al-Ce and Al-Nd binary systems supported by critical experiments and first-principles energy calculations.", *Acta Materialia*, submitted 2006.
6. F.J. Presuel-Moreno, M.Jakab, R.G. Kelly, J.R. Scully, "Barrier, Electrochemical Sacrificial Cathodic Prevention and Active Corrosion Inhibition Properties of Al-Co-Ce Coatings on A2024-T3," CORROSION Journal Special Issue on Smart Coatings, submitted, (2006).
7. D. Little, J.R. Scully, "The Effect of Heat Treatment on the IGSCC Behavior of Al-Cu-Mg-Ag Alloys," accepted, *Corrosion Science J.*, (2006).
8. D. Ho, N. Brack, J.R.. Scully, T. Markley, M. Forsyth and B. Hinton, "Cerium dibutylphosphate as a corrosion inhibitor for AA2024-T3 Aluminum alloys," Accepted for Publication in *J. Electrochem. Soc.*, 153(9), (2006).
9. F.J. Presuel-Moreno, M.A. Jakab, R.G. Kelly, J.R. Scully, "Computational Modeling of Active Chemical Inhibition Provided by a Al-Co-Ce Metal Coating Coupled and Uncoupled to A2024-T3," *Journal of the Electrochemical Soc*, accepted, June, (2005).
10. Brian J. Connolly, J.R. Scully, "The Transition from Localized Corrosion to SCC in a Severely Underaged Temper of Al-Li-Cu-Ag Alloy AA 2096," *Corrosion J.*, **61**(12), pp.1145-1166, (2005).
11. M. A. Jakab, F. Presuel-Moreno and J. R. Scully, "Effect of Molybdate, Cerium and Cobalt Ions on the Oxygen Reduction Reaction on AA2024-T3 and Selected Intermetallics: Experimental and Modeling Studies," *J. Electrochem. Soc.*, **153**(7), pp.244-252, (2006).
12. D. Little, J.R. Scully, "The Effect of Surface Pretreatment on the Under-Paint Corrosion of AA 2024-T3 at Various Temperatures," *Corrosion J.*, **62**(4), pp. 300-315, (2006).
13. M.E. Goldman, N. Unlu, G.J. Shiflet, J.R. Scully, *"Selected Corrosion Properties of a New Al-Co-Ce Alloy," J. Electrochem. and Solid State Letters*," **8**(2), B1-B5, (2005).

14. M.A. Jakab, F. Presuel, J.R. Scully, "Critical Concentrations Associated with Cobalt, Cerium and Molybdenum Inhibition of AA 2024-T3 Corrosion, Delivery from Al-Co-Ce-(Mo) Alloys," *Corrosion J.*, **61**(3), pp. 246-263, (2005).
15. J.G. Hoekstra, *S.B. Qadri, J.M. Fitz-Gerald, J.R. Scully, "Laser Surface Modification of a Crystalline Al-Co-Ce Alloy for Enhanced Corrosion Resistance," *Advanced Engineering Materials*, **7**(9), pp. 1-5, (2005).
16. M.A. Jakab, J.R. Scully, "Storage and Release of Inhibitor Ions from Amorphous Al-Co-Ce Alloys: Controlled Release on Demand," *Nature Materials*, 4, September, pp. 667-670, (2005).
17. F.J Presu-Morenoel, M.A. Jakab, J.R. Scully, "Inhibition of the Oxygen Reduction Reaction on Copper Using Ce, Mo, and Co Compounds," *J. Electrochem. Soc.*, **152**(9), pp. B376-387, (2005).
18. M.A. Jakab, F. Presuel, J.R. Scully, "The Oxygen Reduction Reaction on AA 2024-T3; Experiment and Modeling Using the Theory of a Heterogeneous Electrode" *J. Electrochem. Soc.*, **152**(8), B311-B320, (2005).
19. F.J. Presuel-Moreno, M.E. Goldman, R.G. Kelly, J.R. Scully, "Electrochemical Sacrificial Cathodic Prevention Provided by a Al-Co-Ce Metal Coating Coupled to A2024-T3," *J. Electrochem. Soc*, **152**(8), pp. B302-B310, (2005).
20. N. Unlu, F.Q. Guo, G.J. Shiflet, S.J. Poon, J.R. Scully, " The Effect of Pd Addition on the Glass Formation Ability and Electrochemical Corrosion Behavior of a Ternary ($Al_{75}Cu_{17}Mg_8$) Alloy, submitted to *Materials Science and Engineering*, (2005).
21. N. Unlu, F.Q. Guo, J. Ferrel, G.J. Shiflet, S.J. Poon, J.R. Scully, "The Effect of Ni Additions on Corrosion Behavior of $(Al_{75}Cu_{17}Mg_8)_{(100-x)}Ni_x$ (x=0,1,3,5,7 at%) Amorphous and Crystalline Alloys, submitted to *Materials Science and Engineering*, (2005).
22. J.E. Switzer, G.J. Shiflet, J.R. Scully, "Localized Corrosion of $Al_{90}Fe_5Gd_5$ and $Al_{87}Ni_{8.7}Y_{4.3}$ Alloys in the Amorphous, Nanocrystalline, and Crystalline States: Resistance to Micrometer-Scale Pit Formation", *Electrochimica Acta*, **48**, pp. 1223-1234, (2003).
23. B.J. Connolly, Q. Meng, A.L. Moran, R. McCaw, "Mechanical and Precorroded Fatigue Properties of a Coated Aluminum Aircraft Skin System as a Function of Various Thermal Spray Processes", *Corrosion Engineering, Science and Technology*, **39**, 137-142 (2004).
24. P. Moongkhamklang and S.R. Taylor, "The Delineation of Ionic Pathways Through Organic Coatings Using a Molecular Probe", *Progress in Organic Coatings*, **46**(4):259-265 (2003).
25. S.R. Taylor and K. Sieradzki, "The Development of a Multi-Functional Aerospace Coating: Considerations in the Use of Nano-Dimensioned Materials", *Progress in Organic Coatings*, **47**(3-4):169-173 (2003).
26. S.R. Taylor, "The Delineation of Ionic Pathways in Organic Coatings Using Molecular Probes", *J. Corr. Sci. and Engr.*, (in review).
27. S.R. Taylor and P. Moongkhamklang, "The Delineation of Local Water Interaction with Epoxy Coatings Using Fluorescence Microscopy", *Progress in Organic Coatings*, (in press).
28. F. Contu, S.R. Taylor, L. Fenzy, "An FT-IR Investigation of Epoxy Coating Interactions with Simulated Corrosion Blister Electrolytes", *Progress in Organic*

Coatings, (accepted).
29. S.R. Taylor, S. Raman, F. Contu, P. Moongkhamklang, "The Use of Cationic Fluoroprobes to Characterize Ionic Pathways in Organic Coatings", *Progress in Organic Coatings*, (accepted).
30. B.D. Chambers, S.R. Taylor, and M.W. Kendig, "The Rapid Discovery of Corrosion Inhibitors and Synergistic Combinations Using High Throughput Screening Methods", *Corrosion*, **61**(5):480-489 (2005).
31. B.D. Chambers and S.R. Taylor, "The High Throughput Assessment of Inhibitor Synergies on AA2024-T3 through Measurement of Surface Copper Enrichment", *Corrosion*, (in press).
32. B.D. Chambers, S.R. Taylor, "The High Throughput Assessment of Aluminum Alloy Corrosion Using Fluorometric Methods, Part I: Development of a Fluorometric Method to Assess Aluminum Concentration", *Corrosion Science*, (in review).
33. B.D. Chambers, S.R. Taylor, "The High Throughput Assessment of Aluminum Alloy Corrosion Using Fluorometric Methods, Part II: Rapid Evaluation of Corrosion Inhibitors and Synergistic Combinations", *Corrosion Science*, (in review).
34. B.D. Chambers and S.R. Taylor, "Multiple Electrode Methods to Massively Parallel Test Corrosion Inhibitors for AA2024-T3", NACE 2006 - San Diego, CA, Paper No.06678, National Association of Corrosion Engineers, Houston, TX (2006).
35. S.R Taylor and B.D. Chambers, "The Discovery of Non-Chromate Corrosion Inhibitors for Aerospace Alloys Using High-Throughput Screening Methods", 4th International Symposium on Aluminum Surface Science and Technology, Ed. By H. Terryn (in press).
36. Singh S, Houston J, van Swol F, Brinker CJ, "Drying transition of confined water". *Nature*, Aug 3 2006, **442**, p. 526. (Nature does not allow acknowledgements in *Brief Communication*)
37. Brinker CJ, Dunphy DR. "Morphological control of surfactant-templated metal oxide films", *Current Opinion in Colloid & Interface Science*, Jun 2006, **11**, p. 126-132
38. Jiang XM, Brinker CJ, "Aerosol-assisted self-assembly of single-crystal core/nanoporous shell particles as model controlled release capsules", *Journal of the American Chemical Society*, April 2006, **128**, no 14, p. 4512-4513.
39. Yang K, Fan HY, Malloy KJ, Brinker CJ, Sigmon TW, "Optical and electrical properties of self-assembled, ordered gold nanocrystal/silica thin films prepared by sol-gel processing", *Thin Solid Films*; **491**, p.38; 2005.
40. Doshi DA, Shah PB, Singh S, Branson ED, Malanoski AP, Watkins EB, Majewski J, van Swol F, Brinker CJ, "Investigating the interface of superhydrophobic surfaces in contact with water", *Langmuir*; **21**, p.7805; 2005.
41. Gogte S., Vorobieff P, Truesdell R, Mammoli A, van Swol F, Shah P, Brinker CJ, "Effective slip on textured superhydrophobic surfaces", *Physics of Fluids*; May 2005; **17**, no.5, p.1-4.
42. Brinker CJ, "Evaporation-induced self-assembly: Functional nanostructures made easy" (Text of MRS MEDALIST Invited Lecture).. *MRS Bulletin*; Sep 2004, **29**, no. 9, p.631-640.
43. Fan H, Brinker CJ, "Evaporation-Induced Self-Assembly of Functional Nanostructures", *Studies in Surface Science and Catalysis;* 2004, **148**, p. 213-240

44. Liu N, Dunphy DR, Atanassov P, Chen Z, Lopez GP, Brinker CJ, "Photoregulation of mass transport through a photoresponsive azobenzene-modified nanoporous film", *NanoLetters*, 2004; **4**, no.4, p. 551-554.
45. Garnweitner G, Smarsly B, Assink, R, Dunphy DR, Scullin C, Brinker CJ, "Characterization of self-assembled lamellar thermoresponsive silica-hydrogel nanocomposite films", *Langmuir*; Oct 26 2004; **20**, no.22, p.9811-9820
46. Fan H, Yang K, Boye DM, Sigmon T, Malloy KJ, Lopez GP, Brinker CJ, Xu H. "Self-assembly and integration of ordered, robust, three-dimentional gold nanocrystal/silica arrays", *Science,* 2004; **304,** no.5670, p567-571.
47. Dunphy DR, Singer S, Cook AW, Smarsly B, Doshi DA, Brinker CJ, "Aqueous stability of mesoporous silica films doped or grafted with aluminum oxide", *Langmuir*; 2003, **19,** no.24, p.10403-10408..
48. Smarsly B, Garnweitner G, Assink R, Brinker CJ, "Preparation and Characterization of Mesostructured Polymer-Functionalized Sol-Gel-Derived Thin Films", *Progress in Organic Coatings,* 2003, **47**, 393-400.
49. Doshi DA, Gibaud A, Goletto V, Lu MC, Gerung H, Ocko B, Han SM, Brinker CJ, "Peering into the self-assembly of surfactant templated thin-film silica mesophases" *Journal of the American Chemical Society,* 2003, **125,** no.38, p.11646-11655.
50. Smarsly B, Xomeritakis G, Yu K, Liu N, Fan H, Assink RA, Drewien CA, Ruland W, Brinker CJ, "Microstructural Characterization of Polystyrene-block-poly(ethylene oxide)-Templated Silica Films with Cubic-Ordered Spherical Mesopores", *Langmuir*; 2003, **19,** No. 18, 7295-7301.
51. Doshi DA, Gibaud A, Liu NG, Sturmayr D, Malanoski AP, Dunphy DR, Chen HJ, Narayanan S, MacPhee A, Wang J, Reed ST, Hurd AJ, van Swol F, Brinker CJ, "In-situ X-ray scattering study of continuous silica-surfactant self-assembly during steady-state dip coating", *Journal of Physical Chemistry B,* 2003, **107**, no.31, p.7683-7688.
52. Yang Y, Lu Y, Lu M, Huang J, Haddad R, Xomeritakis G, Liu N, Malanoski AP, Sturmayr D, Fan. H, Sasaki DY, Assink RA, Shelnutt JA, van Swol F, Lopez GP, Burns AR, Brinker CJ, "Functional Nanocomposites Prepared by Self-Assembly and Polymerization of Diacetylene Surfactants and Silicic Acid", *Journal of the American Chemical Society*, 2003, **125,** No. 5, 1269-1277.
53. Garnweitner G, Smarsly B, Assink R, Ruland W, Brinker CJ, "Self-Assembly of an Environmentally Responsive Polymer/Silica Nanocomposite", *Journal of the American Chemical Society*, 2003, **125**, 5626-5627.
54. Liu NG, Assink RA, Smarsly B, Brinker, CJ, "Synthesis and characterization of highly ordered functional mesoporous silica thin films with positively chargeable -NH2 groups", *Chemical Communications*, 2003, p.1146-1147.
55. Liu NG, Chen Z, Dunphy DR, Jiang YB, Assink RA, Brinker CJ, "Photoresponsive nanocomposite formed by self-assembly of an azobenzene-modified silane", *Angewandte Chemie - International Edition*; 2003, **42**, p.1731-1734.
56. Liu N, Dunphy DR, Rodriquez MA, Singer S, Brinker CJ, "Synthesis and Crystallographic Structures of a Novel Photoresponsive Azobenzene-Containing Organosilane", *Chemical Communications*; 2003, p.1144-1145.

56. Gibaud A, Grosso D, Smarsly B, Baptiste A, Bardeau JF, Babonneau F, Doshi DA, Chen Z, Brinker CJ, Sanchez S, "Evaporation Controlled Self-Assembly of Silica Surfactant Mesophases", *Journal of Physical Chemistry B.*, 2003, **107,** p.6114-6118.
57. Wu X; Yu K Brinker CJ, Ripmeester J, "Mesostructured MTES-derived silica thin film with spherical voids investigated by TEM: 2. Dislocations and strain relaxation", *Langmuir*; 2003, **19**, p.7289.
58. Wu X; Yu K Brinker CJ, Ripmeester J, "Mesostructured MTES-derived silica thin film with spherical voids investigated by TEM: 1. Mesostructure determination", *Langmuir*; 2003, **19**, p.7282.
59. Liu N, Yu K, Smarlsy B, Dunphy DR, Jiang Y-B, Brinker CJ, "Self-Directed Assembly of Photo-Active Hybrid Silicates Derived from an Azobenzene-Bridged Slsesquioxane", *Journal of the American Chemical Society*, 2002, **124,** No. 49, 14540-14541.
60. Liu N, Assink RA, Brinker CJ, "Synthesis and Characterization of Highly Ordered Mesoporous Thin Films with –COOH Terminated Pore Surfaces", *Chemical Communication,* 2002, **No. 3**, 370-371.
61. Yifeng W, Bryan CS, Huifang, Pohl P, Yang Y, Brinker CJ, "Interface Chemistry of Nanostructured Materials: Ion Adsorption on Mesoporous Alumina," *Journal of Colloid and Interface Science*, 2002, **254**, 23-30.
63. Lu Y, Yang Y, Lu M, Huang J, Fan H, Haddad R, Lopez GAR, Sasaki DY, Shelnutt J, Brinker CJ, "Self Assembly of Mesoscopically Ordered Chromatic Polydiacetylene /Silica Nanocomposites, , *Nature*, 2001, **410**: p. 913-917.
64. Fan H, Bentley HR, Kathan K, Clem P, Lu Y, Brinker CJ, "Self-Assembled Aerogel-Like Low Dialectric Constant Films" *Journal of Non-Cryst. Solids*, 2001. **285**:79-83.
65. Fan H, van Swol F, Lu Y, Brinker CJ, "Multiphased Assembly of Nanoporous Silica Particles, *Journal of Non-Cryst. Solids*, 2001, 285, p. 71-78.
66. Yu K, Hurd AJ, Eisenberg A, Brinker CJ, "Syntheses of Silica/Polystrene-block-Poly (ethylene oxide) Films with Regular and Reverse Mesostructures of Large Characteristic Length Scales by Solvent Evaporation-Induced Self Assembly", *Langmuir*, 2001, **17**, p.7961.
67. F. Wong, R. G. Buchheit, "Utilizing the structural memory effect of layered double hydroxides for sensing water uptake in organic coatings," *Progress in Organic Coatings* **51**(2): 91-102 (2004).
68. R.G. Buchheit, H. Guan, S. Mahajanam, F. Wong, "Active Corrosion Protection and Corrosion Sensing in Chromate-free Organic Coatings," *Progress in Organic Coatings*, **47**, 174 (2003).
69. R. G. Buchheit, S. P. V. Mahajanam, "Ion Exchange Compounds for Corrosion Inhibiting Pigments in Organic Coatings," ACS Symposium Series, New Developments in Coatings Technology, ACS, Philadelphia, PA (2006) accepted for publication.
70. A. Seth, W.J. van Ooij, P. Puomi, T. Metroke and A. Appblett, "Characterization of Novel Primer Systems using liquid-state ^{29}Si and ^{13}C NMR", will be submitted to *Prog. Org. Coat.*
71. A. Seth, W.J. van Ooij, P. Puomi, Z. Yin, A. Ashirgade, S. Bafna and C. Shivane, "Novel, One-step, Chromate-free Coatings Containing Anticorrosion Pigments for Metals – an Overview and Mechanistic Study", accepted in *Prog. Org. Coat.*

72. W.J. van Ooij, D. Zhu, M. Stacy, A. Seth, T. Mugada, J. Gandhi and P. Puomi, "Corrosion Protection Properties of Organofunctional Silanes – An Overview", *Tsinghua Science and Technology*, **10** (2005) 639-664.
73. D. Zhu and W.J. van Ooij, "Enhanced Corrosion Resistance of AA2024-T3 and HDG using a Silane Mixture of Bis-[trimethoxysilylpropyl]amine and Bis-[triethoxysilylpropyl] tetrasulfide", *Electrochimica Acta*, **47** [5], 1113-1125 (2004)
74. D. Zhu and W.J. van Ooij, "Corrosion Protection by Water-based Silane Mixtures of bis-[trimethoxysilylpropyl]amine and Vinyltriacetoxysilane", *Prog. Org. Coat.*, **49** [1], 42-53 (2004).
75. W.J. van Ooij, D. Zhu and V. Palanivel, "Nanoparticle-filled Silane Films as Chromate Replacements for Aluminum Alloys", *Prog. Org. Coat.*, **47** [3-4], 384-393 (2003)
76. D. Zhu and W. J. van Ooij, "Corrosion Inhibition of AA 2024-T3 by Bis-[3-(triethoxysilyl)propyl]tetrasulfide in neutral Sodium Chloride solution - Part 2: Mechanism of Corrosion Protection", *Corrosion Sci.*, **45** [10] 2177-2197 (2003)
77. D. Zhu and W.J. van Ooij, "Corrosion Control of Metals by an Environmentally-Friendly Silane Surface Treatment", *J. Corr. Sci. and Prot. Metals.*, submitted, 2003 (in Chinese)
78. V. Palanivel, D. Zhu and W. J. van Ooij, "Effects of Addition of Corrosion Inhibitors to Silane Films on AA2024-T3 Alloy", submitted to *Progress in Organic Coatings.*
79. W.J. van Ooij, D. Zhu, V. Palanivel, J.A. Lamar and M. Stacy, "Potential of Silanes for Chromate Replacement in Metal-Finishing Industries", *Silicon Chemistry*, accepted, 2002
80. D. Zhu and W.J. van Ooij, "Structural Characterization of bis-[triethoxysilylpropyl] tetrasulfide and bis[trimethoxysilylpropyl]amine by FTIR and Electrochemical Impedance Spectroscopy", *J. Adhesion Sci. Technol.*, **16** (2002) 1235-1260.
81. S.R. Taylor and K. Sieradzki, "The development of a multi-functional aerospace coating: considerations in the use of nano-dimensioned materials", *Prog. Org. Coat.*, Vol. 47 pp. 169-173 (2003).
82. M.A. Correa-Duarte, M. Grzelczak , V. Salgueirino-Maceira V, M. Giersig , L.M. Liz-Marzan , M. Farle , K. Sierazdki , R. Diaz , "Alignment of carbon nanotubes under low magnetic fields through attachment of magnetic nanoparticles" , *J. of Phys. Chem. B*, **109,** pp.19060-19063 (2005).
83. M. Grzelczak , M.A. Correa-Duarte, V. Salgueirino-Maceira , M. Giersig , R. Diaz, L.M. Liz-Marzan, "Photoluminescence quenching control in quantum dot-carbon nanotube composite colloids using a silica-shell spacer", *Advanced Materials*, **18,** 415-420 (2006).
84. V. Salgueirino-Maceira, M.A. Correa-Duarte, M. Farle, M.A. Lopez-Quintela, K. Sieradzki, R. Diaz, "Synthesis and Characterization of Large Colloidal Cobalt Particles", *Langmuir*, 22, pp.1455-1458 (2006).
85. V. Salgueirino-Maceira , M.A. Correa-Duarte, M. Farle, A. Lopez-Quintela, K. Sieradzki, R. Diaz, "Bifunctional gold-coated magnetic silica spheres", *Chem. of Mat.*, **18,** pp. 2701-2706 (2006).
86. M.Grzelczak, M.A. Correa-Duarte, V. Salgueiriño-Maceira, M.Giersig, R. Diaz, and L.M. Liz-Marzán, "Photoluminescence Quenching Control in Quantum Dot–Carbon Nanotube Composite Colloids Using a Silica-Shell Spacer", *Advanced Materials*, adma.200501523.

87. A Zhu and GJ Shiflet, "Thermodynamics of Aluminum-based Glasses" Chapter 6 in Advanced Structural Materials, Taylor and Francis Group, LLC, in press
88. Section Editor: ASM Metals Handbook, Vol. 13, Section on Fundamental Corrosion Processes, pp. 42-86, (2004).
89. Section Editor: Section on *Forms of Corrosion*, ASTM Manual 20 on Corrosion Tests and Standards, Version II, pp. 205-322, ASTM Philadelphia, PA. (2005).
90. J.R. Scully, A.M. Lucente, Chapter on Corrosion of Amorphous Metals, in ASM Metals Handbook, Vol. 13B, CORROSION, (accepted – in press), ASM, Metals Park OH (2004).
91. J.R. Scully, R.G. Kelly, Chapter on Electrochemical Methods in Laboratory Corrosion Testing, in ASM Metals Handbook, Vol. 13A, CORROSION, Fundamental, Testing and Protection, pp. 68-80, ASM, Metals Park OH (2004).
92. J.R. Scully, Chapter on Electrochemical Methods in Laboratory Corrosion Testing, in ASTM *Manual on Corrosion Tests and Standards, Application and Interpretation 2nd ed.*, ASTM West Conshohoken, PA, pp. 107-130, (2005).
93. Lu, Yunfeng; Brinker, C. Jeffrey; Antonietti, Markus; Bai, Chunli (editors). Self-Assembled Nanostructured Materials, Materials Research Society Proceedings, Volume 775 (2004).
94. C.J. Brinker, *Co-Editor of:* Proceedings on Hybrid Organic/Inorganic Materials, *Mat. Res. Soc. Symp. Proc., (Spring 2002)*
95. C.J. Brinker, *Co-Editor of* Aerogels 6 Proceedings of the Sixth International Symposium on Aerogels, *J. Non-Crystal. Solids 285 (2001).*
96. R.G. Buchheit, "Corrosion Resistant Coatings and Paints," in Handbook of Environmental Degradation of Materials,' Myer Kutz, Ed., William Andrew Publishing, New York (2005).
97. R.G. Buchheit, A.E. Hughes, "Chromate and Chromate-Free Conversion Coatings," p. 720 in Metals Handbook Vol. 13A, S.D. Cramer, B.S. Covino, Eds., ASM International (2003).
98. A. Seth and W.J. van Ooij, 'Optimization of One-step, Low-VOC, Chromate-free Novel Primer coatings using Taguchi Method approach', in press for Publication in ACS Symposium Series Book, P. Zarras, editor
99. D. Zhu and W.J. van Ooij, 'Surface Modification of Metals by Silanes' in 'Adhesion Aspects of Polymeric Coatings', Vol. 2, K.L. Mittal, editor, VSP, Utrecht, 2003, pp. 81-99.
100. S.R. Taylor, "Coatings for Corrosion Protection: An Overview", Encyclopedia of Materials: Science and Technology, Ed. by K.H.J. Buschow, R.W. Cahn, M.C. Fleming, B. Ilschner, E.J. Kramer, and S. Mahajan, Pergamon, London, (2002).
101. S.R. Taylor, "Coatings for Corrosion Protection: Non-Metallic", Encyclopedia of Materials: Science and Technology, Ed. by K.H.J. Buschow, R.W. Cahn, M.C. Fleming, B. Ilschner, E.J. Kramer, and S. Mahajan, Pergamon, London, (2002).
102. S.R. Taylor, "Coatings for Corrosion Protection: Metallic", Encyclopedia of Materials: Science and Technology, Ed. by K.H.J. Buschow, R.W. Cahn, M.C. Fleming, B. Ilschner, E.J. Kramer, and S. Mahajan, Pergamon, London, (2002) .
103. S.R. Taylor, "Coatings for Corrosion Protection: Organic", Encyclopedia of Materials: Science and Technology, Ed. by K.H.J. Buschow, R.W. Cahn, M.C. Fleming, B. Ilschner, E.J. Kramer, and S. Mahajan, Pergamon, London, (2002).

104. S.R. Taylor, "The Role of Intrinsic Defects in the Protective Behavior of Organic Coatings", Handbook of Environmental Degradation of Materials, Ed. By M. Kutz, William Andrews Publishing, NY, (2005).

Note: Other publications from this MURI are in preparation and will be forthcoming.

b. Other Non-refereed Publications

1. S.R. Taylor, J.R. Scully, R.G. Kelly, and G.J. Shiflet, R.G. Buchheit, W.J. van Ooij, K. Sieradzki, C.J. Brinker, and A.L. Moran, "The Development of a Multi-Functional Coating for Aerospace Application Using Molecular and Nano-Engineering Methods: An Overview", in Proceedings of 2002 Tri-Service Conference, Ed. by R.A. Mantz and P.C. Trulove, AFRL, San Antonio, TX (2003).
2. B.D. Chambers, S.R. Taylor, and M.W. Kendig, "The Rapid Discovery of New Inhibitors Using Combinatorial Methods", in Proceedings of 2002 Tri-Service Conference, Ed. by R.A. Mantz and P.C. Trulove, AFRL, San Antonio, TX (2003).
3. P. Moongkhamklang and S.R. Taylor, "The Role of Coating Heterogeneities in the Long-Term Performance of Coated Aluminum Alloys: Delineation of Ionic Pathways Using a Molecular Probe", in Proceedings of 2002 Tri-Service Conference, Ed. by R.A. Mantz and P.C. Trulove, AFRL, San Antonio, TX (2003).
4. S.R. Taylor, J.R. Scully, and G.J. Shiflet, R.G. Buchheit, W.J. VanOoij, K. Sieradzki,R.E. Diaz,C.J. Brinker, and A.L. Moran, "The Development of a Multi-functional Aerospace Coating Using Nano-Engineering Methods: A MURI Overview and Progress Report", in Proceedings of 2003 Tri-Service Conference, Ed. by V. Agarwala, NSWC, Las Vegas, NV (2003).
5. P. Moongkhamklang and S.R. Taylor, "Delineation of Ionic Pathways in Organic Coatings Using Molecular Probe Technique and Local Electrochemical Methods", in Proceedings of 2003 Tri-Service Conference, Ed. by V. Agarwala, NSWC, Las Vegas, NV (2003).
6. S.R. Taylor, G.J. Shiflet. J.R. Scully, R.G. Buchheit, W.J. vanOoij, C.J. Brinker, K.S. Sieradzki, R.E., Diaz, and A.L. Moran, "Increasing the Functionality of Military Coatings Using Nano-dimensioned Materials" in Proceeding of First World Congress on Corrosion in the Military: Cost Reduction Strategies, Sorrento, Italy, June 6-8, 2005.
7. S.R. Taylor and B.D. Chambers, "The Discovery of Non-Chromate Corrosion Inhibitors for Aerospace Alloys Using High-Throughput Screening Methods", in Proceeding of First World Congress on Corrosion in the Military: Cost Reduction Strategies, Sorrento, Italy, June 6-8, 2005.
8. B.D. Chambers and S.R. Taylor, "High Throughput Corrosion Assessment of AA2024-T3 in the Presence of Corrosion Inhibitors", in Coatings and Inhibitors, Ed. by M.W. Kendig, G.O. Ilevbare, R. Granata, and S. Kuroda, The Electrochemical Society, Pennington, NJ, (in press).
9. MC Gao, GJ Shiflet, "Phase formation sequence map for Al-Ni-Gd glass-forming system devitrified at 250°C.", THERMEC'2003, Materials Science Forum **245-250**, Pt. 1 (2003) pp. 426-432.
10. JP Hadorn and GJ Shiflet, "A Survey of Eutectoid Decomposition in Three Lanthanide-Magnesium Systems", , Proc. Int. Conf. Solid-Solid Phase Transformations in Inorganic Materials 2005 (PTM'05), J.M. Howe, D.E. Laughlin,

J.K. Lee, U. Dahmen and W.A. Soffa -eds., TMS (Warrendale, PA) 2005, pp. 701-706.

11. M. Goldman, N. Unlu, G.J. Shiflet, and J.R. Scully, *"Amorphous Metallic Coatings with Tunable Corrosion Properties Based on Al-Co-Ce-(Mo) Alloy Compositions,"* Paper No. 04276, CORROSION/2004, New Orleans, LA, March (2004).
12. M. Goa, N. Unlu, M. Jakab, J. Scully, G.J. Shiflet, "Amorphous Al-Co-Ce Alloy with Potential Excellent Corrosion Resistance," Military Tri-Service Conference on Corrosion, San Antonio, TX (2002).
13. J.R. Scully, B.A. Kehler, Y. Lee and R.P. Gangloff, "Strategies for Mitigation of Hydrogen Environment Assisted Cracking of High Strength Steels", Tri-Service Corrosion Conference, NACE, Houston, TX, November (2005).
14. J.R. Scully, B.A. Kehler, Y. Lee and R.P. Gangloff, "Strategies for Mitigation of Hydrogen Environment Assisted Cracking of High Strength Steels", 16th International Corrosion Congress: Corrosion tech. in the High Technology Era, Sept. 19-24, Beijing, China, (2005).
15. J.R. Scully and Marta Jakab, *"Design of Cathodic Inhibitors for AA2024-T3 Guided by Understanding Heterogeneous Cathodic Reaction Kinetics"*, 208th ECS Meeting, in LA-E3 Coatings and Inhibitors, Editors: M. Kendig, R. Granata, G. O. Ilevbare, and S. Kuroda, ECS Transactions, Vol 1. The Electrochemical Society, Pennington, NJ, (2005).
16. Q. Meng and A. L. Moran, N. Tailleart, M. A. Jakab and J. R. Scully, "Characterization and Mechanical/Corrosion Properties of Amorphous Al-Co-Ce Coatings," Proc. Of the Tri-Service Corrosion Conference, Orlando, November (2005).
17. F.J. Presuel-Moreno, M.E. Goldman, R.G. Kelly, J.R. Scully, *"Electrochemical Sacrificial Cathodic Prevention Provided by a Al-Co-Ce Metal Coating Coupled to A2024-T3,"* the Electrochemical Soc. Proc. On Corrosion of Light Metals and Alloys, Ed., R. Buchhiet, B. Shaw, R. Kelly, pp. 235-254, (2004).
18. M.A. Jakab, F.J. Presuel-Moreno, J.R. Scully, *"Critical Concentrations associated with cobalt, cerium and molybdenum inhibition of AA2024-T3 corrosion: delivery from Al-Co-Ce(-Mo) alloys,"* the Electrochemical Soc. Proc. On Corrosion of Light Metals and Alloys, Ed. R. Buchhiet, B. Shaw, R. Kelly, pp. 236-254, (2004).
19. S. Chrisanti, R.G. Buchheit, "Use of Ce-modified bentonite clay as a pigment for corrosion inhibition and sensing," ABSTRACTS OF PAPERS OF THE AMERICAN CHEMICAL SOCIETY 228: U360-U360 240-POLY Part 2 AUG 22 2004.
20. R.G. Buchheit, S. Chrisanti, S. Mahajanam, "Corrosion Inhibiting and Sensing Ion Exchange Pigments for Organic Coatings," Corrosion in Marine and Saltwater Environments II, D. A. Schifler, Ed., ECSPV 2004-xx, The Electrochemical Society, Pennington, NJ (2005).
21. S. Chrisanti, S. Mahajanam, R.G. Buchheit, "The Use of Ion Exchange Compounds as Corrosion Inhibiting and Sensing Pigments in Organic Coatings," in 2004 Surface Engineering Conference Proceedings, ASM International, Materials Park, OH (2005).
22. R.G. Buchheit, H. Guan, F. Wong, S. Mahajanam, "Organic Coating Pigments for Corrosion Resistance and Corrosion Sensing," Tri-Service Corrosion Conference, January 14-18, 2002, San Antonio TX.

23. S.P.V. Mahajanam, R.G. Buchheit, "Characterization of Zn-Al-$V_{10}O_{28}^{6-}$ Corrosion Inhibiting Hydrotalcite Pigments in Epoxy Resins," p. 270 in the Proceedings of the Electrochemical Society, PV2003-23, The Electrochemical Society, Pennington, NJ (2004).
24. A. Ashirgade, P. Puomi, W.J. van Ooij, S. Bafna, A. Seth, C. Shivane and Z. Yin, 'Novel, One-step, Chromate-free Coatings Containing Anticorrosion Pigments for Metals that can be used in a Variety of Industries', paper to be published on a conference CD, Eurocorr 2006 in Maastricht, Sep 24-28, 2006
25. P. Puomi, W.J. van Ooij, A. Seth, Z. Yin, A. Ashirgade, S. Bafna and C. Shivane Novel, 'One-step, Chromate-free Coatings Containing Anticorrosion Pigments for Metals', Extended Abstract in the Book of Abstracts of Coatings Science International, Noordwijk, The Netherlands, 26-30 June (2006) 74-78
26. W.J. van Ooij, P. Puomi, A. Ashirgade, S. Bafna, A. Seth, C. Shivane and Z. Yin, 'Low-VOC, Chromate-free, Anti-corrosion Primers for Aluminum Alloys and HDG steel', presented at Megarust 2006, June 12-15, Norfolk, Virginia, http://www.nstcenter.com/RUST2006/presentations/thu/MR2006-22P.Puomi.pdf
27. W.J. van Ooij, A. Seth, L. Yang, Z. Yin and C. Shivane, 'Novel approaches in the development of environmentally compliant coatings for corrosion protection of metals', Proceedings of Hawaii PPF XI Conference 2005
28. W.J. van Ooij, A. Seth, C. Shivane, A. Ashirgade, S. Bafna, L. Yang and P. Puomi, 'Superprimer: Chromate-free, low-VOC, systems eliminating chromate conversion coatings', Poster Presented in Tinker Air Force Base Conference 2005
29. A. Seth and W.J. van Ooij, 'A Novel, low-VOC, Chromate-free, one-step primer system for the corrosion protection of metals and alloys", presented at the Fifth International Symposium on Silanes and Other Coupling agents Toronto, Canada, June 22-24, 2005 and has been accepted for publication in Silanes and Other Coupling agents Ed. K.L. Mittal
30. L. Yang, N. Simhadari, A. Seth and W.J. van Ooij, 'Novel Corrosion Inhibitors for Silane Systems on Metals", presented at the Fifth International Symposium on Silanes and Other Coupling agents Toronto, Canada, June 22-24, 2005 and has been accepted for publication in Silanes and Other Coupling agents Ed. K.L. Mittal
31. W.J. van Ooij, V. Palanivel, D. Zhu and A. Seth, "Mechanisms of Corrosion Protection of Metals by Silane Films", International Conference on Corrosion, UMIST, Manchester, UK, July 7-11, 2003
32. W.J. van Ooij, H. Yang, H. Mu and R. Manian, "Novel Chromate Replacement Paint Pigments based on Water-Soluble Inhibitors coated with a Plasma-Polymerized Membrane Film", Proceedings 16th International Symposium on Plasma Chemistry (ISPC 16), June 22-27, 2003, Taormina, Italy
33. R. Manian, W.J. van Ooij and Y. Huang, "Magnetic Properties and Corrosion Resistance of Plasma Polymer- stabilized Cobalt Nanoparticles", Proceedings 16th International Symposium on Plasma Chemistry (ISPC 16), June 22-27, 2003, Taormina, Italy
34. W.J. van Ooij, V. Palanivel, D. Zhu, M. Stacy, A. Lamar and A. Seth, "Overview of Mechanisms of Corrosion Protection of Metals by Silane Films", Fourth International Symposium on Silanes and other Coupling Agents, June 11-13, 2003, Orlando, FL; to be published in the Proceedings

35. .J. van Ooij and D. Zhu,'Corrosion Resistance of Metals Coated with Organofunctional Silanes', Presented at the 3rd International Conference on Surface Engineering, ICSE2002, Chengdu, P.R. China, October 10-13, 2002, Published in the Proceedings "Contributions of Surface Engineering to Modern Manufacturing and Remanufacturing", Southwest Jiaotong University Press, Chengdu, P.R. China (2002), pp. 594-598.
36. W.J. van Ooij, D. Zhu, A. Lamar, M. Stacy, A. Seth and V. Palanivel, 'The Potential of Organofunctional Silanes for Corrosion Protection of Metals', Presented at RUST 2002, US Navy & Industry Corrosion Technology Exchange, Louisville, KY, July 8-11, 2002, Published in the Proceedings (on CD)
37. D. Zhu, M. Stacy, J.A. Lamar, V. Palanivel and W.J. van Ooij, " Surface Finishing of Metals by Silanes for Corrosion Protection and Improved Paint Adhesion", 2002 Surface Modification and Metal Finishing International Symposium, June 24-29, 2002, Chicago, IL
38. J.A. Lamar, D. Zhu and W.J. van Ooij, "Corrosion Protection of AA2024-T3 by Bis-non-functional Silanes", Proc. Tri-Service Corrosion Conference, January 14-18, 2002, San Antonio, TX
39. W.J. van Ooij, J.A. Lamar and D. Zhu, "Corrosion Protection of AA2024-T3 by Organofunctional Silanes", Proc. Tri-Service Corrosion Conference, January 14-18, 2002,
40. K. Sieradzki, M. Vukmirovic, and R. Vasill, *Photonic Crystal Structures as Nanoengineered Coatings*, Proceedings of The Tri-service Corrosion Conference, January 2002.
41. Lim, D., Diaz, R. E., "Classical emulation of molecular fluorescence and the modification of its quantum efficiency by nearby material structures", *Proceedings of the 9th International Conference on Electromagnetics in Advanced Applications and 11th European Electromagnetic Structures Conference*, pp. 953-955, Torino 12-16 September 2005.
42. B.J. Connolly, A.L. Moran, R. McCaw, J. Pugh, K. Scandell, "Thermal Sprayed Aluminum Alloy Cladding for Aircraft Skin Replacements," in Proceedings of the 2002 Tri-Service Corrosion Conference, Organized by AFOSR/AFRL (Tri-services Committee on Corrosion, U.S. Department of Defense, 2002).
43. Q. Meng, A.L. Moran, N. Tailleart, M.A. Jakab, J.R. Scully, A.L. Moran, "Characterization of Mechanical/Corrosion Properties of Amorphous and Al-Co-Ce Coatings," in Proceedings of the 2005 Tri-Service Corrosion Conference, (Tri-services Committee on Corrosion, U.S. Department of Defense, 2005).

c. Patents

Patents Awarded

1. Fluid Light Guide Having Hydrophobic Aerogel Cladding Layer, U.S. Patent No. 6,983,093, Issued January 3, 2006
2. Fan, Hongyou; Lopez, Gabriel P.; Brinker, Charles Jeffrey; Lu, Yunfeng; Prototyping of Patterned Functional Nanostructures, US Patent Application 10/163,425 (allowed April 2005).
3. Doshi, Dhaval; Fan, Hongyou; Hurd, Alan; Brinker, C. Jeffrey, Photo-Definable Self-Assembled Materials, US Patent Application 6,808,867 (issued October 26, 2004.

4. Brinker, C. Jeffrey; Tsai, Chung-Yi; Lu, Yungfeng, Inorganic Dual-Layer Microporous Supported Membranes, U.S. Patent No. 6,536,604 Issued March 25, 2003
5. Brinker, C. Jeffrey; Ashley, Carol S; Rimple, Bhatia; Singh, Anup K, Sol-Gel Method for Encapsulating Molecules, U.S. Patent No. 6,495,352 Issued December 17, 2002
6. Fan, Hongyou, Lopez, Gabriel P., Brinker, C. Jeffrey, Lu, Yunfeng, Protyping of Patterned Functional Nanostructures, U. S. Patent No. 6,471,761 issued October 29, 2002

Patent Applications

1. C. Jeffrey Brinker; Pratik Shah; Eric D. Branson; Frank van Swol, Processing and Patterning of Hydrophobic Coatings, DOE No./Sandia No. S-103,479/SD-7616 (application filed March 2004)
2. Fan, H.; Lu, Y.; Brinker, J.; Lopez, G.P., Rapid Prototyping of Patterned Organic/Inorganic Functional Nanostructures, UNM-560.
3. Fan, H.; C.J. Brinker, S.T. Reed, Plasma Treatment to Remove Organic Templates to Create Porous Silica Materials
7. C.J. Brinker, H. Fan, Y. Lu, Method for Making Hybrid Bridged Silsesquioxane Thin Film and Particulate Mesophases
5. S.R. Taylor and B.D. Chambers, "Novel Synergistic Combinations of Chromate-free Corrosion Inhibitors and Methods for Discovery Using High Throughput Screening", Provisional Patent Application No. 60/657,298.(March 2005)
6. S.R. Taylor and B.D. Chambers, "Synergistic Combinations of Chromate-Free Corrosion Inhibitors", PCT Application, March 1, 2006.
7. R. G. Buchheit, H. Guan, V. N. Laget, "Corrosion Resistant Coating," Utility U.S. Patent filing, OSU1159-174A, January 2004.
8. W.J. van Ooij and Matt Stacy, PCT Application, July 24, 2003, *"Superprimer"*
9. W.J. van Ooij and V. Palanivel, PCT Application, July 24, 2003, *"Reduced Chromate Silane Film"*
10. W.J. van Ooij, Max Sorenson and Matt Stacy, US Patent Application, assigned to UC and Aeromettech, about August 1, 2003, *"Hydrolyzed Silane Mixture for Bonding Rubber to Metals"*
11. Doshi, Dhaval; Fan, Hongyou; Huesing, Nicola; Hurd, Alan; Brinker, C. Jeffrey, Photo-Definable Self-Assembled Materials, U.S. Patent Application Number 20020127498, Filed September 12, 2002
12. Brinker, C. Jeffrey; Tsai, Chung-Yi; Lu, Yunfeng, Inorganic Dual-Layer Microporous Supported Membranes, U.S. Patent Application Number 20020142172, Filed October 3, 2002

Patent Disclosures

1. C. Jeffrey Brinker; Pratik Shah; Eric D. Branson; Frank van Swol, Processing and Patterning of Hydrophobic Coatings, DOE No./Sandia No. S-103,479/SD-7616
2. Helen K. Baca; C. Jeffrey Brinker; Dunphy, Darren; Brozik, Susan; Flemming, Jeb; Klavetter, Elmer, A Cell-Based Biosensor, DOE No./Sandia No. S-102,154/SD-7431
3. Paul D. Calvert; Helen K. Baca; Eric D. Branson; C. Jeffrey Brinker; Pratik Shah High Resolution Ink-Jet Printing, SD-7515/S-102,263

4. Ying-bing Jiang; Joseph L Cecchi; C. Jeffrey Brinker, Method of Making Dense, Conformal, Ultra-Thin Cap Layers for nanoporous Low-K LLD by Plasma-Assisted Atomic Layer Deposition, UNM#745.
5. Robert C. Hughes, C. Jeffrey Brinker, Susan M. Brozik, Darren W. Branch Mesoporous Sol-gel Supported Lipid Bilayer for Biosensor Applications DOE No./Sandia No. S-102,107/SD-7397(January 28, 2004).
6. Helen K. Baca; C. Jeffrey Brinker; Dunphy, Darren; Brozik, Susan; Flemming, Jeb; Klavetter, Elmer, A Cell-Based Biosensor, DOE No./Sandia No. S-102,154/SD-7431
7. Paul D. Calvert; Helen K. Baca; Eric D. Branson; C. Jeffrey Brinker; Pratik Shah High Resolution Ink-Jet Printing, SD-7515/S-102,263
8. C. Jeffrey Brinker; Pratik Shah; Eric D. Branson; Frank van Swol, Processing and Patterning of Hydrophobic Coatings, DOE No./Sandia No. S-103,479/SD-7616 (Oct 31,2003)
9. S Shiflet, SJ Poon and JR Scully, "Amorphous Metallic Coatings with Tunable Corrosion Properties Based on Al-Co-Ce-(Mo) Alloy Compositions"
10. J.R. Scully, An Al-Cu-Mg-Ni alloy with an Open Circuit Potential Tailored to AA 2024-T3.
11. W.J. van Ooij and V. Palanivel, "Chromate-containing Silane Films for Corrosion Protection of Metals"
12. W.J. van Ooij and H. Yang, "Slow-Release Paint Pigments for Corrosion Control of Metals"
13. W.J. van Ooij and A. Seth, "Use of Silanes for Improvement of Fatigue Life and Resistance to Corrosion Fatigue Cracking of Aerospace Al Alloys"
14. W.J. van Ooij and V. Palanivel, "Novel Corrosion Protection Compound (CPC) based on Silanes"
15. W.J. van Ooij, M. Sorenson, "Hydrolyzed Silane Mixture for Bonding Metals to Unsaturated Rubbers"
16. W.J. van Ooij and J.G. Singh, "Electrodeposition of Organofunctional Bis-Silanes on Metals"
17. W.J. van Ooij, D. Zhu, and R.G. Buchheit, "Chromate-Free Primer System for Aluminum Alloys"
18. C. Jeffrey Brinker; Dunphy, Darren; Brozik, Susan; Flemming, Jeb; Klavetter, Elmer A Cell-Based Biosensor, DOE No./Sandia No. S-102,154/SD-7431

SUMMARY OF MURI GRAs AND PDRAs

STUDENT	ADVISOR	DEGREE
Laetitia Fenzy	Taylor	MS
Brian Chambers	Taylor	PhD
Santhanam Raman	Taylor	PDRA
Francesco Contu	Taylor	PDRA
Jason Hadorn	Shiflet	MS.
Michael Gao	Shiflet	PDRA
Aiwu Zhu	Shiflet	Research Scientist
Necip Unlu	Shiflet	PDRA
Marta Jakab	Scully	Ph.D
Nicole Tailleart	Scully	MS.
Meghan Goldman	Scully	MSE
J.G. Hoekstra	Scully	MS
Tomohiro Aburada	Scully	PhD
Geoff Biddick	Scully	BS
Leah Stohr	Scully	BS
Francisco Presuel-Moreno	Scully	PDRA
Fariaty Wong	Buchheit	MS
Sudhakar Mahajanam	Buchheit	PhD
Santi Chrisanti	Buchheit	PhD
Kevin Ralston	Buchheit	PhD
Hong Guan	Buchheit	PDRA
Henry Gerung	Brinker	PhD
Ying-Bing Jiang	Brinker	PhD
Nanguo Liu	Brinker	PhD
Gerog Garnweitner (U. Vienna)	Brinker	PhD
Shailendra Rathod	Brinker	PhD
Xingmao Jiang	Brinker	PhD
Adam Cook	Brinker	BS
Eric Branson	Brinker	BS
Chris Hartshorn	Brinker	BS
David Bullock	Brinker	BS
Alex Mace	Brinker	BS
Devang Butani	Brinker	BS
Angela Triplett	Brinker	BS
Hongyou Fan	Brinker	PDRA
Yi Yang	Brinker	PDRA
Evelyn Bond	Brinker	PDRA
Anthony Malanoski	Brinker	PDRA
George Xomeritakis	Brinker	PDRA
Seema Singh	Brinker	PDRA

STUDENT	ADVISOR	DEGREE
Rishikesh Manian	van Ooij	MS
Lin Yang	van Ooij	MS
Hai Yang	van Ooij	MS
Danqing Zhu	van Ooij	PhD
Anuj	van Ooij	PhD
Zhangzhang Yin	van Ooij	PhD
Paula Puomi	van Ooij	PDRA
Jeffrey Thomson	Sieradzki	PhD
Toni Tang	Sieradzki	PhD
Veronica Salgueirino	Sieradzki	PDRA
Ratsko Vasill	Sieradzki	PhD
Misa Vukmirovic	Sieradzki	PhD
N. Dimitrov	Sieradzki	PDRA
Derrick Lim	Diaz	PhD
Mat Manusharow	Diaz	MS
Amy Powers	Diaz	MS
Miguel Correa	Diaz	PDRA
MIDN R. Kurrle	Moran	BS
MIDN R. Martin	Moran	BS
MIDN J. Lipscomb	Moran	BS
Rachel Carr	Moran	BS
Brian Connolly	Moran	PDRA
Qingjiang Meng	Moran	PDRA

MURI PROGRAM OVERVIEW

I. PROGRAM OBJECTIVES

The materials that are most critical to the function of current military aerospace coating systems are limiting in that they are either toxic (e.g., chromate compounds), not maintained for the life of the coating system (e.g., unintentional removal of cladding during the de-painting process), or have limited mission function (e.g., low glint, fixed-color camouflage). This Multi-Disciplinary University Research Initiative (MURI) seeks to establish the scientific basis for a military aerospace coating with expanded function using environmentally benign materials. This advancement will require, in some cases, the use of molecular- and nano-engineered materials.

This MURI is seeks to develop the scientific basis for a coating system that will:

(1) Provide corrosion protection using environmentally compliant materials
(2) Sense corrosion and mechanical damage of the aircraft skin
(3) Initiate coating repair responses to sensed chemical and physical damage
(4) Provide color change-on-demand
(5) Achieve optimal adhesion using environmentally compliant materials
(6) Improve the fatigue resistance and mechanical integrity of the fuselage
(7) Provide self-cleaning, water-rejection, and icephobicity via super hydrophobicity

This significant advancement will be accomplished through the development of a new and complete coating system that will include:

(1) The development of a field-replaceable, multi-functional, nano-engineered metallic cladding
(2) The use of molecular engineering, micro-electro-mechanical, and integrated circuit approaches to develop sensing capability of mechanical and environmental conditions of the surface of the aircraft.
(3) The development of new approaches for the identification, encapsulation, and delivery of environmentally compatible inhibitor compounds.
(4) The optimization of organic coating adhesion through the use of environmentally compliant surface treatments.
(5) The development of biomimetic surface structures

The academic team for this MURI is comprised of nine investigators from seven U.S. academic institutions, and has received guidance and other assistance from U.S. industries, DoD, and DoE laboratories. Non-academic partners have collaborated to date, through one of the following types of interactions: (1) as an advisor or (2) as a technical partner which has contributed materials and/or services.

II. SUMARY OF ACTIVITIES

The MURI has made significant progress in all areas of endeavor and has established collaborations amongst the MURI team as well as with outside institutions. These collaboration will be highlighted within the topical discussions of this report.

Specific team interactions have included:

- Conference calls amongst the MURI academic team.
- Internal review meetings of the MURI academic team.
- Multiple AFOSR/AFRL/DoD reviews including a final review at the Tri-Service Corrosion Conference in Orlando.

The specific details of each investigator research effort for the period 9/1/05 though 8/31/06 are provided in this section which is divided into six areas representing the components of the proposed multi-functional coating system. These areas and the individual PIs working within each area are:

(1) Nano-Engineered Metallic Cladding – Scully, Shiflet, Moran,
(2) Identification of Environmentally Compliant Inhibitors – Taylor
(3) Inhibitor Encapsulation and Delivery Strategies – Brinker, Buchheit, van Ooij, Taylor
(4) Added Coating Functionality (Sensing) – Sieradzki, Diaz
(5) Enhanced Adhesion Using Nano-Engineered Materials – van Ooij
(6) System Performance – S.R. Taylor

This segment of the report will present the activities, status of effort, and accomplishments for these respective research efforts for the time period of 9/1/09 through 8/31/06.

PROJECT PERFORMANCE

NANO-ENGINEERED METALLIC CLADDING

J.R. Scully, G.J. Shiflet, A.L. Moran

I. PROJECT OVERVIEW

The goal of this effort is to create a field-applied metallic cladding that has a range of functions: tunable barrier and cathodic protection properties, improved adhesion of subsequent organic layers, the ability to store and release corrosion inhibitors for self-healing, and improvement of fatigue resistance of the aircraft skin structure. This cladding will be developed by the use of Al-transition metal (TM)- rare earth (RE) nanocrystalline and metallic glasses (Shiflet) and applied via either thermal spray (Moran), laser deposition (Fitz-gerald) or kinetic metallization (Moran) technology. Spray-applied Al-based materials (e.g., Al, Al-Zn) have already been applied to steels and age-hardened aluminum materials, but this technology has not been extended to emerging novel multi-functional materials.

A critical characteristic of new amorphous/ nano-crystalline materials developed through this MURI is the ability to supersaturate desired alloying elements (e.g., Co, Ce, Mo) to produce a material with simultaneous superior corrosion performance, high strength, ductility, and wear resistance. Because of the wide composition range in the Al-Co-Ce family of amorphous alloys, "tunable" corrosion properties may be obtained with user-selected corrosion properties governed by manipulation of Co or Ce contents. Moreover, the composition can be controlled to produce a compositionally graded cladding material such that the base composition is tailored to place the skin in compression and minimize fatigue damage, while the outer composition incorporates transition metals to optimize barrier type corrosion protection, active inhibition, adhesion, and possibly sensing agents. The surface exposed nanocrystals in partially vitrified glasses could be selectively etched to provide molecular sized pockets for the incorporation of bonding agents. Moreover, because spray applied metals are not fully consolidated; the micron-dimensioned porosity could be exploited for the incorporation of other components used to optimize mechanical bonding of subsequent organic layers. The ability to utilize rare-earth elements make it possible to produce cladding materials that possess active corrosion protection to suppress corrosion at through-thickness scratches that expose underlying AA2024-T3 or steels.

II. EFFORT REPORT

A. Corrosion Attributes and Functions of New Multi-Functional Metallic Coatings - J.R. Scully

Objectives

The goal of this effort is to replace the hot roll-bonded cladding systems currently used on military aircraft with a thermally sprayed or cold sprayed aluminum or aluminum alloy coating. Specifically the new coating system will possess multi-function corrosion properties such as tunable barrier properties, ability to provide tunable sacrificial cathodic protection, as well as the capability to act as a pigmented paint that releases an inhibitor species which actively inhibits corrosion. Moreover, the new coating will ideally improve the corrosion fatigue lifetime of the aircraft skin. The metallic coating of current focus is an aluminum - transition metal – rare earth (Al-TM-RE) alloy which could by spray applied using various deposition routes or deposited as a powder that is subsequently laser surface treated. Regardless of deposition route, the goal is to produce a metallic coating that is partially or wholly amorphous and possesses tunable properties. Moreover, the methodology and protocols used to demonstrate and quantify corrosion functions, properties, and capabilities are broadly transferable to any new coating system.

The opportunity exists to create a metallic cladding/multi-functional coating that is easily field-applied and has a range of functions to improve corrosion performance, coating adhesion, and provide active corrosion protection (i.e., self-healing). This will ultimately be accomplished through implementation of thermal spray (Moran), laser deposition (Fitz-Gerald) and or kinetic metallization (Moran) technology, and the use of nanocrystalline or amorphous matrix metallic glasses such as the Al-TM-RE glasses developed by Prof. Gary Shiflet. Spray-applied Al-based materials (e.g., Al, Al-Zn) have already been applied to steels and Al age-hardened materials. A critical characteristic of new amorphous/ nano-crystalline materials developed through this MURI is the ability to supersaturate desired alloying elements (e.g., Co, Ce, Mo) to produce a material with simultaneous superior corrosion performance, high strength, ductility, and wear resistance. Because of the wide composition range in the Al-Co-Ce family of alloys, "tunable" corrosion properties may be obtained with user-selected corrosion properties. Moreover, the composition can be controlled to produce a compositionally graded cladding material such that the base composition is tailored to place the skin in compression and minimize fatigue damage, while the outer composition incorporates transition metals to optimize barrier type corrosion protection, active corrosion inhibition, adhesion, and possibly sensing agents. The surface-exposed nanocrystals in partially vitrified glasses could be selectively etched to provide molecular sized pockets for the incorporation of bonding agents. Moreover, because spray-applied metals are often not fully consolidated; the micron-dimensioned porosity could be further exploited for the incorporation of other components or used to optimize mechanical bonding of the subsequent coatings. Further, the ability to utilize alloy compositions that contain rare-earth elements make it possible to produce a cladding material with active corrosion

protection (inhibition) properties that can control corrosion at scratches that expose the underlying substrate alloy such as AA 2024-T3 or steels.

The primary goal of this project is to synthesize (with Group Shiflet of the MURI) and investigate new Al-based metallic coating alloys with the aim of developing a fundamental understanding of how various compositions, amorphous/crystalline microstructures and other attributes achieve and govern the various desired corrosion functions that we have targeted. Desired corrosion functions include:

- The incorporation of alloying elements into metal coatings that can be released in corrosive environments and serve as active corrosion inhibitors. Examples include Mo (released as Mo(VI)), Ce (released as Ce(III) or (IV)), Co (released as Co(II) and Co(III)), and other rare earth elements. Mechanisms of storage, release and inhibition associated with a metallic coating capable of functioning in a similar manner as a pigmented paint will be elucidated. Objectives not only include the investigation of storage, release, transport and inhibition, but modeling and experiments which verify the protection of AA 2024-T3 in the presence of an Al-Co-Ce alloy by chemical means. The ultimate goal will be to produce a long-lived, rapid-response, active corrosion inhibitor system in a metal coating.

- The incorporation of alloying elements into metallic coatings that optimize the composition and metallurgical state in order to enhance the corrosion barrier properties of the metallic coating. Examples include incorporation of alloying elements to improve amorphicity, passivity in acids and bases, halide-induced pit initiation resistance, pit propagation behaviors, and/or act to retard devitrification (i.e., nanocrystal or transitional phase formation) with the ultimate goal to enhance barrier corrosion resistance. Mechanisms responsible for good barrier properties will be elucidated. The objective includes establishing the connection between composition and barrier corrosion properties such that tunable alloy properties can be achieved.

- The incorporation of alloying elements e into metallic coatings that enhance sacrificial cathodic prevention attributes including throwing power. The alloying additions that achieve this function are not necessarily mutually exclusive with those discussed in (1) or (2). Mechanisms responsible for development of attributes favorable to sacrificial cathodic protection will be elucidated. The objective not only includes investigation of storage, release, and inhibition, but modeling and experiments that verify the protection of AA 2024-T3 in the presence of an Al-Co-Ce alloy by chemical means.

A second goal is to reproduce or duplicate these functions in a field-applicable spray or laser treated powder deposit on a structural material. With these goals in mind, there were several thrust areas aimed at achieving these goals over the lifetime of the project.

2. Summary of Activities – Status of Effort

- The cladding team of the MURI (Shiflet, Scully, Kelly, Moran, Fitz-Gerald) designed a novel amorphous and partially amorphous Al-Co-Ce alloy aimed at achieving multi-functional corrosion functions. There are several fundamental corrosion issues concerning development of metallic claddings to enable implementation of a new generation of novel, multi-functional metallic cladding alloys.
- The compositions and coating attributes sought for optimal barrier corrosion properties, active corrosion inhibition (remote healing) properties, and sacrificial corrosion protection properties were hypothesized, designed into a metal coating, tested, verified, and mechanisms for operation proposed. Progress was made in the MURI towards all of these activities and is reported below.
- Alloys must be produced first in ribbon form and then in spray applied or laser treated form. The achievement of functions must be verified in each. Phase I studies centered on characterizing and understanding the corrosion properties of amorphous and devitrified alloy ribbons. Phase II studies focused on corrosion properties of spray applied and laser treated metallic coatings. During the past two year of the MURI, most research emphasis has shifted from spun melt ribbon characterization to investigation of spray and laser applied deposits. Investigation of laser melted and spray applied deposits has been undertaken and compared to spun melt ribbons.

Phase I

Metal Coating Functions: Active Corrosion Inhibition

- The MURI has continued to address the scientific basis for incorporation of alloying elements into a metal coating that could be released, transported and function as active corrosion inhibitors. To address the scientific basis for incorporation of alloying elements that could be released, transported and function as active corrosion inhibitors, experiments have focused on storage and release of Mo(VI), Ce(III) and Co(II).
- Ms. Marta Jakab (Ph.D. Chemical Engineering, 2005) completed a program of study under the direction of Professor J.R. Scully that led to the Ph.D. Thesis. It was of particular interest to explore the possibility of active corrosion inhibition in a novel class of Al-Co-Ce(-Mo) alloys that can release Co^{2+}, Ce^{3+} and MoO_4^{2-} ions. Therefore, the scientific goals of this thesis were to characterize cerium, cobalt and molybdenum storage, release and inhibition when delivered from bulk Al-Co-Ce and Al-Co-Ce-Mo alloys. The final step was to characterize and elucidate mechanisms of oxide storage, release, delivery, and corrosion inhibition. The effect of environmental triggers (pH, chloride concentration) on the mechanism and reaction order of ion release was also a part of these release studies.
- In the past year, both experimental and modeling studies were conducted to confirm storage and release of Co(II), Mo(VI) and Ce(III) ions from an Al-Co-Ce alloy in both acidic neutral and alkaline solutions. Storage has been investigated by X-ray Photoelectron and Auger Electron Spectroscopy. Both pH and Cl^- ion concentration have been found to control release form oxides into aqueous solutions. Release can be triggered via alkaline and acidic solutions but is not detected in neutral solutions or

weak acids. This is one of the first reports of chemical inhibition of corrosion via a metal coating serving as a source of inhibitor ions. Advanced models of the role of heterogeneous reaction sites and the blocking of these sites by inhibitors were also developed in the last year. Several models were adapted from the literature including pinhole and membrane models of inhibition. These models help to elucidate what inhibitor functions might be beneficial.

- In complimentary modeling studies, finite element modeling was completed to demonstrate that inhibitor storage, release rates, transport rates and accumulation levels associated with an Al-Co-Ce alloy functioned in a similar manner as a pigmented paint, and was capable of providing active corrosion inhibiting of various lengths of AA2024-T3. The release and transport of these soluble ions from an Al-Co-Ce metallic coating under atmospheric corrosion conditions were modeled. Most of the input parameters were abstracted from experimental tests. The criterion for protection was met once a determined critical concentration was reached by one of the soluble ions in the aqueous solution over all the exposed AA2024. This critical inhibitor concentration was a level necessary to inhibit corrosion at a given NaCl concentration. The goal was to quantitatively understand what metallic cladding inhibitor release rates and loading levels are needed to protect a scratch exposing AA2024-T3, and to otherwise quantitatively understand the parameters that control the release and transport of active corrosion inhibitors from inorganic cladding matrices to areas of active corrosion, and to give feedback to the corrosion (Scully, Jakab) and metallurgy design teams (Shiflet) to help optimize the design of loading and release mechanisms for long-lived but rapidly responsive functional coatings.

Metal Coating Function: Corrosion Barrier Properties

- Professors Scully, Shiflet and their students have synthesized, patented and characterized a series of Al-Cu-Mg-Ni, Al-Cu-Mg-Pd and Al-Co-Ce-(Mo) alloys with the goal of elucidating barrier corrosion properties. Meghan Goldman completed her M.S. studies in 2005 on this subject. Additional work was conducted by Necip Unlu (PDRA – UVA) and Jack Ferrel (UGRA – UVa) on the corrosion properties of the Al-Cu-Mg-(Ni) and Al-Cu-Mg-(Pd) systems. This work is in the publication stage.
- Studies completed by M. Goldman (M.S. degree 2004) under the direction of Prof. Scully address the fundamental mechanisms governing the potency of various TM and RE alloying additions retained in solid solution in improving uniform alkaline dissolution and localized pit initiation, stabilization and propagation resistance. These studies demonstrated tunable barrier and sacrificial anode properties. Research studies have shifted to verifying similar properties in spray and laser treated deposits. (See below).

Metal Coating Function: Tunable Sacrificial Cathodic Protection

- The concept of tunable cathodic protection using a sacrificial anode coating was demonstrated through experiment and modeling. Dr. Francisco Presuel interacted

with Meghan Goldman and was directed by Prof. John R. Scully to demonstrate through finite element modeling that an Al-Co-Ce alloy can cathodically protect AA 2024-T3 of various scratch lengths in Cl^- ion solution of various concentrations. In the past year, the electrochemical (or electrolytic) throwing power of such an Al-Co-Ce metallic coating under various atmospheric corrosion conditions was modeled.

- The criterion for protection is a galvanic couple potential distribution below the pitting potential of AA2024-T3. The effects of scratch size, pH and chloride concentration, metallic coating composition, and electrochemical kinetics of the materials involved were studied. Substantial sacrificial cathodic prevention of AA2024-T3 scratches could be achieved with Al-Co-Ce alloys serving as a metallic coating with performance superior to conventional Alclad™ coatings in terms of both polarization and maximum scratch size protected.
- The metallic coating provides the best protection (*i.e.*, largest cathodic polarization of a AA 2024-T3 scratch) when it contains a low Co content, is exposed to either high or low pH solutions of low chloride concentration, and the AA2024-T3 scratch exhibits slow cathodic kinetics. The Co content of the alloy should be minimized, consistent with the retention of amorphicity, in order to maximize the throwing power, especially for lower pH solutions. A conference proceedings paper and archival paper in the journal of the electrochemical society were developed.

Phase II.

Metal Coating Functions: Laser Treatment of Al-Co-Ce Alloy Ingot Surfaces for Optimization of Corrosion Properties and Functions

- This effort, directed by Professors Scully and Fitz-Gerald working with Mr. Jeff Hoekstra (M.S. UVA, 2006) and Tomohiro Aburada (Ph.D. 2008), was aimed at extending results from ribbons to actual coatings on aerospace alloys. Laser surface treatments were conducted in the Al-Co-Ce based alloy surfaces both in the form of crystalline ingots and powders applied to aerospace alloy surfaces. A pulsed (25 ns duration FWHM) excimer laser operating at 248 nm was used to irradiate bulk ingot alloys and powders. At this wavelength and pulse duration, typical cooling rates are generally on the order of 10^6 K/s. However, there were significant questions surrounding the homogeneity of the starting bulk surfaces and powders as materials with large inhomogeneous phases will require additional melting and diffusion times.
- Laser energy densities ranging from 0.5 J/cm^2 to 3.5 J/cm^2 were explored while surface doses were varied from 1 to 5000 pulses/area. Cross-sectional analysis of fractured bulk specimen surfaces showed melt depths ranging from 0.5 to 3 microns largely dependent on the total surface dose. The resulting microstructures are being correlated with electrochemical analysis and devitrification behavior. Results indicated that surface cracks could dominate coating corrosion properties.
- Potentiodynamic polarization results, electrochemical noise, and impedance measurements showed improvement over native materials, exhibiting several characteristics of amorphous surface layers. Additional characterization is being performed by scanning electron microscopy (SEM), energy dispersion (EDS),

diffraction (XRD), and electrochemical (EC) techniques. Mr. Hoekstra has completed all degree requirements and the work has been reported at TMS, ASM and AMP.

Metal Coating Functions: Spray Applied Al-Co-Ce Alloy Surfaces for Optimization of Corrosion Properties and Functions

- The optimal glass forming chemistries determined by Scully and Shiflet in 2004 have been sprayed and produced by laser surface melting in 2005. USNA and UVa have collaborated on the purchase of several materials from Arris International and Valimet using a recently developed process. PTS and HVOF coatings are being deposited using the amorphous feedstock and evaluated in terms of metallurgical, mechanical and corrosion properties. A new student, Nicole Tailleart has joined the research team to perform these studies. The following coatings have been tested for corrosion and fatigue properties.

TABLE 1. Coatings Sprayed/To Be Sprayed by Various Thermal Spray Methods (from Moran, USNA)

Powders	HVOF	PTS	Cold Spray	FS	APS
Al, 45 um	+		+	+	+
nano-Al agglomerated	+				+
AlPoCo Al-6Co-5Ce, 45 μm	+	+			
AlPoCo Al-6Co-5Ce, 45 μm cryomilled					
AlPoCo Al-18Co-9Ce, 10 μm		+			
Arris/Valimet Al-13Co-26Ce, 10 μm		+	+		
Arris/Valimet Al-13Co-26Ce, 45 μm	+				
Arris/UCD Al-17Co-16.1Ce	*	*	*		
Arris/UCD Al-12.2Co-16.6Ce	*	*	*		

- All the compositions are given by weight percentage
- The composition of Al-6Co-5Ce powder was measured while others AlCoCe powders have nominal compositions

* Future coatings under ONR program

3. Accomplishments and New Findings

Phase I

- Critical inhibitor concentration for Co(III), Ce(III) and Mo(VI) inhibition of corrosion of AA 2024-T3 were further defined as a function of chloride concentration using two criteria over an expanded range of Cl^- concentrations.
- As a part of this effort, a protocol for rapid determination of critical inhibitor concentration for Cu rich Al precipitation age hardened alloys used in aerospace was

perfected. Electrochemical results were recently confirmed via studies of pit diameters and treatments where verified to improve fatigue lifetimes of AA 2024-T3 (joint with USNA).

- Mechanisms for the inhibition of the oxygen reduction reaction on both pure Cu and AA2024-T3 by Ce(III), Co(II), and Mo(VI) were further elucidated based on concepts of cathode site blocking via homogeneous chemical precipitation and direct electrochemical reduction. As a part of this research a model was adapted from the literature to explain both the charge and mass transport controlled oxygen reduction reaction rates on a heterogeneous electrode such as 2024-T3 as a function of Cu coverage with and without inhibitors.
- Additionally, the pinhole heterogeneous electrode and membrane models were adapted and developed to explain the effect of inhibitors that block reactive Cu rich sites on heterogeneous electrodes. The latest discovery in this area is that depending on heterogeneous electrode nature and mass transport distances, several functions of inhibitors may be ineffective while others are more effective.
- Tunable intrinsic barrier corrosion properties of Al-Co-Ce alloys, sacrificial cathodic protection capabilities combined with inhibitor release capability creates a metal coating that exhibits all three strategies combined in one coating. The novel concept of a metal coating serving like a pigmented coating as a substrate capable of releasing inhibitors was successfully published in Nature Materials.
- The mechanistic explanation for the effects of alloy composition on repassivation potential and open circuit potential were elucidated through diagnostic electrochemical and surface science studies. Co mediates cathodic oxygen reduction electron transfer reactions (ETR) in both the active and mass transport limited regimes to control cathodic kinetics and open circuit potential of Al-Co-Ce alloys. Co controls acid dissolution rates of activated Al-Co-Ce in pits to control the repassivation potential. The latest finding is that pit acidification may be in part mitigated by the dissolution of Co which at equilibrium does not hydrolyze nearly to the extent as Al. Thus, less acidic environments are created in metastable pits making it more difficult to form and maintain the critical pit chemistry required to stabilize pits.
- A regression type model optimized for alloy composition was developed to enable prediction of pitting, repassivation potential and open circuit potential for solid solution glass alloys. The model enables prediction of the effects of alloying content on these properties.
- The chemical throwing power of an Al-Co-Ce coating galvanically coupled to a AA 2024-T3 scratch was successfully modeled and experimental studied as a function of initial pH, release rates, electrolyte thickness and Cl^- concentration. Chemical inhibition and throwing power was maximized at low pH and high pH in low Cl^- solutions. The conclusions were that the metallic cladding studied can provide active corrosion protection (e.g., healing capability) to scratches up to 2500 mm of exposed 2024-T3. Low initial solution pH results in a faster coverage of Ce^{3+} over the scratch. Increasing the [Cl^-] from 0.05 M to 0.1 M dramatically reduces the size of scratch that can be protected. Sharp transitions of the percentage of scratch covered with the critical Ce(III) concentration are observed, especially for the more conductive solutions and Diffusion is the mass transport mode that most affects Ce^{3+}

and Co^{2+} concentration profiles. Migration has a modest contribution that becomes more evident at longer times. Migration appears to be relevant in some cases where the initial pH < 4 and S<1500 □m). The release rate is found to depend in part on the cathodic reaction rate on the cladding which causes pH rise due to OH^- production. The anode cathode relationship is also found to be important through its influence on migration as well as the discover that when the cladding acts as an anode then hydrolysis of Al^{+3} due to cladding dissolution competes with pH rise due to OH^- production. The pH over the cladding can even drop in certain circumstances.

- Chemical throwing power and sacrificial corrosion protection has been successfully experimentally investigated in a thin electrolyte scratch cell. Protection by chemical inhibition has been isolated from electrochemical inhibition in thin electrolyte cells using electrical coupling and decoupling methods. Both forms of protection have been demonstrated and verified via cyclic voltammetry methods, solution analysis by UV-vis to detect inhibitor release and post-test examination for 2024-T3 corrosion.
- Based on the modeling and experimental methods investigated here, generic methods have been developed to assess protection of aerospace alloys at exposed sites such as scratched. These methods have generic applicability to aerospace materials regardless of exact corrosion protection or inhibitor type.
- The concept of tunable cathodic protection using a sacrificial anode coating was demonstrated through experiment and modeling. The metallic coating provides the best protection (*i.e.*, largest cathodic polarization of a AA 2024-T3 scratch) when it contains a low Co content, is exposed to either high or low pH solutions of low chloride concentration, and the AA2024-T3 scratch exhibits slow cathodic kinetics. The Co content of the alloy should be minimized, consistent with the retention of amorphicity, in order to maximize the throwing power, especially for lower pH solutions. This work has been published in JECS and a special issue of CORROSION Journal.

Phase II

- Laser surface treatments were applied to a Al-Co-Ce alloy ingot as well as powders. Preliminary electrochemical and metallurgical/structural characterization was achieved on laser deposited surfaces. Glancing angle XRD confirms amorphous surface layers. A major finding was that homogenization of cast Al-Co-Ce alloys is required prior to laser surface treatment to produce amorphous layers. Secondly, good barrier corrosion resistance is governed by physical defects such as cracks in the highly corrosion resistant amorphous layer. This work has been published in Advance Materials and Processes.

- The optimal glass forming chemistries were recently determined by Scully and Shiflet at UVa. USNA and UVa have collaborated on deposition of Al-13Co-26Ce (approximately by weight) ingot materials from *Arris International*. Fatigue and Corrosion testing has been accomplished. To date, Pulsed Thermal Spray and HVOF spray deposits have been investigated for barrier corrosion properties. PTS materials can be amorphized and display excellent barrier corrosion properties in Cl^- solutions.

- A method has been developed to distinguish the intrinsic corrosion properties of various spray deposited alloys from their properties as defective coatings on 2024-T3.
- HVOF spray deposited and cold spray Al-Co-Ce coatings have also been investigated for corrosion barrier properties after being deposited on 2024-T3. Intrinsic barrier corrosion properties of the deposited materials has been successfully isolated and distinguished from the corrosion properties of the "coating." It has been discovered that the intrinsic corrosion resistance of Al-Co-Ce coating materials independent of 2024-T3 is better than as a coating on 2024-T3. The difference is tentatively attributed to defects in the coatings such as cracks and porosity. Barrier corrosion resistance of "coatings" on 2024-T3 is believed to be dominated by these later factors.
- Two compositions of Pulse Thermal Spray Alloys (Al8Co7Ce and AlCo12Ce3) have been investigated for barrier corrosion resistance using electrochemical corrosion testing methods. It has been determined that a high Co alloy possesses superior corrosion resistance after statistical evaluation.
- Two STTR projects have been launched through DOD funding at SAIC/Enigmatics and at SWRI/Plasma Tech. aimed at advancing the commercialization of Al-Co-Ce coatings. Both STTR projects are being conducted in collaboration with the Univ. of Virginia. SEAS.

MURI – Inter-team Accomplishments

- Techniques to study inhibitor release and accumulation have been adapted to the study of inhibitor release from porous silica (Brinker MURI team). Porous silica has been added as a pigment to epoxy coatings to tests inhibition of coating scribe creep by underpaint corrosion via inhibitor release. Recently, UV-vis and Capillary Electrophoresis have confirms release of the Ce(III) inhibitor from the porous silica using similar procedures as for Al-Co-Ce alloys.
- Contributed to team development of high throughput assessment of inhibitor synergies on AA2024-T3 through Measurement of Surface Copper Enrichment. The method was subsequently used by Brian Chambers and Ray Taylor.
- Developed a spray applicable amorphous and nanocrystalline Al-Co-Ce coating with possible multi-functional corrosion properties for application on aerospace precipitation aged hardened alloys in conjunction with Shiflet and USNA.

4. Personnel Supported

J.R. Scully	co-PI	10% effort
J. Fitzgerald	Assistant professor	4%
Marta Jakab	GRA	100%
Nicole Tailleart	GRA	100%
J. Hoekstra	GRA	100%
F.J. Presuel-Moreno	Post-Doc	50 %
C. Marks	CESE Technician	5%
Tomohiro Aburada	GRA	100%
Geoff Biddick	Undergrad. RA	50%
Leah Stohr	Undergrad. RA	50%

5. Publications

a. Referred Journals

1. F.J. Presuel-Moreno, M.Jakab, R.G. Kelly, J.R. Scully, "Barrier, Electrochemical Sacrificial Cathodic Prevention and Active Corrosion Inhibition Properties of Al-Co-Ce Coatings on A2024-T3," CORROSION Journal Special Issue on Smart Coatings, submitted, (2006).
2. D. Little, J.R. Scully, "The Effect of Heat Treatment on the IGSCC Behavior of Al-Cu-Mg-Ag Alloys," accepted, *Corrosion Science J.*, (2006).
3. D. Ho, N. Brack, J.R.. Scully, T. Markley, M. Forsyth and B. Hinton, "Cerium dibutylphosphate as a corrosion inhibitor for AA2024-T3 Aluminum alloys," Accepted for Publication in J. Electrochem. Soc., 153(9), (2006).
4. F.J. Presuel-Moreno, M.A. Jakab, R.G. Kelly, J.R. Scully, "Computational Modeling of Active Chemical Inhibition Provided by a Al-Co-Ce Metal Coating Coupled and Uncoupled to A2024-T3," *Journal of the Electrochemical Soc*, accepted, June, (2005).
5. Brian J. Connolly, J.R. Scully, "The Transition from Localized Corrosion to SCC in a Severely Underaged Temper of Al-Li-Cu-Ag Alloy AA 2096," *Corrosion Journal*, 61(12), pp. 1145-1166, (2005).
6. M. A. Jakab, F. Presuel-Moreno and J. R. Scully, "Effect of Molybdate, Cerium and Cobalt Ions on the Oxygen Reduction Reaction on AA2024-T3 and Selected Intermetallics: Experimental and Modeling Studies," *J. Electrochem. Soc.*, 153(7), pp.244-252, (2006).
7. D. Little, J.R. Scully, "The Effect of Surface Pretreatment on the Under-Paint Corrosion of AA 2024-T3 at Various Temperatures," *Corrosion J.*, 62(4), pp. 300-315, (2006).
8. M.E. Goldman, N. Unlu, G.J. Shiflet, J.R. Scully, *"Selected Corrosion Properties of a New Al-Co-Ce Alloy," J. Electrochem. and Solid State Letters*," 8(2), B1-B5, (2005).
9. M.A. Jakab, F. Presuel, J.R. Scully, *"Critical Concentrations Associated with Cobalt, Cerium and Molybdenum Inhibition of AA 2024-T3 Corrosion, Delivery from Al-Co-Ce-(Mo) Alloys," Corrosion Journal*, 61(3), pp. 246-263, (2005).
10. J.G. Hoekstra, *S.B. Qadri, J.M. Fitz-Gerald, J.R. Scully, "Laser Surface Modification of a Crystalline Al-Co-Ce Alloy for Enhanced Corrosion Resistance," *Advanced Engineering Materials*, *Advanced Engineering Materials*, 7(9), pp. 1-5, (2005).
11. M.A. Jakab, J.R. Scully, "Storage and Release of Inhibitor Ions from Amorphous Al-Co-Ce Alloys: Controlled Release on Demand," *Nature Materials*, 4, September, pp. 667-670, (2005).
12. F.J Presu-Morenoel, M.A. Jakab, J.R. Scully, "Inhibition of the Oxygen Reduction Reaction on Copper Using Ce, Mo, and Co Compounds," *J. Electrochem. Soc.*, 152(9), pp. B376-387, (2005).
13. M.A. Jakab, F. Presuel, J.R. Scully, "The Oxygen Reduction Reaction on AA 2024-T3; Experiment and Modeling using the Theory of a Heterogeneous Electrode" *J. Electrochem. Soc.*, 152(8), B311-B320, (2005).

14. F.J. Presuel-Moreno, M.E. Goldman, R.G. Kelly, J.R. Scully, "Electrochemical Sacrificial Cathodic Prevention Provided by a Al-Co-Ce Metal Coating Coupled to A2024-T3," *Journal of the Electrochemical Soc*, 152(8), pp. B302-B310, (2005).
15. N. Unlu, F.Q. Guo, G.J. Shiflet, S.J. Poon, J.R. Scully, " The Effect of Pd Addition on the Glass Formation Ability and Electrochemical Corrosion Behavior of a Ternary ($Al_{75}Cu_{17}Mg_8$) Alloy, submitted to Materials Science and Engineering, (2005).
16. N. Unlu, F.Q. Guo, J. Ferrel, G.J. Shiflet, S.J. Poon, J.R. Scully, "The Effect of Ni Additions on Corrosion Behavior of $(Al_{75}Cu_{17}Mg_8)_{(100-x)}Ni_x$ (x=0,1,3,5,7 at%) Amorphous and Crystalline Alloys, submitted to Materials Science and Engineering, (2005).
17. J.E. Switzer, G.J. Shiflet, J.R. Scully, "Localized Corrosion of $Al_{90}Fe_5Gd_5$ and $Al_{87}Ni_{8.7}Y_{4.3}$ Alloys in the Amorphous, Nanocrystalline, and Crystalline States: Resistance to Micrometer-Scale Pit Formation", *Electrochimica Acta*, 48, pp. 1223-1234, (2003).

b. Books/Book chapters/Books edited

Book Chapters

1. Section Editor: ASM Metals Handbook, Vol. 13, Section on Fundamental Corrosion Processes, pp. 42-86, (2004).
2. Section Editor: Section on *Forms of Corrosion*, ASTM Manual 20 on Corrosion Tests and Standards, Version II, pp. 205-322, ASTM Philadelphia, PA. (2005).
3. J.R. Scully, A.M. Lucente, Chapter on Corrosion of Amorphous Metals, in ASM Metals Handbook, Vol. 13B, CORROSION, (accepted – in press), ASM, Metals Park OH (2004).
4. J.R. Scully, R.G. Kelly, Chapter on Electrochemical Methods in Laboratory Corrosion Testing, in ASM Metals Handbook, Vol. 13A, CORROSION, Fundamental, Testing and Protection, pp. 68-80, ASM, Metals Park OH (2004).
5. J.R. Scully, Chapter on Electrochemical Methods in Laboratory Corrosion Testing, in ASTM *Manual on Corrosion Tests and Standards, Application and Interpretation 2nd ed.*, ASTM West Conshohoken, PA, pp. 107-130, (2005).

c. Proceedings

1. M. Goldman, N. Unlu, G.J. Shiflet, and J.R. Scully, *"Amorphous Metallic Coatings with Tunable Corrosion Properties Based on Al-Co-Ce-(Mo) Alloy Compositions,"* Paper No. 04276, CORROSION/2004, New Orleans, LA, March (2004).
2. M. Goa, N. Unlu, M. Jakab, J. Scully, G.J. Shiflet, "Amorphous Al-Co-Ce Alloy with Potential Excellent Corrosion Resistance," Military Tri-Service Conference on Corrosion, San Antonio, TX (2002).
3. J.R. Scully, B.A. Kehler, Y. Lee and R.P. Gangloff, "Strategies for Mitigation of Hydrogen Environment Assisted Cracking of High Strength Steels", Tri-Service Corrosion Conference, NACE, Houston, TX, November (2005).
4. J.R. Scully, B.A. Kehler, Y. Lee and R.P. Gangloff, "Strategies for Mitigation of Hydrogen Environment Assisted Cracking of High Strength Steels", 16th

International Corrosion Congress: Corrosion tech. in the High Technology Era, Sept. 19-24, Beijing, China, (2005).
5. J.R. Scully and Marta Jakab, *"Design of Cathodic Inhibitors for AA2024-T3 Guided by Understanding Heterogeneous Cathodic Reaction Kinetics"*, 208th ECS Meeting, in LA-E3 Coatings and Inhibitors, Editors: M. Kendig, R. Granata, G. O. Ilevbare, and S. Kuroda, ECS Transactions, Vol 1. The Electrochemical Society, Pennington, NJ, (2005).
6. Q. Meng and A. L. Moran, N. Tailleart, M. A. Jakab and J. R. Scully, "Characterization and Mechanical/Corrosion Properties of Amorphous Al-Co-Ce Coatings," Proc. Of the Tri-Service Corrosion Conference, Orlando, November (2005).
7. F.J. Presuel-Moreno, M.E. Goldman, R.G. Kelly, J.R. Scully, *"Electrochemical Sacrificial Cathodic Prevention Provided by a Al-Co-Ce Metal Coating Coupled to A2024-T3,"* the Electrochemical Soc. Proc. On Corrosion of Light Metals and Alloys, Ed., R. Buchhiet, B. Shaw, R. Kelly, pp. 235-254, (2004).
8. M.A. Jakab, F.J. Presuel-Moreno, J.R. Scully, *"Critical Concentrations associated with cobalt, cerium and molybdenum inhibition of AA2024-T3 corrosion: delivery from Al-Co-Ce(-Mo) alloys,"* the Electrochemical Soc. Proc. on Corrosion of Light Metals and Alloys, Ed. R. Buchheit, B. Shaw, R. Kelly, pp. 236-254, (2004).

6. Interactions/Transitions

Participation at Professional Meetings, Conferences and Seminars

1. Marta Andrea Jakab, Francisco Jose Presuel-Moreno, and John R. Scully, "Cerium, Cobalt and Molybdate Ion Storage, Release and Corrosion Inhibition when Delivered from Oxides on Aluminum - Transition Metal - Rare Earth Metal Alloys", ISE Symposium on Corrosion, Edinburgh, Scotland, 2006. (invited)
2. Nicole Tailleart, Q.Ming, A. Moran, John R. Scully, "Barrier Corrosion Properties of Spray Applied ALUMINUM - TRANSITION METAL - RARE EARTH METAL ALLOYS," Gordon Research Conference on Corrosion – Poster Session, July, 2006.
3. Marta Andrea Jakab, Francisco Jose Presuel-Moreno, and John R. Scully, "Cerium, Cobalt and Molybdate Ion Storage, Release and Corrosion Inhibition when Delivered from Oxides on Aluminum - Transition Metal - Rare Earth Metal Alloys", Topical Research Symposium on Smart Coatings and Inhibitors, CORROSION 2005, Houston TX, April, 2005. (Invited)
4. J.R. Scully, "Hidden Corrosion, What Should Be Measured to Improve Emerging Anticipate and Manage Strategies," 32nd[d] Annual Review of Progress In Quantitative Non-destructive Evaluation," QNDE –Brunswick, Maine (2005). {Key Note Lecture for Symposium Kick-off General Session).
5. Francisco Presuel, Marta Jakab, Robert Kelly, and John Scully "Computational Modeling of Active Corrosion Inhibitor Release from an Al-Co-Ce Metallic Coating: Protection of Exposed 2024-T3", E3 - Coatings and Inhibitors, Abstract #289, 208th ECS Meeting, Los Angeles CA, October, 2005.

6. J.R. Scully and Marta Jakab, "Design of Cathodic Inhibitors for AA2024-T3 Guided by Understanding Heterogeneous Cathodic Reaction Kinetics", in E3 - Coatings and Inhibitors, 208th ECS Meeting, Los Angeles, CA, October 2005.
7. T. Aburada, J.R. Scully, and J.M. Fitz-Gerald, "Laser Processing of Al Based Alloy for Enhanced Corrosion Resistance", presented at the 61st Annual National Association for Corrosion Engineering (NACE) International Meeting, San Diego, CA, March 12th – 16th, 2006.
8. T. Aburada, J.G. Hoekstra, M.A. Jakab, S.B. Qadri, G. J. Shiflet, S. J. Poon, J.R. Scully, and J.M. Fitz-Gerald, "Laser Processing of Crystalline Technologically Relevant Glass-Forming Alloys for Enhanced Corrosion Resistance", presented at the 52nd International American Vacuum Society Fall Meeting, Boston, MA, October 30th - November 4th, 2005.
9. T. Aburada, J.G. Hoekstra, M.A. Jakab, S.B. Qadri, G. J. Shiflet, S. J. Poon, J.R. Scully, and J.M. Fitz-Gerald, "Laser Processing of Crystalline Fe and Al Based Glass-Forming Alloys for Enhanced Corrosion Resistance", presented at the 8th International Conference on Laser Ablation, Banff, Canada, September 11th - 16th, 2005.
10. Marta Jakab, John R. Scully, "Cerium, Cobalt and Molybdate Ion Storage, Release and Corrosion Inhibition when Delivered from Oxides on Aluminum - Transition Metal - Rare Earth Metal Alloys," CORROSION/05, Research in Progress Symposium, NACE, Houston, April, 2005.
11. Marta Jakab, John R. Scully, "Cerium, Cobalt and Molybdate Ion Storage, Release and Corrosion Inhibition when Delivered from Oxides on Aluminum - Transition Metal - Rare Earth Metal Alloys," CORROSION/05, Student Poster Session, NACE, Houston, April, 2005.
12. Marta Jakab, John R. Scully, "Cerium, Cobalt and Molybdate Ion Storage, Release and Corrosion Inhibition when Delivered from Oxides on Aluminum - Transition Metal - Rare Earth Metal Alloys," Gordon Research Conference on Corrosion – Poster Session, July, 2004.
13. J.G. Hoekstra, G. J. Shiflet, S. J. Poon, J. R. Scully, and J. M. Fitz-Gerald, "Laser Processing of Bulk Crystalline Alloys for Improved Corrosion Resistance", *TMS International Meeting*, San Francisco, CA, February 2005.
14. J.G. Hoekstra, G. J. Shiflet, S.B. Qadri, J. R. Scully, and J.M. Fitz-Gerald, "Laser Processing and Characterization of Materials", *American Vacuum Society Meeting*, Orlando, FL March 2005.
15. J.M. Fitz-Gerald, J.G. Hoekstra, G. J. Shiflet, S.B. Qadri, J. R. Scully, "Laser Processing and Surface Modification of Bulk Crystalline Glass-Forming Alloys for Enhanced Corrosion Resistance", the *American Vacuum Society Meeting*, New England, Burlington, MA June 27-30 2005.
16. M. E. Goldman, N. Unlu, G.J. Shiflet, J.R. Scully, "Barrier Corrosion Properties of Amorphous Aluminum-Based Metallic Glasses" NACE Corrosion 2003, San Diego, CA, March 17-20 2003 (2nd Place Marcel Pourbaix Science Division).
17. M. E. Goldman, N. Unlu, G.J. Shiflet, J.R. Scully, "Amorphous Metallic Coatings with Tunable Corrosion Properties Based on Al-Co-Ce-(Mo) Alloy Compositions," Tri-Service Corrosion Conference, Las Vegas, NV, November 17-21, 2003.

18. John R. Scully, "A New Amorphous Aluminum-Based Metallic Glass with Tunable Corrosion Properties," Sandia National Labs, May 2003, [Invited].
19. John R. Scully, M. A. Jakab; M. E. Goldman; F. J. Presuel; N. Unlu; G. J. Shiflet, "Amorphous Metallic Coatings With Tunable Corrosion Properties Based On Al-Co-Ce-(Mo) Alloy Compositions", Partners in Environmental Technology Technical Symposium & Workshop, Washington, D.C., Sponsored by SERDP, December 2003. *(invited).*
20. M. Jakab, F. Presuel-Moreno, and J. Scully "Cerium, Cobalt and Molybdate Cation Storage States, Release and Corrosion Inhibition when Delivered from Oxides on Aluminum - Transition Metal - Rare Earth Metal Alloys", The 204 Electrochemical Society Meeting, Orlando, Florida, October, 2003.
21. F. Presuel, M. Goldman, J. Scully, and R. Kelly "Modeling of Electrochemical Sacrificial Cathodic Prevention Provided by a Novel Al-Ce-Co Metal Coating Coupled to AA-2024 Under Atmospheric Conditions", The 204 Electrochemical Society Meeting, Orlando, Florida, October, 2003.
22. Meghan Goldman, Necip Unlu, Francisco J. Presuel, Gary J. Shiflet, and John R. Scully, Amorphous Metallic Coatings with Tunable Corrosion Properties Based on Al-Co-Ce-(Mo) Alloy Compositions , paper No 04276, Corrosion/2004, New Orleans, LA, March 28–April 1, 2004 •NACE International. (In - Advances and Future Directions in Military Coating Systems).
23. F.J. Presuel-Moreno, H. Wang, M.A. Jakab, R. G. Kelly, and J.R. Scully, "Computational Modeling of Active Corrosion Inhibitor Release from an Al-Co-Ce Multifunctional Metallic Coating and Protection of Exposed 2024-T3", Gordon Research Conference – Aqueous – Corrosion, Poster Session, New London, NH, July 2004.
24. R.G. Kelly, J.R. Scully, D. Peeler, M. Altynova, "An Algorithm for Modeling the Effects of Corrosion on the Structural Integrity of Lap Joints in Aerospace Structures," NACE Topical Research Symposium on Modeling and Life prediction for Corrodible Structures," J.R. Scully, D.W. Shoesmith, editors, NACE CORROSION/2003, San Diego, March 2003 [Invited].

Consultation and Advisory Activities

- Consultant to S&KT on the Effects of Corrosion on Structural Integrity (CESI) program run by Dr. Deb Peeler of AFRL. The program aims to factor corrosion into the Structural Integrity KC-135 Tanker Aircraft and develop prediction and management tools to forecast future aircraft maintenance
- Consultant to Columbia Accident Investigation Board (CAIB) regarding corrosion issues associated with the Orbiter Columbia and the remaining Orbiter Fleet.
- John R. Scully, appointed to Defense Science Board Task Force on Corrosion Control, (2003-2005).
- Consultant to S&KT regarding development of a predictive model to factor in the effects of environment severity including photonic radiation (UV light) on AF paint degradation. The project compares exposure dosing to molecular analysis of coatings to coating function based on EIS method and salt spray exposure.

- Consultant to Faraday, Inc. regarding a Phase I SBIR for development of a predictive model for degradation of AF paint barrier properties by EIS using theory based data mining. The project compares exposure dosing to molecular analysis of coatings to coating function based on EIS method and salt spray exposure.
- Consultant to Faraday, Inc. regarding phase II SBIR regarding a predictive model for degradation of AF paint barrier properties by EIS using theory based data mining. The project compares exposure dosing to coating function based on EIS methods.

Transitions - Professional Communications

- Dr. Airan Perez
  Office of Naval Research
  800 N. Quincy Street
  Arlington, VA 22217-5660
  Phone:
  Email: PEREZA@ONR.NAVY.MIL
  Phone:
  Dates: Summer, 2005-6 and via conference, email, phoncon
  Objective: to discuss opportunities for mitigation of the cracking of high strength ferrous alloys in marine applications via use of a tunable Al-Co-Ce coating

- Dr. Martin Kendig
  Rockwell Science Center
  1049 Camino Dos Rios
  Thousand Oaks CA, 91360
  Phone: (805)373-4341
  e-mail: mkendig@rwsc.com
  Dates: July 25-29, 2004 and via email
  Objective: use of inhibitors to suppress hydrogen environment assisted cracking

- David L. Book
  President, Enigmatics, Inc.
  9215 51st Avenue, No. 7
  College Park, MD 20740
  Tel (work/cell): 301-486-1725/202-285-2431
  Dates: Various in 2006
  Objective: Collaboration with Enigmatics and SAIC on development of a spray applied Al-Co-Ce coating via pulse thermal spray methods under STTR funding

- Dr. Edelman Schmuel
  SAIC, Inc.
  Dates: Various in 2004-2006
  Objective: Collaboration with Enigmatics and SAIC on development of a spray applied Al-Co-Ce coating via pulse thermal spray methods at first under MURI and then under STTR funding

- Dr. Marta Jakab
  Research Engineer
  Mechanical and Materials Engineering Division
  Southwest Research Institute
  6220 Culebra Road
  San Antonio, TX, 78228-0510
  Phone: 210-522-5240
  Email: marta.jakab@swri.org
  Dates: Various in 2006
  Objective: Collaboration with SWRI and Plasma Inc. on development of a spray applied Al-Co-Ce coating via pulse thermal spray methods under STTR funding

- Dr. Satish Dixit, Ph.D.
  Plasma Technologies, Inc.
  1754 Crenshaw Blvd.
  Torrance, CA 90501
  Dates: Various in 2006
  Objective: Collaboration with SWRI and Plasma Inc. on development of a spray applied Al-Co-Ce coating via pulse thermal spray methods under STTR funding

- George E. Kim, Ph.D.
  Consultant - NANOTECHNOLOGY
  Materials and Surface Engineering
  Perpetual Technologies, Inc.
  tel: 514-240-7932
  fax: 514-762-9022
  email: gkim@perpetualtech.ca
  www.perpetualtech.ca
  Dates: Various in 2006
  Objective: Collaboration with SWRI and Plasma Inc. on development of a HVOF spray applied Al-Co-Ce coating via HVOF spray methods under both MURI and STTR funding

- Laura B. Simon
  Senior Materials Engineer
  S&K Technologies, Inc.
  1600 Brown St. Suite 201
  Dayton, OH 45409
  Objective: ongoing 2002-03, supplier of AA 2024-T3 sheet with intact and scratched cladding after exposure – goal is to compare cathodic protection afforded by cladding to model results

- Dr. Mark F. Smith (Manager)
  Joining and Coating Department
  Sandia National Laboratories
  P.O. Box 5800, MS 0889

Albuquerque, NM 87185-0889 USA
voice: 505-845-3256, fax: 505-844-4816, pager: 505-540-1984
mfsmith@sandia.gov
Objective: ongoing 2002-03 discussions regarding use of cold spray application method applied to Al-Co-Ce alloys

- Robert C. McCune,
  Materials Research and Advanced Engineering Department
  Ford Motor Company
  Mail Drop 3182 SRL
  P.O. Box 2053
  Dearborn, MI 48121-2053
  phone: (313)845-0610
  fax: (313)323-1129
  e-mail: rmccune@ford.com
  Objective: On-going discussion of automotive and Naval Cold spray application of Al-base alloys for corrosion mitigation

7. New Discoveries, Inventions, Patent Disclosures

- Patent Disclosure on Al-Co-Ce alloys with Tunable Corrosion Properties
- Patent Disclosure on an Al-Cu-Mg-Ni alloy with an Open Circuit Potential Tailored to AA 2024-T3

8. Honors and Awards

- John R. Scully, paper published in Nature Materials on Inhibitor Storage and Release from Al-Co-Ce alloy
- Marta Jakab: A.B. Campbell Award, Best paper in published in Corrosion Journal for an author under 35 years of age, 2005. *"Critical Concentrations Associated with Cobalt, Cerium and Molybdenum Inhibition of AA 2024-T3 Corrosion, Delivery from Al-Co-Ce-(Mo) Alloys," Corrosion Journal*, 61(3), pp. 246-263, (2005).
- Marta Jakab: Best Graduate Student in Chemical Engineering, University of Virginia, School of Engineering and Applied Science, 2005.
- Marta Jakab: 1st Place Marcel Pourbaix Award, NACE Corrosion/2005 Student Poster Session
- Meghan Goldman: 2nd Place Marcel Pourbaix Award, NACE Corrosion/2004 Student Poster Session
- Marta Jakab: 3rd Place Marcel Pourbaix Award, NACE Corrosion/2003 Student Poster Session
- Meghan Goldman: 3rd Place Marcel Pourbaix Award, NACE Corrosion/2003 Student Poster Session
- John R. Scully, Fellow of the Society, The Electrochemical Society, 2005
- John R. Scully, The Francis LaQue Award, The American Society for Testing and Materials, 2005.

- John R. Scully and D.G. Kolman, Selected for Institute of Corrosion (UK) T.P. Hoar Award for Best Paper in the journal CORROSION SCIENCE published in the prior year.
- John. R. Scully, was elected Chairman of the Gordon Research Conference on Aqueous Corrosion, to be held July 14-19, 2004 New London, New Hampshire

B. The Design of Amorphous Aluminum Alloys – G.J. Shiflet

1. Objectives

- The goal of this portion of the MURI program was to design a metallic glass coating using computational thermodynamics and a considerable number of experiments for subsequent modeling validation and for thermodynamic data acquisition
- In this Final Report a new approach is discussed to obtain data for thermodynamic modeling, namely utilizing First Principles (FP) to secure information on stable phases to help guide alloy design.
- An Al-RE-TM system with RE=Ce and TM=Co was selected to form the base alloy to optimize both thermodynamically, utilizing the CALculation of PHAse Diagram (CALPHAD) technique, and electrochemically, e.g., pitting resistance.
- Because fundamental thermodynamic information is incomplete for the Al-Ce-Co ternary system a more complete database required construction using techniques including DSC, DTA, C_p measurements, phase identification and detailed chemical analyses, and partitioning studies. Alloy ingots were produced by arc- and induction-melting high purity elements.
- High-speed melt-spinning was employed to identify the Glass Formation Range (GFR). Considerable effort was spent over the past several years to fix the binary Al-Ce diagram. This effort along with the completed Al-rich portion of the Al-Ce-Co phase diagram will be reported below.
- Finally, a new binary system (Al-Sm) was made to test the basic idea that a metallic glass is more inherently corrosion resistant than its crystalline form.

2. Summary of Activities – Status of Effort

Re-assessment of Al-Ce Binary Phase Diagram

a. First principles energy calculations

- The Al-Ce binary system is analyzed using first principles calculations that employ the first principles, plane-wave code VASP, which solves for the electronic band structure using electronic density functional theory. Because of the presence of rare-earth element Ce, PAW potentials are used as supplied with

VASP (a commercial software package for this purpose). The entire f-levels are treated within the valence band. All structures are fully relaxed (both lattice parameters and atomic coordinates) until, again, energies converge to a precision of 10 meV/atom. The plane-wave energy cutoff is held constant at 300 eV for Al-Ce, the defaults for the rare-earth potentials. Spin polarization is considered in all calculations other than pure aluminum. To obtain enthalpy of formation values ΔH_f, a composition-weighted average of the pure elemental cohesive energies is subtracted from the cohesive energy of a given compound. The resulting energy is an "enthalpy" because its volume is relaxed (at zero pressure). It is at T=0 K because its atomic coordinates are relaxed.

- Vertices of the convex hull of a scatter plot of ΔH_f versus composition identify stable structures. Points above the convex hull represent thermodynamically unstable structures, though they may be metastable, or stable at higher temperatures in some cases. Most of the structures examined are mechanically stable, in the sense that atomic displacements during relaxation are generally small (less than 0.03 nm at worst). The $Al_4La.oI30$ type structures have large displacements because the starting crystallographic structure is not good.

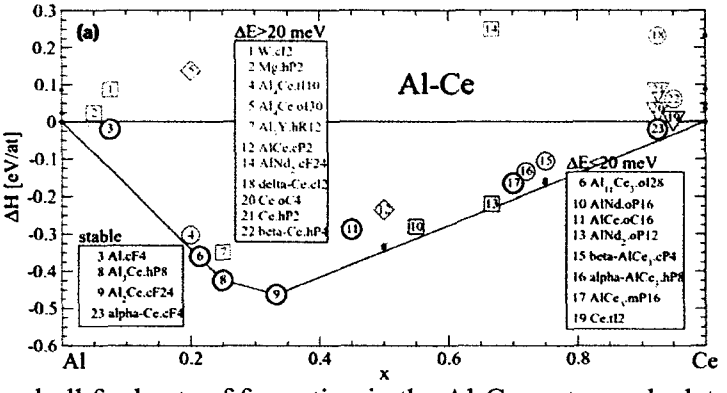

Figure 1. Convex hull for heats of formation in the Al-Ce system calculated with VASP.

- For the resulting enthalpies of formation displayed in Fig. 1, the plotting symbol notation is: heavy circles for known stable binary phases; light circles for known high temperature phases; diamonds for known metastable phases; triangles for known high pressure phases; squares for imperfectly known, unknown or hypothetical structures. Tie-lines run along convex hull edges, joining low enthalpy structures at the vertices of the convex hull. Structures are labeled using the notation {prototype}.{Pearson} where the prototype is the name of some commonly known isostructural compound, and the Pearson symbol gives point symmetry, translational symmetry and number of sites per unit cell. For example, the structure in the Al-Ce binary diagram (Fig. 1) labeled $AlNd_2.oP12$ contains Al and Ce atoms arranged as in $AlNd_2$ with Ce substituting for Nd. This structure is orthorhombic, primitive (no centering) with a twelve atom unit cell.
- The binary phase diagram is fairly well reproduced, but the overall level of agreement is lower than found in similar studies of compounds not containing rare earth elements. The following discussion addresses Al-Ce, starting from pure Al and ending with pure Ce. For pure Al comparison is made between FCC (cF4),

HCP (hP2) and BCC (cI2) structures, finding the known FCC structure favored.

- The low temperature stable $\alpha Al_{11}RE_3$.oI28 phases are just 2 meV/atom above the convex hull for Al-Ce. The high temperature β phases with Pearson symbol tI10 lie above the convex hulls by about 40 meV/atom in each case. According to the experimental phase diagrams the composition of β matches that of α,but the ideal composition of tI10 is more Al-rich than oI28. Introducing an Al vacancy on the 4e site of tI10 is found to raise the energy by an additional 40 meV/atom (i.e., 400 meV/vacancy) above the convex hull. Other sites are even more unfavorable. In the current thermodynamic modeling, the previously reported $\beta Al_{11}RE_3$ phase is corrected to be a stoichiometric Al_4RE compound. Reports of Al_4RE phases with structure type oI30 (prototype Al_4La) are highly doubtful because their enthalpies of formation are all found to be positive. There is thus no driving force to create such a crystal structure from its constituent elements.
- The next two phases, Al_3Ce.hP8 and Al_2Ce.cF24 are correctly placed on the convex hull. As a candidate for the previously unreported structure βAl_3Ce, the prototype Al_3Y.hR12 is first considered. At a ΔE of around 20 meV/atom, this could easily arise as a high temperature phase. As suggested by Cacciamani and Ferro[1] the possibility of sublattice mixing in the cF24 structures is explored. To test this possibility the compositions $Al_{(1-x)}RE_x$ (x=0.292, 0.333 and 0.375) are investigated by taking a 24-atom unit cell of Al_2RE.cF24 and replacing a single atom with one of the opposite type. The calculated energy costs is found to be around 1 eV for each replacement. Estimating entropy gains upon replacement from the numbers of available sites yields temperatures exceeding 4000 K at which sublattice disorder should be important. Since this temperature greatly exceeds the melting temperature it is concluded that sublattice mixing can safely be ignored in these alloy systems.
- At composition x=0.5, the experimental phase diagram shows stable phases. In both cases calculations find these phase lie slightly above the convex hulls.
- At composition $AlCe_3$, the established phase diagram shows a sequence of phases, mC16, hP8 and cP4 at progressively higher temperatures. Current energy data reproduces this sequence, but it is found that even the lowest energy lies slightly above the convex hull.
- Pure elemental Ce exhibits a complicated sequence of structures as temperature rises, α (FCC, low volume), β (cP4), γ (FCC, high volume), δ (BCC). Because the cell volume is relaxed, the high volume γ phase is not found, but the others (α, β and δ) are properly ordered in enthalpy. Likewise the high pressure phases lie correctly above the α phase in enthalpy. Although spin polarization is considered, current calculations for pure Ce did not find spin polarized states, probably because the actual magnetic structures are spin canted in various manners. Calculations place these in the proper sequence, and find the high pressure FCC structure properly above α.

b. Thermodynamic Models

- The Gibbs free energy of individual phases is described by sublattice models and is defined relative to the Stable Element Reference (SER), *i.e.*, the enthalpies of

the pure elements in their defined reference phase at 298.15K and 1 atm.

- All the disordered solutions including liquid are modeled with a single sublattice, with the Gibbs energy expressed as for a binary phase with components A and B:

$$G^{\phi} = x_A {}^{o}G_A^{\phi} + x_B {}^{o}G_B^{\phi} + RT(x_A \ln x_A + x_B \ln x_B) + {}^{ex}G^{\phi} + {}^{mag}G^{\phi}.$$

where ${}^{o}G_i^{\phi}$ is the molar Gibbs energy of the pure element i in the structure of phase ϕ in the non- magnetic state, taken from the values tabulated by Dinsdale[2], and x_i is the mole fraction of each component.

- The excess Gibbs energy is expressed in Redlich-Kister-Muggianu polynomial form:

$${}^{ex}G^{\phi} = x_A x_B \sum_i {}^{i}L_{A,B}^{\phi}(x_A - x_B)^{i}.$$

- ${}^{i}L_{A,B}^{\phi}$ are the binary interaction parameters evaluated in the present work, which is typically modeled as: ${}^{i}L = {}^{i}a + {}^{i}bT + {}^{i}cT\ln(T) + {}^{i}dT^2$.
- The magnetic contribution to the Gibbs energy (${}^{mag}G^{\phi}$) for all binary compound phases is set to zero because of a lack of experimental data.
- Stoichiometric compounds are modeled as if the enthalpy and entropy are constants and only one element occupies one sublattice. For example, the Gibbs free energy for a binary stoichiometric compound A_xB_y is modeled as (J/mole of atoms):

$$G^{A_xB_y} = \frac{x}{x+y} {}^{o}G_A + \frac{y}{x+y} {}^{o}G_B + a + bT.$$

- The C15 Laves phase A_2B (cF24, Cu_2Mg) consists of only two crystallographic sites (A atoms occupy Wyckhoff sites 16d and B atoms occupy 8a).

c. Re-assessed Al-Ce Phase diagram

- The Al-Ce was calculted (Fig. 2) using first-principles energy calculations and critical experiments, reaching the following new conclusions:
  (1) An equilibrium phase $AlCe_2$ exists and is stable at high temperatures (647-775 °C). Its structure is likely oP12.
  (2) The previously described $Al_{11}RE_3$ (RE=La,Ce,Nd,Pr) should ideally have a stoichiometry of Al_4RE (tI10).
  (3) There exist an $\alpha/\beta Al_3Ce$ polymorphous transition occurring at 973°C in Al-Ce system. The βAl_3RE phase may be isostructural with βAl_3Y (hP12).
  (4) The cF24 structures of Al_2Ce should be treated as a stoichiometric compound phase.
  (5) $\alpha/\beta AlCe_3$ polymorphous transition is confirmed, but the exact transition temperature (between 200-500 °C) is not identified.
  (6) The invariant temperatures detected during the heat segment were emphasized during optimization rather than the liquidus temperatures. The former are always easier to identify during thermal analysis and thus are of higher accuracy and reproducibility. Therefore, they should be assigned more weight during optimization.
  (7) The Al-Ce system was thermodynamically reoptimized. The calculated heat (absorbed or released) for all the invariant reactions agrees well with those from

thermal measurements on a relative scale. The process to obtain these conclusions were done as using both First Principles calculations and computational thermodynamics coupled with many experiments on a series of alloys.

- Based upon these new measurements and other literature information, the Al-Ce system is optimized using the PARROT module (Fig. 2a). The newly computed Al-Ce phase diagram agrees very well with DTA data points, and excellent agreement for all the invariant reactions is achieved. On the other hand, agreement of the computed liquidus boundary is good overall but less satisfactory, and this may be due to (1) the intrinsic uncertainty in terms of liquidus measurement; (2) lack of sufficiently reliable thermodynamic measurements of the liquid phase; (3) the high susceptibility to oxidation for RE-rich alloys.

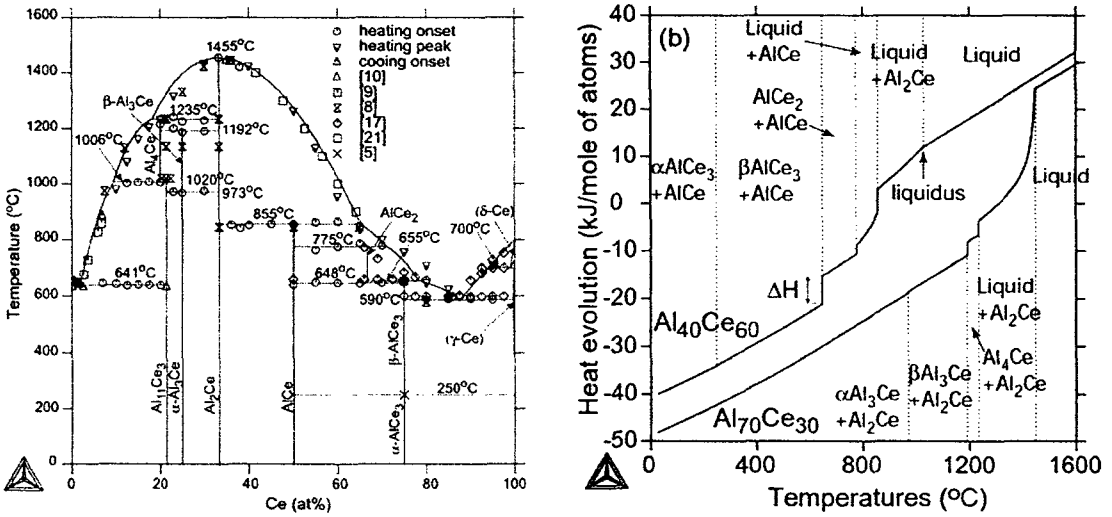

Figure 2 (a) Optimized Al-Ce phase diagram and (b) temperature dependent enthalpies associated with phase transformations for $Al_{40}Ce_{60}$ and $Al_{70}Ce_{30}$ determined from our database.

- Figure 2b shows total enthalpy as a function of temperature for two alloys, namely, $Al_{70}Ce_{30}$ and $Al_{40}Ce_{60}$. All the first-order phase transitions can be recognized by a discontinuity of the total enthalpy at its particular transition temperature, and is indicated by a vertical dotted line on the figure. The calculated enthalpy change for the $\alpha/\beta AlCe_3$ polymorphous phase transformation in $Al_{40}Ce_{60}$ is ~0.1 kJ/mole of atoms. This calculated value is very reasonable in the sense that this transformation was not detected by DSC, probably because the enthalpy change is so small. Quenching experiments showed that the kinetics are actually very fast for the $\alpha/\beta AlCe_3$ transformation. For all the invariant reactions, it is further found that the calculated enthalpy change is in very good agreement with those obtained from DTA measurements (obtained by the integrated area under the peak in the DTA plot), given the fact that the error in DTA enthalpy measurement is typically ~20%. Similar conclusions can be drawn for alloy $Al_{40}Ce_{60}$ and other Al-Ce alloys.

d. Re-assessment of the Al-Ce-Co Ternary Phase Diagram

Introduction

Along with identifying and designing a new amorphous metal coating, the thermodynamics and a usable CALPHAD database was a deliverable. The phase equilibria of the Al-rich Al-Ce-Co ternary system using a range of experimental techniques including melt spinning, transmission electron microscopy (TEM), electron probe microanalysis (EPMA), X-ray diffraction (XRD) and differential thermal analysis (DTA). The glass formation range (GFR) in the Al-rich corner is determined, and a partial 500 °C isotherm is constructed. Three stable ternary phases are confirmed, namely, Al_8CeCo_2, Al_4CeCo and AlCeCo, while a metastable phase, Al_5CeCo_2, was discovered. Also confirmed are our previous results [detailed above for Al-Ce] that a polymorphous transformation of $\alpha/\beta Al_3Ce$ exists in the Al-Ce binary system, and that the transformation between $Al_{11}Ce_3$.oI28 and Al_4Ce.tI10 can't be polymorphous. Further, a series of DTA measurements were performed with repeated heating/cooling cycles to obtain accurate phase transition temperatures. The equilibrium and metastable phases identified by the present and earlier reported experiments, together with many hypothetical ternary compounds, are further studied by first-principles (FP) calculations. Based on new experimental data and FP calculations, the thermodynamics of the Al-rich Al-Co-Ce system is optimized using the CALPHAD method. Model calculated phase equilibria and phase boundaries conform with the present experimental results. Disagreement with other reports concerning the Ce-Co and Co-rich Al-Ce-Co phase diagrams are addressed. Application to glass formation is discussed in light of present studies.

Experimental Procedures

One hundred and thirty four alloys, many of which were used to identify the GFR as marked in Fig. 3, were synthesized through arc-melting pieces of Al (99.999% purity), Co (99.9995%) and Ce (99.9%) on a water-cooled copper hearth using a tungsten electrode in a partial argon atmosphere. Individual ingots were melted 5 to 6 times in total; each time the ingot was flipped over prior to melting to improve homogeneity. The weight loss after melting was found to be less than 1.0 wt.%. Oxides formed on the ingot surface during arc-melting were ground away using SiC paper, and then the sample surfaces were cleaned with acetone followed by methanol. Ingots free of surface contaminants were then cut into pieces and inserted into a quartz crucible with an inner diameter of 6 mm and placed inside a single-wheel melt-spinner. All melting and casting of the alloys was done in a He atmosphere to prevent oxidization and improve heat conduction. The wheel was operated at a constant circumferential speed of 48 m/s. Following melt-spinning, several experimental techniques including DSC, XRD and TEM were used to check whether the as-spun ribbon was amorphous, partial amorphous or crystalline. This resulted in the glass formation range (GFR) as shown in Fig. 3, where earlier reported results [**Error! Reference source not found.,Error! Reference source not found.**] have also been included.

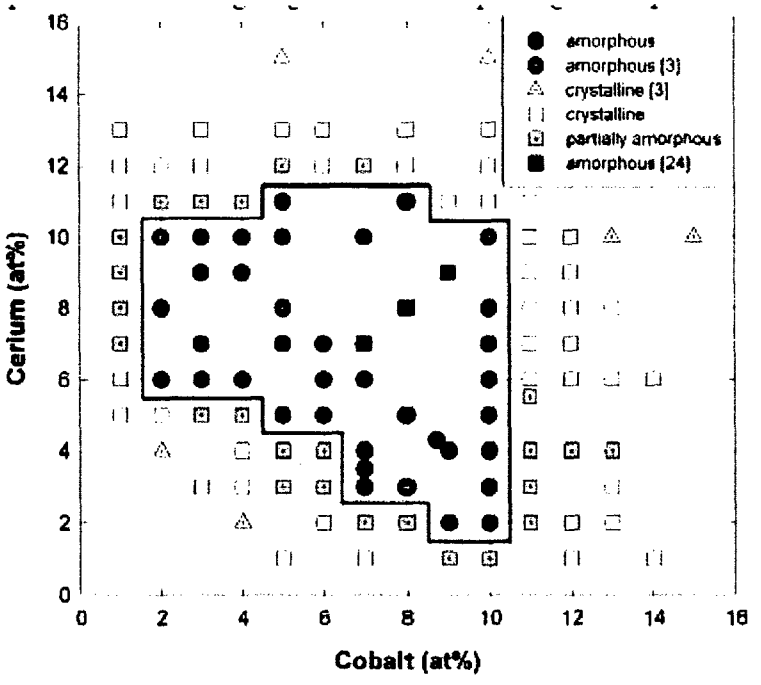

Figure 3. The glass forming range (GFR) determined in the Al-rich Al-Ce-Co system, whose border is marked by the solid lines. The early reported work from Refs. [**Error! Reference source not found.,Error! Reference source not found.**] is also shown. The as-quenched alloys were synthesized with a constant circumferential speed of 48 m/s using single-wheel melt spinning technique.

Thirty-three alloys were selected for the partial 500 °C isotherm study. The temperature of 500 °C was chosen to avoid active reaction of the samples with the quartz tube, because the Al-rich Al-Ce-Co alloys melts at ~640 °C. Small ingots were cut from the master ingot and sealed inside quartz tubes under a partial pressure of argon to prevent oxidization, then annealed at 500 °C for 3 weeks. The annealed samples were quenched into cold water, ground with a series of SiC papers, polished using diamond paste, and finally examined in a LaB_6 and an FEG-scanning electron microscopes (SEM) for microstructure analysis. Electron Probe Microanalysis (EPMA), using pure element samples as external standards, was employed to perform all chemical analysis. The accuracy of the EPMA measurement in this study is about 1 at%.

Thirty-one alloy compositions within the GFR were initially melt spun into amorphous ribbons and then annealed in quartz tubing for a variety of times to check whether the equilibrium state was appropriately achieved for each composition. Annealed ribbons were analyzed with XRD using Cu-K_α radiation. Specimens for TEM were made by electropolishing melt-spun and annealed ribbons in a solution of 1 part nitric acid to 3.5 parts methanol at 6-10 volts and -23 °C. These thin foils were first examined in a conventional TEM operating at 200 kV, where the phases were identified using selected area diffraction (SAD). The chemical composition of the matrix and compound particles was then determined using quantitative energy-dispersive x-ray spectroscopy (EDS) in a field-emission gun TEM (FEG-TEM) also operating at 200 kV, in which a low-

background specimen holder was employed. Spectra were collected from probes placed on individual particles. The integrated intensities I_{Al}, I_{Co} and I_{Ce} from the Al $K\alpha_{1,2}$, Co $K\alpha_1$ and Ce $L\alpha_1$ peaks, respectively in each spectrum were used to calculate the phase composition using the Cliff-Lorimer equations.

DTA measurements were performed on all the 134 arc-melted samples in a Perkin-Elmer DTA7 at a heating/cooling rate of 10 K/min up to 1400 °C in a dynamic argon environment. For each sample the heating/cooling cycle was repeated at least twice to ensure the reproducibility of all the thermal events. The DTA was calibrated with high-purity aluminum and gold with an uncertainty of ±1 °C on the measured melting points after calibration. All the thermal events during the heating cycles are characterized by the heating onset temperature. The onset is defined by finding the intersection of the baseline and the extrapolated tangent at the inflection point of the leading edge of the peak. However, in certain cases, some thermal events were too weak to give a well-defined onset on heating, but still did show a well-defined cooling onset. In such cases, the peak temperature observed on heating is used.

Experimental Results for Al-Co-Ce

The GFR determined in this study is shown in Fig. 3, together with some earlier reported data. Alloys with compositions of $Al_{99-y}Ce_yCo_1$ (y=8-10, all the composition are in atomic percent unless otherwise specified) were found to be partially amorphous in this study. The GFR determined in this report is referred to the specific wheel speed of 48 m/s used. As-spun $Al_{90}Ce_3Co_7$ is truly amorphous since no crystalline phase(s) was detected in the dark-field image and the selected area electron diffraction pattern. Examination shows that the amorphous alloy completely decomposes into equilibrium phases of fcc-Al, Al_4Ce and Al_9Co_2 (Pearson Symbol mP22) after annealing at 500 °C for 24 h.

The experimentally constructed Al-Ce-Co equilibrium 500 °C isotherm is shown in Fig. 4. There are three stoichiometric compounds confirmed, namely, Al_8CeCo_2.oP44 (τ_1), Al_4CeCo.oP12 (τ_2), and AlCeCo.mC12 (τ_3). A metastable stoichiometric compound Al_5CeCo_2 (it is proposed to be isostructural with Al_5CeNi_2.oI16, based on current FP calculations) was also discovered in the present study (it is not shown in the equilibrium isotherm to avoid confusion). It was found that the Co solubility in the $Al_{11}Ce_3$.oI28 and αAl_3Ce.hP12 binary compounds is negligible, in agreement with the observation made by Zarechnyul *et al.* [3]. The same is true for Ce solubility in Al-Co binary compounds. However, the Co solubility in the Al_2Ce.cF24 was found to be ~2.5 at% Co at 500 °C, while the previously reported Co solubility is ~10 at% Co [3]. The solubility limit of Co in Al_2Ce has significant influence on the phase relations and phase tie triangles in its vicinity. Details of the experimental results are presented below.

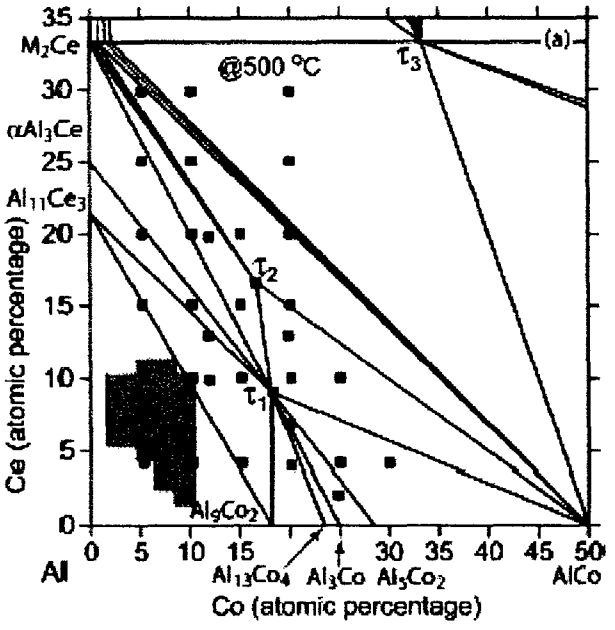

Figure 4. The Al-rich Al-Ce-Co 500 °C isotherm determined in this study. Samples chosen for equilibrium study are marked as filled squares. The shaded area highlights the observed GFR.

The EDX analysis on alloy $Al_{65}Ce_{25}Co_{10}$ demonstrates that the Co solubility in M_2Ce.cF24 is essentially zero, contradicting Zarechnyul's report of ~5 at% [3]. It is concluded that Zarechnyul *et al.* [3] overestimated the Co solubility in M_2Ce.cF24. The as-annealed microstructure contains a large volume fraction of M_2Ce.cF24 (white), a slightly smaller volume fraction of Al_4CeCo.oC20, and a very small volume fraction of AlCo.cI2. The coarse primary M_2Ce and τ_2 develop above 1155 °C at which the invariant reaction U_{11} occurs, i.e. $L + \tau_2 \leftrightarrow AlCo + M_2Ce$ (see Table 6), during solidification from arc-melting. The fine eutectic-like features in the microstructure may be due to the very small mole fraction of τ_2 phase involved in the U_{11} reaction, thus this reaction can be approximated as "quasi-eutectic". The DTA thermal events observed are marked in the calculated isopleth with fixed Co contents of 10 at.%. The continuous changes in mole fractions of the equilibrium phases at temperatures below 1155 °C are a result of the gradual changes in the Co solubility in M_2Ce and in the compositional homogeneity range of AlCo, which both vary as a function of temperature especially for the AlCo phase. Note the Al_5CeCo_2.oI16 (it is observed in alloy $Al_{68}Ce_{13}Co_{20}$) is *not* observed in this sample, indicating that it is not an equilibrium phase at 500 °C.

The overall DTA plots for most of the alloys are complex, which often consist of several thermal events, for example, in alloys $Al_{75}Ce_{20}Co_5$ and $Al_{70}Ce_{20}Co_{10}$. It is not immediately possible to identify which phases are involved in each thermal event if only the DTA plot is available. However, this can be done fairly easily once the thermodynamic descriptions for the system are determined. Based on the thermodynamic

database developed in this study, the 1st thermal event with an onset temperature of ~961 °C observed in $Al_{75}Ce_{20}Co_5$ during heating segment is concluded to reflect the allotropic transformation of $\alpha/\beta Al_3Ce$, which was recently identified by in our Al-Ce binary phase diagram study (see above). This phase transition is also observed in alloy $Al_{75}Ce_{15}Co_{10}$ whose 1st thermal event has a peak temperature of 970 °C, further confirming the existence of allotropes of $\alpha/\beta Al_3Ce$. The 1st heating peak in alloy $Al_{70}Ce_{20}Co_{10}$ occurs at 1089 °C, and this event is also observed in several other alloys whose compositions lie within the tie triangles of αAl_3Ce-τ_1-M_2Ce and αAl_3Ce-τ_1-$Al_{11}Ce_3$. Thus it is concluded that this event must belong to an invariant reaction, and the current thermodynamic calculations actually predicts that it results from the phase relation change, namely, $\beta Al_3Ce + \tau_2 \leftrightarrow M_2Ce + \tau_1$ (see U6 in Table 6).

e. First-Principles Energy Calculation

- The Al-Ce-Co ternary system and its constituent binary systems are further analyzed using first-principles calculations that employ the plane-wave code VASP [4,5], which solves for the electronic band structure using electronic density functional theory. Because of the presence of the rare-earth element Ce, projector augmented wave (PAW) potentials are used as supplied with VASP [6]. These are similar to pseudopotentials except that the core levels are solved simultaneously with the valence electrons. Two choices are available for the Ce potential, a "standard" version in which the entire set of f-levels is treated within the valence band, and a trivalent version (named "Ce_3") in which some f-electrons are kept frozen in the core. Since the trivalent Ce_3 potential incorrectly predicts a positive enthalpy of formation (ΔH_f =+5.7 kJ/mol) for the stable C15-$CeCo_2$.cF24 compound, the standard Ce potential was used throughout the Al-Ce-Co system. The exchange-correlation functional used is the Perdew-Burke-Ernzerhof (PBE) gradient approximation. Reciprocal space (k-point) meshes are increased to achieve convergence to a precision of 1 meV/atom. All structures are fully relaxed (both lattice parameters and atomic coordinates) until, again, energies converge to a precision of 1 meV/ atom. The plane-wave energy cutoff was held constant at 300 eV, the default for the Ce potential. All calculations were performed using the ''Accurate'' setting which avoids wrap-around errors. Spin polarization was considered in all calculations other than pure Al.
- To obtain T=0 K enthalpy of formation values ΔH_f, a composition-weighted average of the pure elemental cohesive energies is subtracted from the cohesive energy of a given compound. The resulting energy is an "enthalpy" because its volume was relaxed (at zero pressure). It is at T=0K because its atomic coordinates are relaxed. Stable structures are identified as the vertices of the convex hull of a scatter plot of ΔH_f *vs.* composition. Points above the convex hull represent thermodynamically unstable structures, though they may be metastable or high temperature stable in some cases. All the structures examined were mechanically stable, in the sense that atomic displacements during relaxation were generally small (less than 0.03 nm at worst). For each binary, and the ternary, however, disagreements are found between the calculated phase diagrams and the experimentally established ones. Some of the disagreements probably reflect poor approximations made in the calculated cohesive energies, for example the use of non-relativistic quantum mechanics. Other, stronger disagreements require further study, both theoretical and experimental. The binary

diagrams are fairly well reproduced, but the agreement in the case of Al-Ce is less impressive than in other studies of non-RE containing alloys. The binary Al-Ce phase diagram was already discussed above.

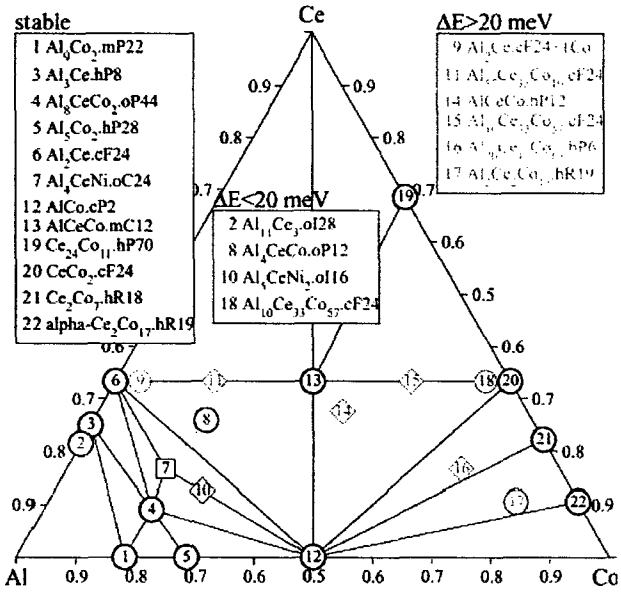

Figure 5. Convex hull and metastable/unstable phases of the Al-Co system. The plotting symbol notation is: heavy circles for known stable binary phases; light circles for known high temperature phases; diamonds for known metastable phases; triangles for known high pressure phases; squares for imperfectly known, unknown or hypothetical structures. Tie-lines run along convex hull edges, joining low enthalpy structures at the vertices of the convex hull.

- Binary Al-Co exhibits several interesting structures in the Al-rich region. Experimental investigation of the phase diagram is ongoing, with the greatest uncertainty in the composition range $Al_{13}Co_4$-Al_3Co, where a variety of "quasicrystal approximant" structures are observed. Recalling the thermodynamic rule that multiple phases of nearly identical composition should not coexist over a wide temperature range, it is evident that not all reported structures should meet the convex hull. Additionally, certain of the crystal structures (e.g. $Al_{13}Co_4$.mC102) exhibit partial occupancy, which should not be present in a low temperature phase. The well-known stable phases Al_9Co_2.mP22 and Al_5Co_2.hP28 are found on either side of this problematic composition range.
- Ce-Co yields excellent agreement with the established phase diagram provided the standard Ce potential is used, as opposed to trivalent Ce_3 in which the f-level is kept frozen. The calculated enthalpy of formation is listed in Table 1. The calculated lattice parameters are listed in Table 2, and they agree with experimentally determined values. The cluster of reported stable phases from $CeCo_3$ to Ce_5Co_{19} is

thermodynamically implausible, and the present calculation is more consistent with a single low temperature phase (possibly Ce_2Co_7) together with two high temperature or metastable phases on either side of it. The hP6 structure of $CeCo_5$ is properly identified as a high temperature phase.

- The ternary diagram is well reproduced. The enthalpy of formation data set is listed in Table 3. The calculated lattice parameters for stable and hypothetical compounds are listed in Table 4, and they closely agree with those determined by experiments. The known stable phases that are confirmed are: Al_8CeCo_2.oP44, which is recognized as a decagonal quasicrystal approximant, and AlCeCo.mC12. The alternate reported structure AlCeCo.hP12 is high in energy by 144 meV/atom and most likely is metastable. At the composition of Al_4CeCo.oP12, a different structure was found, namely, Al_4CeNi.oC24 lower in energy by 5 meV/atom. Since it was not possible to perfectly reproduce the Al-Ce binary diagram, it is difficult to assert which structure is the true low energy state. Rather, further experimental and theoretical effort is required to resolve the matter. Finally, it was found that Al_5CeNi_2.oI16 has a low energy of only 15 meV/atom, indicating a possible metastable or high temperature phase. This is more likely the structure for a metastable phase obtained in the experimental portion of this work.

f. Thermodynamic Models

- The Gibbs free energy of individual phases is described by sublattice models and is defined relative to the Standard Element Reference (SER), i.e., the enthalpies of the pure elements in their defined reference phase at 298.15K and 1 atm. All the disordered solutions including the liquid are modeled with a single sublattice, with the Gibbs energy expressed as for a ternary complete disordered solution (e.g., liquid) with components Al, Ce and Co:

$$G^{\phi} = \sum_{i=Al,Ce,Co} x_i {}^{o}G_i^{\phi} + RT \sum_{i=Al,Ce,Co} x_i \ln x_i + {}^{ex}G^{\phi}_{Al,Ce,Co} + {}^{mag}G^{\phi}_{Al,Ce,Co} \qquad (1)$$

where ${}^{o}G_i^{\phi}$ is the molar Gibbs energy of the pure element i in the structure of phase ϕ in the non- magnetic state, taken from the values tabulated by Dinsdale [2], and x_i is the mole fraction of each component.

- The excess Gibbs energy, ${}^{ex}G^{\phi}_{Al,Ce,Co}$, is expressed in Redlich-Kister-Muggianu polynomial form:

$$\begin{aligned} {}^{ex}G^{\phi}_{Al,Ce,Co} &= x_{Al}x_{Ce}\sum_{k=0}^{k} {}^{k}L^{\phi}_{Al,Ce}(x_{Al}-x_{Ce})^k + x_{Ce}x_{Co}\sum_{k=0}^{k} {}^{k}L^{\phi}_{Ce,Co}(x_{Ce}-x_{Co})^k \\ &+ x_{Al}x_{Co}\sum_{k=0}^{k} {}^{k}L^{\phi}_{Al,Co}(x_{Al}-x_{Co})^k + x_{Al}x_{Ce}x_{Co}\left({}^{0}L^{\phi}_{Al,Ce,Co}x_{Al} + {}^{1}L^{\phi}_{Al,Ce,Co}x_{Ce} + {}^{2}L^{\phi}_{Al,Ce,Co}x_{Co}\right) \end{aligned} \qquad (2)$$

where ${}^{k}L^{\phi}_{i,j}$ are the binary interaction parameters (k is an integer), and are taken directly from individual assessed edge binary databases.

- ${}^{k}L^{\phi}_{Al,Ce,Co}$ are the ternary interaction parameters, which are to be optimized in this study. Both the binary and ternary interaction parameters have the following general form:

$$^{k}L^{\phi} = {}^{k}a + {}^{k}b\,T + {}^{k}c\,T\ln(T) + {}^{k}d\,T^{2} + {}^{k}e\,T^{-1} + {}^{k}f\,T^{-3} \quad (3)$$

- The magnetic contribution to the Gibbs energy ($^{mag}G^{\phi}$) for all the ternary compound phases in the Al-rich corner was set to zero because they all order at very low temperatures less than 100 K. It is only significant for the Ce-Co binary and Co-rich ternary alloys, neither of which are the focus of this study.
- Stoichiometric compounds are modeled as if the enthalpy and entropy are constants and only one element occupies one sublattice. For example, the Gibbs free energy for a ternary stoichiometric compound $Al_xCe_yCo_z$ (x,y,z denotes the chemical formula) is modeled as (J/mole of total atoms):

$$G^{Al_xCe_yCo_z} = \frac{x}{x+y+z}{}^{o}G_{Al}^{fcc} + \frac{y}{x+y+z}{}^{o}G_{Ce}^{fcc} + \frac{z}{x+y+z}{}^{o}G_{Co}^{hcp} + a + bT \quad (4)$$

where a, b are parameters to be determined, namely, the enthalpies of formation and entropies of formation for the compound $G^{Al_xCe_yCo_z}$ respectively. ${}^{o}G_{Al}^{fcc}$, ${}^{o}G_{Ce}^{fcc}$ and ${}^{o}G_{Co}^{hcp}$ are the Gibbs energies of the pure components, Al, Ce and Co with respect to its enthalpies in the SER state respectively. Note that, both Ce and Co have several allotropes in the solid state. At the SER state, both Al and Ce have a crystal structure of fcc, while Co has a crystal structure of hcp.

- The Gibbs energy of those binary $(Al,Co)_xCe_y$ compound phases that have ternary solubility (i.e., Al and Co substitute for each other in ternary phase) is expressed as:

$$G^{(Al,Co)_xCe_y} = \sum_{i=Al,Co} y_i\,{}^{o}G_{i:Ce}^{(Al,Co)_xCe_y} + \frac{x}{x+y}RT\sum_{i=Al,Co} y_i \ln y_i + y_{Al}y_{Co}\sum_{k=0}^{k} {}^{k}L_{Al,Co:Ce}^{(Al,Co)_xCe_y}(y_{Al}-y_{Co})^{k} \quad (5)$$

where ${}^{k}L_{Al,Co:Ce}^{(Al,Co)_xCe_y}$ are the interaction parameters and have a form in Eq. (3). ${}^{o}G_{Al:Ce}^{(Al,Co)_xCe_y}$ and ${}^{o}G_{Co:Ce}^{(Al,Co)_xCe_y}$ represent the Gibbs energy of the compound Al_xCe_y and Co_xCe_y respectively. These two expressions were obtained from the binary assessments without change during optimization. Only the interaction term ${}^{k}L_{Al,Co:Ce}^{(Al,Co)_xCe_y}$ which contains a series of parameters *a*, *b*, *c*...(see Eq. (3)) was optimized in this study to obtain best fitting between the calculated phase diagram and experimental data achieved in this study and those assessed in Refs. [3]. It was found in Ref. [3] and the present study that in the Al-rich corner only Al_2Ce.cF24 extends into ternary solubility, but $CeCo_2$.cF24 also has significant ternary solubility [3]. Therefore, both are treated as one ternary phase M_2Ce (M=Al, Co) with a two-sublattice model of $(Al,Co)_2(Ce)_1$. This choice makes physical sense because (1) both Al_2Ce and $CeCo_2$ are A_2B type Laves phases (prototype Cu_2Mg, Pearson symbol cF24), and their lattices consist of only two crystallographic sites (A atoms occupy Wyckoff sites 16d and B atoms occupy 8a) and (2) substitution between Al and Co in the 16d site is energetically favored and is confirmed while substitution between Al/Co and Ce in the 8a site is not found in Ref. [3] and this study.
- The Al-Ce-Co ternary phase diagram assessed in Ref. [7] is mainly based on the work by Zarechnyul *et al.* [3] in 1980, who constructed the partial 600 °C isotherm in the range of 0-33.3 at.% Ce. The ternary stoichiometric compounds assessed in Ref. [7] include Al_8CeCo_2.oP44 [3], Al_4CeCo.oP12 [3], $Al_2Ce_2Co_{15}$.hR19 [8], $Al_4Ce_3Co_3$.oP [9], AlCeCo.hP12 [10] and AlCeCo.mC12 [11]. In addition, Zarechnyul *et al.* [3]

found three binary compounds that show ternary solubility between Al and Co atoms at 600 °C. Specifically, Co solubility in Al_2Ce.cF24 is ~10 at% Co, Al solubility in $CeCo_2$.cF24 is ~10 at% Al, and Al solubility in $CeCo_5$.hP6 is ~20 at% Al. Note that in the assessed Al-Ce-Co ternary phase diagram [7], the $CeCo_5$.hP6 binary compound is treated as unstable, and the Ce_5Co_{19}.hR24 binary compound is assigned with a solubility of ~20 at% Al instead. Since the metastability of the $CeCo_5$.hP6 phase at low temperatures in the Ce-Co binary system is not convincingly established in experiments, its decomposition mechanism (i.e., by spinodal or eutectoid decomposition) remains controversial.

g. Modeling Results

- The Thermo-Calc® package [12] is used to optimize the ternary system using the PARROT module. The optimization is based on the experimental data from this study, such as DTA measurements, phase relationships, phase compositions and phase crystal structures. It is usually difficult to obtain the liquidus temperatures accurately and, furthermore, rare earth elements are susceptible to oxidation. Thus the liquidus data are assigned with lower weight during optimization. In contrast, the invariant reaction temperatures are seen to be reproducible and thus more reliable, and they are set with higher weight during the global optimization. The thermodynamic parameters obtained in this study are listed in Table 5. As an example of the database, Fig. 6 shows the calculated partial isopleths (vertical sections) through the Al-Co-Ce phase diagram at fixed Ce contents of 4, 10, 15 and 20 at.%. These figures illustrate how alloy compositions and temperature affect the equilibrium phase diagrams and demonstrate that the phase transformations during equilibrium solidification for compositions within the GFR are complicated. Other calculations show that the agreement is excellent between calculated phase transition temperatures and experimental DTA data. For other compositions whose DTA measurements were performed in this study, good agreement is also obtained.
- Isothermal sections at any temperature, e.g., 1000 and 1100 °C can be calculated from thermodynamic descriptions obtained in the present work. These thermodynamic descriptions predict that a reaction of $\beta Al_3Ce + \tau_2 \leftrightarrow M_2Ce + \tau_1$ (see Table 6) occurs at ~1090 °C, and consequently the composition triangle relationship among τ_1, τ_2, βAl_3Ce and M_2Ce changes when the temperature is raised from 1000 to 1100 °C. This is not common because there is no additional solid phase formation, and no liquid is yet formed at these temperatures for both composition triangles. Surprisingly, the predicted invariant temperature for the reaction of $\beta Al_3Ce + \tau_2 \leftrightarrow M_2Ce + \tau_1$ agrees extremely well with the DTA thermal events at ~1089 °C recorded for alloys $Al_{70}Ce_{25}Co_5$ and $Al_{70}Ce_{20}Co_{10}$ during heating segment. This phase transition was not detected during DTA measurements in alloys with lower Ce contents such as $Al_{70}Ce_{15}Co_{15}$ because the amount of heat associated for this transition is lower for alloys of lower Ce contents. The calculated enthalpy change for this reaction based on current thermodynamic descriptions is ~200 J/mol for $Al_{70}Ce_{15}Co_{15}$, and ~400 J/mol for $Al_{70}Ce_{20}Co_{10}$. Again, this further demonstrates that current thermodynamic descriptions are accurate.

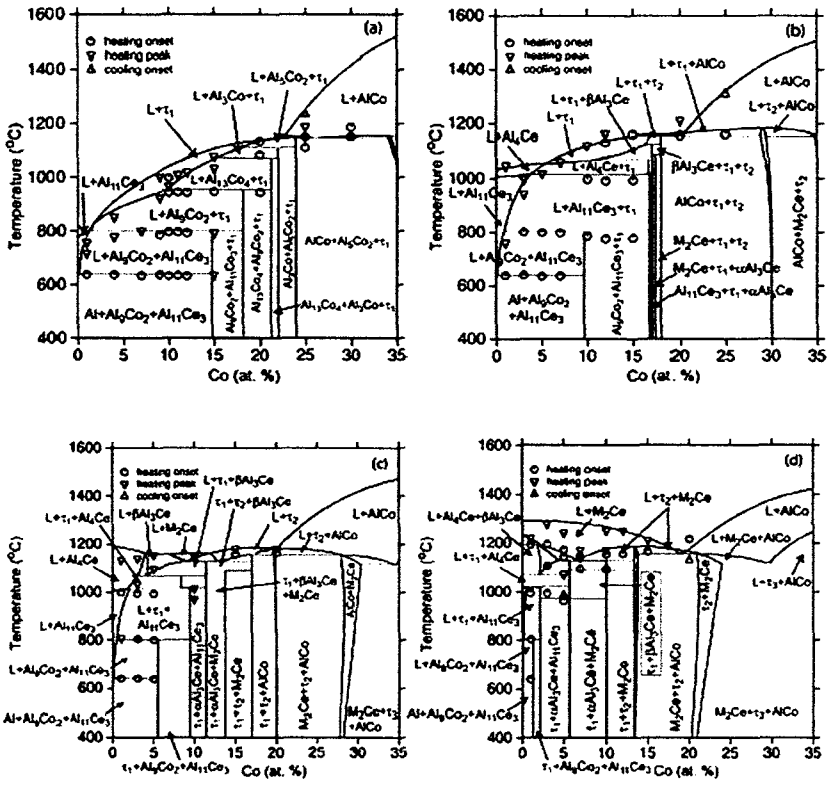

Figure 6. Calculated isopleth plot of (a) Al-4Ce-Co, (b) Al-10Ce-Co, (c) Al-15Ce-Co and (d) Al-20Ce-Co from the thermodynamic descriptions obtained in the present work.

- Calculated liquidus surface projection with liquidus isocontours reveal the univariant equilibria between the liquid and two solid phases, and an invariant reaction point where four phases co-exist at equilibrium. All the invariant reactions involving the liquid are listed in Table 6. The majority of the predicted invariant reaction temperatures agree exceptionally well with DTA measurements except for a few reactions including U_3, U_8 and U_7 whose agreement is imperfect. For reaction U_3 ($Al_4Ce + \tau_1 \leftrightarrow L + Al_{11}Ce_3$), the current model slightly overestimated the reaction temperature but is still acceptable. This is thought due to possible stabilization of the Al_4Ce.tI10 by impurity or minor solute effects. In order to greatly improve agreement with measured DTA data, the current authors then take a sublattice model of $(Al,Co)_4(Ce)_1$ to model the Al_4Ce phase, i.e. to allow Co atoms to mix with Al atoms. The resulting optimization finds that the agreement of U_3 with experiments cannot be improved substantially unless a significant Co solubility (≥10 at.%) in Al_4Ce is used, which, however, contradicts the present FP prediction. Therefore, this treatment is not progressed further and is not presented here. For reactions U_8 ($L + \tau_2 \leftrightarrow \beta Al_3Ce + \tau_1$) and U_9 ($L + M_2Ce \leftrightarrow \tau_2 + \beta Al_3Ce$), their reaction temperature and liquid composition are so close to each other that their thermal events overlap during DTA

measurements. This makes precise determination of the onset temperature for each reaction difficult. For reaction U_7 ($L + Al_5Co_2 \leftrightarrow Al_3Co + \tau_1$), the uncertainty in reaching equilibrium state for Al_3Co and Al_5Co_2 may be responsible for the imperfect agreement on the reaction temperature with DTA measurement.

h. Applications for GFA

- The liquidus surface projection showed that increasing Ce or Co contents in the alloy monotonically raises the liquidus temperature (beyond the ternary eutectic point E_1), and the compositions within the GFR have liquidus temperatures that lie between ~900 and ~1125 °C. The ternary τ_1 compound has the broadest primary compositional field in the Al-rich corner so it is mainly responsible for the liquidus temperature of alloys within the GFR, and thus impacts the glass formation the most. On the other hand, the ternary τ_2 compound has less impact on the glass formation, and the primary τ_2 phase field has a nearly plateau liquidus temperature of 1175 °C. Further, the observed GFR is very narrow, and is mainly limited by the wide phase fields of the primary M_2Ce and AlCo, which both are very stable in the edge binaries and the ternary and impact the ternary phase equilibria substantially. In order to improve the GFA and broaden the GFR in the Al-Ce-Co system, an alloying strategy could be sought to lower the melting point of the ternary τ_1 compound and destabilize M_2Ce and AlCo solution compounds as one effective measure.
- In this report we also showed that (1) a polymorphous transition of $\beta Al_3Ce \leftrightarrow \alpha Al_3Ce$ occurs at ~973 °C and (2) a catetectic $Al_4Ce \leftrightarrow L + Al_{11}Ce_3$ occurs at 1006 °C in the Al-Ce binary. For the Al-Ce-Co ternary, the $\alpha/\beta Al_3Ce$ transition temperature measured in this study is found to fluctuate slightly, i.e., 961-970 °C, but fairly close to that in the binary i.e., ~973 °C and the first thermal event marked for alloys $Al_{75}Ce_{20}Co_5$ and $Al_{75}Ce_{15}Co_{10}$. Therefore, it is further confirmed that the polymorphism of $\alpha/\beta Al_3Ce$ exists in the Al-Ce system. The slight decrease in the $\alpha/\beta Al_3Ce$ transition temperature in the Al-Ce-Co ternary may be due to the possibility of small Co solid solution in βAl_3Ce or other unidentified reasons. Due to lack of direct measurement of this Co solubility data, this possibility is not considered in the current thermodynamics modeling. On the other hand, the binary catetectic reaction of $Al_4Ce \leftrightarrow L + Al_{11}Ce_3$ becomes the reaction of $Al_4Ce + \tau_1 \leftrightarrow L + Al_{11}Ce_3$ in the Al-Ce-Co ternary that occurs at 996±6°C. Such a change in the reaction temperature provides further experimental support that the phase transition between Al_4Ce and $Al_{11}Ce_3$ cannot be polymorphous.
- What is attractive using CALPHAD modeling is that only some critical experiments are required, including one complete isotherm, a set of reasonably sufficient data of phase transition temperature as a function of composition and temperature, and some reliable thermochemistry data, such as, enthalpy of formation either from experiments or FP calculations.
- The successful production of multicomponent bulk metallic glasses makes thermodynamic modeling even more desirous. Unfortunately, the unusual combination of elements makes it unlikely that the proper set of information exists. Successful modeling of thermodynamics requires an extensive body of reliable phase equilibria and thermochemistry data. However, even today, only a small fraction of

ternary and a vanishingly small fraction of quaternary and higher order diagrams have been reported. Although a large fraction of binary diagrams have been determined, many are still incomplete and some are even incorrect. At the present stage, FP calculation is still not able to fully calculate the free energy of a phase at finite and high temperatures. Meanwhile, the CALPHAD method alone cannot predict any new phase in a system without giving an appropriate energy description in advance. Therefore, experiments remain the most important and reliable means to determine an unknown phase diagram.

- However, experimental determination of an unknown multicomponent system can be very challenging and exhaustive because a lot of information including phase chemistry and crystal structure (e.g., atomic positions in a crystal), phase boundaries (e.g., solidus and solvus), mechanisms of phase transitions, etc. all need to be quantified. This inevitably involves a range of combined techniques, such as XRD, EPMA, TEM and DTA. All the experiments are susceptible to sample purity, equilibration condition, operators' skills, and instrument sensitivity, etc, which all have significant impact on the quality of the phase diagram studied.
- The thermodynamics of Al-Ce-Co in the present work are determined through the classical CALPHAD approach, and the values of the enthalpies of formation of the ternary compounds (see Table 5) through the CALPHAD optimization scheme are found to be comparable with those from FP calculations (see Table 1). The CALPHAD-modeled values of enthalpies of formation are consistently more negative than from FP calculations by ~6 kJ/moles. This report demonstrates that FP calculations may have underestimated the lattice stability of alloy compounds associating with Al and rare earth elements. For example, it was found that the enthalpies of formation of Al-rich Al-Ce compounds measured by experiments are all more negative than from FP calculation by 4-6 kJ/moles. This is due to the imperfect treatment of rare- earth atoms by current calculation methods. Some specific shortcomings are: (1) use of an approximate exchange-correlation potential while tightly bound f-electrons may exhibit strong correlations; (2) use of non-relativistic equations for high atomic number elements; (3) assumption of collinear magnetism while rare-earths often exhibit noncollinear magnetism. Nonetheless, the values of enthalpy of formation data for the Al-Ce-Co compounds are shown to be sufficiently accurate, at least as a starting value for the optimization process to enhance CALPHAD efficiency and accuracy.

References

1. Cacciamani G, Ferro R. CALPHAD 2001;25:583.
2. Dinsdale AT. CALPHAD 1991;15:317.
3. Zarechnyuk OS, Rykhal ZM, Korin VV. Dopo. Akad. Nauk Ukr. A Fiziko.-Mate. Tekh Nauki 1980;42:86.
4. Kresse G, Hafner J. Phys. Rev. B 1993;47:558.
5. Kresse G, Furthmuller J. Phys. Rev. B 1996;54:11169.
6. Kresse G, Joubert D. Phys. Rev. B 1999;59:1758.
7. Villars P, Prince A, Okamoto H. Handbook of ternary alloy phase diagrams, 1995, vol. 3, ASM International, Materials Park, OH 44073.
8. Zarechnyuk OS, Kripyakevich PI. Soviet Phys-Crystall. 1962;7:436.

9. Cordier G, Dorsam G, Kniep R. J. Magn. Magn. Mater. 1988;76:653.
10. Mansey RC, Raynor GV, Harris IR. J. Less-Comm Metals. 1968;14:337.
11. Grin Yu N, Sichevich OM, Bruskov VA, Rykhal RM, Yarmolyuk Ya P. Soviet Phys-Crystall. 1983;28:346.
12. Sundman B, Jansson B, Andersson JO. CALPHAD 1985;9:153.

Table 1: Enthalpies of formation of stable compound phases, $\square H_f$, (kJ/mol of atoms) at T=0 K for Ce-Co system calculated by FP.

Compound	**Pearson symbol-Prototype**	**ΔH_f**	**Comments**
$Ce_{24}Co_{11}$	hP70-$Ce_{24}Co_{11}$	-13.46	Stable
$CeCo_2$	cF24-Cu_2Mg	-24.09	Stable
αCe_2Co_{17}	hR19-Th_2Zn_{17}	-8.23	Low-temperature
βCe_2Co_{17}	hP38-Th_2Ni_{17}	-7.75	High-temperature
Ce_5Co_{19}	hR24-Ce_5Co_{19}	-15.2	Stable
$CeCo_3$	hR12-Be_3Nb	-17.44	Stable
$CeCo_5$	hP6-$CaCu_5$	-10.41	High-temperature
Ce_2Co_7	hR18-Co_7Er_2	-16.67	Stable

Table 2: A comparison of lattice parameters of Ce-Co compounds

Phase	Structure (Pearson symbol)	Lattice parameters *ab initio* (this work)		Experiment [Error! Reference source not found.]	
		a	*c*	*a*	*c*
$Ce_{24}Co_{11}$	hP70	9.351	20.814	9.587	21.825
$CeCo_2$	cF24	7.058		7.160	
$\square Ce_2Co_{17}$	hR19	8.318	12.119	8.378	12.206
$\square Ce_2Co_{17}$	hP38	8.315	8.080	8.378	8.1317
Ce_5Co_{19}	hR24	4.872	49.148	4.948	48.7434
$CeCo_3$	hR12	4.887	24.900	4.964	24.814
$CeCo_5$	hP6	4.876	4.022	4.920	4.029
Ce_2Co_7	hR18	4.882	37.103	4.940	36.52

Table 3: Enthalpies of formation of stable compound phases, ΔH_f, (kJ/mol of atoms) at T=0 K for Al-Ce-Co system calculated by FP.

Compound	Pearson symbol-prototype	ΔH_f	Comments
Al_8CeCo_2 (τ_1)	oP44-Al_8CeCo_2	-46.26	Stable
Al_4CeCo (τ_2)	oC24-Al_4CeNi	-48.12	Stable
AlCeCo (τ_3)	mC12-AlCeCo	-50.51	Stable
Al_4CeCo	oP12-Al_4CeCo	-47.63	Hypothetical
AlCeCo	hP9-AlNdNi	-46.34	Hypothetical
AlCeCo	hP12-AlCeCo	-36.61	Hypothetical
Al_3CeCo	oP20-Al_3NiY	-48.22	Hypothetical
Al_8CeCo_4	tI26-Al_8CeFe_4	-47.71	Hypothetical
Al_5CeCo_2	oI16- Al_5CeNi_2	-48.88	Metastable
$Al_7Co_6Ce_7$	tP40-$Al_7Co_6Pr_7$	-44.54	Hypothetical
$Al_2Ce_2Co_{15}$	hR19-$Al_2Ce_2Co_{15}$	-16.16	Unstable

Table 4: A comparison of lattice parameters of Al-Ce-Co compounds

Phase	Pearson symbol	Lattice parameters *ab initio* (this work)			Experiment [**Error! Reference source not found.**]		
		a	*b*	*c*	*a*	*b*	*c*
Al_8CeCo_2	oP44	14.357	12.389	3.994	14.30	12.41	4.12
Al_4CeCo	oP12	7.594	4.041	6.791	7.59	4.048	7.014
AlCeCo		11.066	4.429	4.726	11.098	4.410	4.807
	mC12	α,γ= 90°;β=106.44°			α,γ= 90°;β=104.61		
Al_4CeCo	oC24	4.094	15.506	6.648			
AlCeCo	hP9	6.824		4.011			
AlCeCo	hP12	5.461		8.300			
Al_3CeCo	oP20	8.130	4.031	10.770			
Al_8CeCo_4	tI26	8.588		5.109			
Al_5CeCo_2	oI16	7.130	9.334	3.947			
$Al_7Ce_6Co_7$	tP40	13.175		4.289			

Table 5: Thermodynamic parameters obtained in the present study

Phase	Parameter (J/mol of atoms)
Liquid	${}^0L^{liq}_{Al:Ce:Co} = +74439 - 3.053T$
	${}^1L^{liq}_{Al:Ce:Co} = -90050 + 1.943T$
	${}^2L^{liq}_{Al:Ce:Co} = +84638 + 6.757T$
$(Al,Co)_2Ce$	${}^0L^{(Al,Co)_2Ce}_{Al,Co:Ce} = -26423 + 5.257T$
	${}^1L^{(Al,Co)_2Ce}_{Al,Co:Ce} = +500$
	${}^2L^{(Al,Co)_2Ce}_{Al,Co:Ce} = +5.0T$
Al_8CeCo_2 (τ_1)	$G^{\tau_1}_{Al:Ce:Co} = \frac{8}{11}{}^oG^{fcc}_{Al} + \frac{1}{11}{}^oG^{hcp}_{Ce} + \frac{2}{11}{}^oG^{fcc}_{Co} - 52223 + 13.744T$
Al_4CeCo (τ_2)	$G^{\tau_2}_{Al:Ce:Co} = \frac{4}{6}{}^oG^{fcc}_{Al} + \frac{1}{6}{}^oG^{hcp}_{Ce} + \frac{1}{6}{}^oG^{fcc}_{Co} - 54802 + 12.705T$
$AlCeCo$ (τ_3)	$G^{\tau_3}_{Al:Ce:Co} = \frac{1}{3}{}^oG^{fcc}_{Al} + \frac{1}{3}{}^oG^{hcp}_{Ce} + \frac{1}{3}{}^oG^{fcc}_{Co} - 54296 + 8.146T$

Table 6. The invariant reactions obtained in the present study

Sym.	T (°C) Cal.	T (°C) Exp.	X(L, at%) Co	X(L, at%) Ce	Reaction[1]
E_1	639	640	0.2	1.9	$L \leftrightarrow Al_{11}Ce_3 + Al_9Co_2 + Al$
U_1	803	798	1.3	4.1	$L + \tau_1 \leftrightarrow Al_{11}Ce_3 + Al_9Co_2$
U_2	955	945	7.6	2.6	$L + Al_{13}Co_4 \leftrightarrow \tau_1 + Al_9Co_2$
U_3	1015	996	4.1	9.0	$Al_4Ce + \tau_1 \leftrightarrow L + Al_{11}Ce_3$
U_4	1068	1073	5.9	10.5	$L + \beta Al_3Ce \leftrightarrow Al_4Ce + \tau_1$
U_5	1073	1085	14.6	2.6	$L + Al_3Co \leftrightarrow Al_{13}Co_4 + \tau_1$
U_6	1090	1089			$\beta Al_3Ce + \tau_2 \leftrightarrow M_2Ce + \tau_1$
U_7	1110	1135	17.9	2.8	$L + Al_5Co_2 \leftrightarrow Al_3Co + \tau_1$
E_2	1116		21.1	28.6	$L \leftrightarrow AlCo + M_2Ce + \tau_3$
U_8	1127	1143	9.7	13.6	$L + \tau_2 \leftrightarrow \beta Al_3Ce + \tau_1$
U_9	1128		9.7	13.7	$L + M_2Ce \leftrightarrow \tau_2 + \beta Al_3Ce$
U_{10}	1147	1151	22.2	4.8	$L + AlCo \leftrightarrow Al_5Co_2 + \tau_1$
U_{11}	1155	1162	19.6	21.5	$L + \tau_2 \leftrightarrow AlCo + M_2Ce$
E_3	1156	1159	20.6	9.0	$L \leftrightarrow AlCo + \tau_1 + \tau_2$
U_{12}	1192		2.8	16.6	$L + M_2Ce \leftrightarrow Al_4Ce + \beta Al_3Ce$

[1] The phases on the left hand side are higher-temperature phases, and those on the right hand side are lower temperature phases.

Appendix: A corrosion comparison between amorphous and crystalline chemically homogeneous structures

Outside the main objective of the Al-Co-Ce thermodynamic study, an experiment was designed to test whether an amorphous phase is intrinsically more corrosion resistant than its crystalline counterpart. The requirement is for a transformation from the wholly amorphous metal structure to occur by way of a massive transformation. That is, there can be no solute partitioning during the crystallization. This is a rare event with metallic glasses devitrification. In this way the corrosion resistance can be examined based on identical chemical distributions in both the crystalline and amorphous materials. The binary Al-Sm system does behave this way. This is ideal for our studies because of the aluminum-rare earth element combination would correlate well with our Al-Co-Ce material. The current report describes the phase transformations involved for an amorphous $Al_{90}Sm_{10}$.

Following alloy synthesis, melt-spinning at 40 m/s produced a metallic glass ribbon that was fully amorphous for $Al_{90}Sm_{10}$. The XRD pattern of the amorphous state is shown in Figure 7:

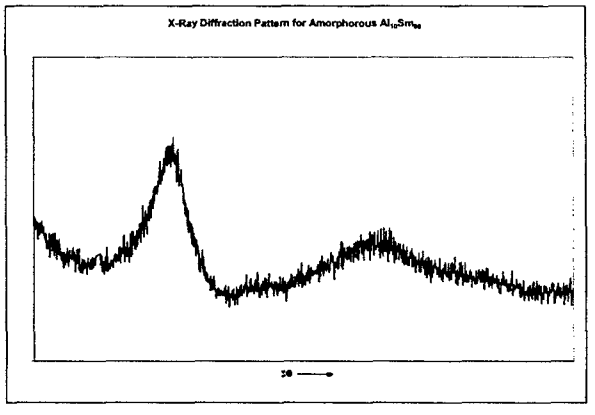

Figure 7. XRD pattern for amorphous $Al_{90}Sm_{10}$. Intensity vs 2θ

An $Al_{90}Sm_{10}$ ingot was cast, broken into pieces and then melt-spun into ribbon. Via XRD, the ribbon was shown to be amorphous. The original ingot was a two-phase mixture of Al + $Al_{11}Sm_3$, consistent with earlier findings. Pieces of the ribbon were isothermally heat-treated in a box furnace for various temperatures and times. Then, via XRD, the isothermal TTT diagram was formed as shown in Figure 8. MS1 and MS2 are metastable intermetallic phases named as such in an earlier publication.

During the transformation sequence, three phase transformations were observed. The first transformation, amorphous → MS2 was observed to occur massively. From TEM and EDS studies, during the transformation, there appears to be no concentration gradient across the interface between the amorphous matrix and the product phase, MS2. A concentration profile was taken across such an interface and EDS analysis shows no observable variation in concentration.

MS2 was determined to have a body-centered cubic crystal structure with a lattice parameter of approximately a = 13.8Å. The MS2 crystals growing into the matrix during the transformation show sparse nucleation and grain size of the order of 1μm (see Figure 9).

The second observed transformation, MS2 → MS1 + Al_{fcc} resembles that of a eutectoid decomposition reaction. The MS2 grains are consumed by growing MS1 + Al lamellar colonies. The distribution of the lamellae is very fine, with a spacing on the order of a few nanometers. After completion of this transformation, the lamellar microstructure appears to globularize with increased heat-treatment even though no additional phase transformation is taking place.

The third observed transformation is MS1 + Al → Al_4Sm + Al, and the resulting microstructure appears to show globular grains of both Al_4Sm and fcc Al. Using EDS, it was possible to distinguish between these two phases. Additionally, during the transformation, it was possible to distinguish between these two phases as well as the MS1 phase; Al_4Sm, MS1, and Al_{fcc} respectively showed increasing richness in aluminum.

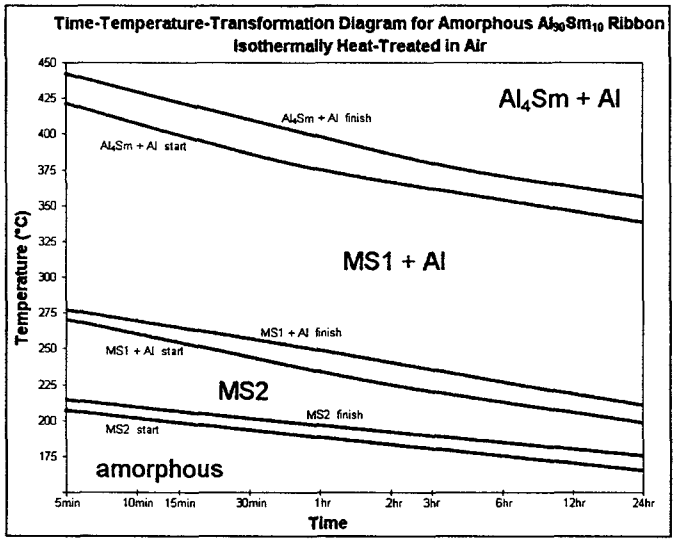

Figure 7: Isothermal TTT Curve for Amorphous $Al_{90}Sm_{10}$ Ribbon

Figure 8: Microstructure of MS2 Grains after Complete am → MS2 Transformation (Heat-Treatment: 200°C for 1hr.)

3. Accomplishments and New Findings

See Section 2 above.

4. Personnel Supported

G.J. Shiflet	co-PI	8%
Michael Gao	PDRA	15%
Aiwu Zhu	PDRA	20%
Jason Hadorn	GRA	60%

5. Publications

a. Refered Journals

1. A Zhu, SJ Poon,; GJ Shiflet, "On glass formability of Al-Gd-Ni (Fe)", *Scripta Materialia*, **50** (2004) pp. 1451-1455.
2. A Zhu, GJ Shiflet, and D Miracle, "Glass Froming Ranges of Al-rare Earth Metal Alloys: Thermodynamics and Kinetic Analysis", *Scripta Materialia*, **50** (2004) pp. 987-991.
3. MC Gao, N Unlü, and GJ Shiflet, M Mihalkovic, M Widom, "Re-assessment of Al-Ce and Al-Nd Binary Systems Supported By Critical Experiments and First-Principles Energy Calculations", *Metallurgical Transactions*, **36A** (2005) pp. 3269-3279. Winner of APDIC Award for best thermodynamic paper published in 2005.
4. MC Gao,.GJ Shiflet, "Devitrification sequence map in the glass forming Al-Ni-Gd system", *Scripta Materialia*, **53** (2005) pp.1129-1134.
5. MC Gao, N Unlu, GJ Shiflet,; M Mihalkovic, M Widom, "Reassessment of Al-Ce and Al-Nd binary systems supported by critical experiments and first-principles energy calculations", *Acta Materialia*, submitted 2006

b. Books/Book Chapters/Books Edited

1. A Zhu and GJ Shiflet, "Thermodynamics of Aluminum-based Glasses" Chapter 6 in Advanced Structural Materials, Taylor and Francis Group, LLC, in press.

c. Proceedings

1. MC Gao, GJ Shiflet, "Phase formation sequence map for Al-Ni-Gd glass-forming system devitrified at 250°C.", THERMEC'2003, Materials Science Forum **245-250**, Pt. 1 (2003) pp. 426-432.
2. JP Hadorn and GJ Shiflet, "A Survey of Eutectoid Decomposition in Three Lanthanide-Magnesium Systems", Proc. Int. Conf. Solid-Solid Phase Transformations in Inorganic Materials 2005 (PTM'05), J.M. Howe, D.E. Laughlin, J.K. Lee, U. Dahmen and W.A. Soffa -eds., TMS (Warrendale, PA) 2005, pp. 701-706.

6. Interactions/Transitions

a. Participation at Professional Meetings, Conferences, and Seminars

1. "Laser Processing of Bulk Crystalline Alloys for Improvement Corrosion Resistance" JG Hoekstra, GJ Shiflet, SJ Poon, JR Scully and JM Fitz-Gerald, TMS San Francisco, Feb. 14, 2005
2. "Eutectoid Decomposition in Lanthanide-Mg Systems", J. Hadorn and GJ Shiflet, PTM05, Phoenix, AZ, May 30, 2005
3. "Two-step Formation of FCC Phases in Al-Glasses", M Gao, GJ Shiflet, TMS, Chicago, IL, Nov. 11, 2003.
4. "Phase Equilibria and Thermodynamic Modeling of Al-Based Metallic Glasses", M. Gao, N. Unlu, and GJ Shiflet, TMS, Charlotte, NC, Mar. 17, 2004.

b. Consultative and Advisory Activities

none

c. Transitions and Professional Communications

7. New Discoveries, Inventions, Patent Disclosures

- Patent disclosure: Al-Co-Ce tunable Amorphous Coating

8. Honors and Awards

- *Scientific American 50 Award* in materials and chemistry for 2004 for work on the development of amorphous metals. This was for general work in amorphous metals including the MURI effort.
- The Alloy Phase Diagram International Commission (APDIC) Best Paper Award: "For the best published manuscript on alloy phase diagram data in the year 2005". This was for the MURI Al-Ce thermodynamic effort, see above.

C. Cladding Application Methods and Fatigue Resistance Characteristics – A.L. Moran

1. Objectives

- The goal of the metallic coatings effort, as part of the integrated multi-functional coating system, is to create a metallic coating that will replace the hot-roll bonded cladding systems currently used on military aircraft. This coating is expected to be easily field applied and have a range of functions to improve corrosion performance, coating adhesion, and provide active corrosion protection. This will be accomplished through implementation of thermal spray or cold spray technology that will provide optimal coating and substrate properties and the use of nanocrystalline or amorphous matrix metallic glasses such as the Al-TM-RE glasses.
- Spray-applied Al-based materials (e.g. Al, Al-Zn) have already been applied to steels and Al age-hardened materials. A critical characteristic of amorphous/nano-crystalline materials is the ability to supersaturate desired alloying elements to produce a material with superior corrosion performance, high strength, ductility, and wear resistance. Further, the ability to utilize alloy compositions that contain rare-earth elements make it possible to produce a cladding material with active corrosion protection properties at coating defects or mechanical scratches.
- High purity aluminum coatings were deposited in air from powder stock using the thermal spray or cold spray techniques[1,2].
- In Stage I of the program a 99.0-99.8 % Al coating/AA2024-T3 skin substrate system has been used to evaluate the corrosion/fatigue performance as a function of thermal spray coating process (i.e., powder flame spray, atmospheric plasma spray, and HVOF spray) and cold spray process such as Kinetic Metallization (KM). It was the specific goal of the first stage of this program to select the process that optimizes the coating's physical, mechanical, and corrosion properties. Moreover, the testing performed on the near pure aluminum coatings in Stage I provided a suitable control for evaluating the inhibitive capability/performance of the exotic/glassy Al-TM-RE alloyed coating system recently developed at the University of Virginia by Scully and Shiflet.
- Additional objectives have been defined as a result of alloy development and process definition completed in the first stage. Specifically, questions concerning the viability of using a thermal spray technique to produce an amorphous or nano-crystalline coating needed to be addressed as well as queries concerning the commercial availability of suitable feedstock in the chosen alloy composition for such a process.

2. Summary of Activities – Status of Effort

Phase I

- Formation of amorphous microstructures by quenching from the liquid phase generally requires cooling rates on the order of 10^4-10^6 K/s during rapid solidification.[3-5]

- As noted in the literature, recent advances in the production of bulk metallic glasses have reduced this rate by orders of magnitude. Several alloy systems have formed amorphous structures at extremely slow cooling rates: $Pd_{40}Ni_{40}P_{20}$ (10^2 K/s),[3] $Ni_{62}Nb_{38}$ (10^3 K/s),[3] $Zr_{65}Al_{7.5}Ni_{10}Cu_{17.5}$ (10^2 K/s),[6] and a Zr-Ti-Be alloy (1 K/s).[7]
- Thermal spray technology combines the processes of very high temperature melting, quenching, and consolidation into a single operation, offering an excellent opportunity to produce amorphous or nano-crystalline coatings. Thermal spray techniques such as atmospheric plasma and HVOF have solidification rates of 10^6-10^8 K/s[8-12] and 10^7 K/s,[13,14] respectively, and are likely candidate processes for amorphous and nano-crystalline/amorphous formation.
- Several amorphous, nano-crystalline, or quasicrystalline alloy coatings have been produced by atmospheric plasma spraying[15-20] as well as by HVOF spraying [3,21-28] and flame spray.[26] It should be noted that although plasma spraying offers a high quench rate, annealing of the thermal spray deposit occurs as a result of both the high temperature plasma flame and adiabatic recalescence associated with particle solidification of one splat droplet upon another.
- This annealing can lead to degrees of devitrification of the sprayed metallic glass.[9,15] A possible alternative deposition method for production of nano-crystalline coatings is cold spray. There are a wide variety of cold or mechanical deposition methods. An evaluation of available, commercially developed methods indicated Kinetic Metallization[29] has been used to consolidate and deposit amorphous aluminum alloyed with transition and rare earth metals without subsequent crystal growth. The resulting coating, however, has the high strength and reduced ductility associated with cold working. Alternative cold spray techniques, recently developed at University of Ottowa, are addressing these issues.
- Initial experimental testing was conducted to evaluate and select the appropriate coating process for optimal corrosion fatigue lifetimes. Coating application processes selected for study include powder flame thermal spray, atmospheric plasma thermal spray, HVOF thermal spray, and Kinetic Metallization. The substrate selected for use throughout the program was AA2024-T3 sheet. The physical (i.e., coating oxide and porosity content), mechanical (i.e., hardness, deflection to coating fracture, fatigue lifetimes), and corrosion (i.e., pre-corroded fatigue lifetimes) properties of 99.0-99.8 % Al coatings applied via the four candidate processes on AA2024-T3 sheet substrate were evaluated.
- Porosity and oxide content were measured via optical microscopy and analyzed via a metallographic computer program. A gray scale delineation technique was used to quantify the area fraction of each of the three constituents (i.e., oxide, porosity, aluminum coating) within each of the coating structures.
- Mechanical property testing of the candidate aluminum coatings included micro-hardness testing of the coating and substrate of the four application systems, coating fracture evaluation via a three-point bend test, and fatigue lifetime evaluation in air utilizing a bending fatigue apparatus. Vickers micro-hardness testing was performed on thermal spray and cold spray coated AA2024-T3 coupons, sandblasted AA2024-T3 coupons, and as received AA2024-T3 coupons. Indentations were made within the thermal sprayed coating, adjacent to the coating/substrate interface, and within the substrate as a function of distance from the coating/substrate interface.

- Hardness values of the aluminum coatings were documented and compared as a function of spray process. Hardness measurements within the substrate were documented to discern any possible metallurgical changes due to the sandblast process and/or the subsequent thermal spray coating application process.
- Three-point bend testing of thermal sprayed and cold sprayed coating/2024-T3 substrate coupons was performed to evaluate the fracture behavior of the coatings as a function of application process. Initiation of coating fracture was documented via optical observation.
- Fatigue testing in lab air was performed on aluminum coated AA2024-T3 applied by the three candidate thermal spray processes, AA2024-T3 Alclad, and AA2024-T3 bare substrate. Fatigue testing in air on KM AA2024-T3 coupons was discontinued due to the poor (i.e., brittle failure) performance of the applied coating.
- The corrosion fatigue properties of a second sample batch of the three candidate thermal sprayed near-pure Al coatings were compared to those of AA2024-T3 and AA2024-T3 Alclad. The effect of a 1000 hour pre-exposure in a 0.6 M NaCl alternate immersion (AI) environment on the fatigue life of AA2024-T3 coupons was evaluated over a range of applied maximum stress levels (i.e., 83, 60, 50, 40, 40, 25 ksi) utilizing a cyclic bending fatigue test frame at 30 Hz (R = -1). The goal of Stage I was to select the process that produces optimal properties with emphasis on corrosion fatigue lifetime.

3. Accomplishments and New Findings

Physical and Mechanical Property Measurements

- Porosity and oxide content of the first sample batch of 99.0-99.8% Al coatings were measured via optical microscopy and metallographic computer analysis. Results indicated that the flame spray coating has the highest area fraction percentage of oxide of 11.6 %, followed by the plasma spray coating, the HVOF spray coating, and the KM coating with area fraction percentages of oxide of 5.48 %, 4.72 % and 4.08%, respectively.
- The flame spray coating also had the highest area fraction percentage of porosity with an 8.3 % measurement. The area fraction percentage of porosity for the plasma sprayed coating, HVOF sprayed coating, and KM coating was 1.35 %, 1.92 % and 1.63%, respectively. Vickers micro-hardness results indicated no difference in the hardness of the 99.0-99.8% aluminum coating as a function of thermal spray application process – all measurements within the coating area were an approximate Vickers hardness of 50.
- Statistical analysis of the hardness results taken from within the AA2024-T3 substrate indicate that no significant change in microstructure or mechanical properties occurs as a function of distance from the coating / base metal interface. Evaluation of deflection at fracture for the thermal spray coatings and KM coating was performed via a three-point bend test.
- Results, as discussed in earlier reports, indicated that the flame spray coating withstands the highest deflection before coating fracture with an average of deflection

of 0.59 inches compared to the deflection sustained by the plasma sprayed coating (0.47 inches) and to the deflection sustained by the HVOF sprayed coating (0.42 inches). The KM coating displayed the lowest deflection at fracture with a deflection of only 0.18 inches. Fatigue testing in lab air was performed on 99.0-99.8% aluminum coated AA2024-T3 as a function of thermal spray application process, AA2024-T3 Alclad, and AA2024-T3 bare substrate.

- Results indicate a loss in fatigue lifetime as a result of hot roll-bonding Alclad onto the AA2024-T3 substrate. Conversely, results indicate an increase in fatigue lifetime as a result of the application of a thermal spray coating onto AA2024-T3. A tentative ranking of the effect on fatigue lifetime of AA2024-T3 was observed as follows: AA2024-T3 + HVOF coating (longest fatigue lifetimes in air), AA2024-T3 + flame spray coating, AA2024-T3 + atmospheric plasma coating, and AA2024-T3 + Alclad (shortest fatigue lifetime in air).

Corrosion Property Measurements

- The effect of unstressed localized corrosion on the fatigue lifetime of AA2024-T3 was evaluated over a range of maximum stress levels applied by a cyclic bend fatigue test frame at 30 Hz (R = -1). Fatigue lifetime results from AA2024-T3 coupons in air were compared to fatigue lifetime results from AA2024-T3 coupons pre-exposed for 1000 hours in an 0.6 M NaCl alternate immersion (AI) environment (see Figure 1).
- An order of magnitude loss in fatigue lifetime was observed in the pre-corroded specimens. The results from the Alclad specimens indicate half an order of magnitude increase in fatigue lifetime compared to the bare substrate.
- An evaluation of the corrosion fatigue lifetime of 99.0-99.8% aluminum coated AA2024-T3 was performed over a range of maximum applied stress levels (i.e., 25 to 60 ksi) as a function of the three candidate thermal spray application processes. A tentative ranking of the thermal spray coating processes was observed according to fatigue lifetime as follows: HVOF (most protective coating – longest fatigue lifetimes over the applied stress levels), powder flame spray, atmospheric plasma spray, AA2024-T3 Alclad, and AA2024-T3 bare substrate (shortest fatigue lifetimes over the applied stress levels).
- Based on initial physical property measurements for porosity and oxide content, the plasma coatings were expected to perform better in pre-corrosion fatigue testing. Oxide and porosity measurements were subsequently conducted on the corrosion fatigue samples indicating significantly higher than expected values of 12.6% oxide content and 4.98% porosity for the plasma coatings in this sample batch. Although this justifies the corrosion fatigue behavior, it also accentuates the requirement to maintain careful spray parameters to assure coating quality and optimal coating performance.
- In summary of Stage 1, using pure aluminum powders as feedstock, HVOF thermal spraying provided the most promising coating in terms of microstructure, mechanical and pre-corroded fatigue properties. The HVOF process used in this phase, however, did not seem to significantly reduce the grain size of the feedstock powders and therefore, to produce an amorphous or nano-crystalline coating, an amorphous or

nano-crystalline feedstock may need to be obtained. Kinetic Metallization needs further development before it can provide appropriate coatings.

Stage II

- The thermal spray Al coatings produced in Stage I were all deposited at CDNSWC and were crystalline since those thermal spray processes could not provide the critical cooling rate required for aluminum during deposition. As a result, it was anticipated that a nano-crystalline or amorphous feedstock must be used to produce the required coating.
- A market survey was conducted to locate nano-crystalline aluminum powders and, as a result, powders were purchased and agglomerated. Due to the nature of the thermal spray technique, individual nano-powders could not be successfully applied because of their low mass and inability to be carried in a moving gas stream for deposition on a substrate, resulting in a clogged thermal spray gun nozzle.
- In order to the spray nano-powders, the individual particles had to be agglomerated into spherical granules or bundles of the appropriate size for deposition. Additionally, nano-powders of pure aluminum are used for propellants and hence are quite reactive, tending to oxidize readily. It was necessary to allow controlled oxidation of the powders to occur during manufacture to insure stability and safety.
- Results for the first attempt at deposition of nano-crystalline aluminum coatings are shown versus the control coatings in Figure 2. Due to the high oxide content in the agglomerated powders, the resulting coatings behaved much more like a ceramic than a metal. Although HVOF was deemed the optimal thermal spray process as a result of Stage I, plasma spraying, typically used for ceramic coating application due to its higher flame temperature, yielded a better nano-powder coating from the oxidized aluminum. Agglomeration does not appear to be a suitable method for production of amorphous or nano-crystalline feedstock for the preferred thermal spray process, HVOF.
- Additional powder sources have also been pursued. Prior to selection of the optimal chemistry, 40 μm size powders of a possible glass-forming composition (Al-6Co-5Ce by weight) were purchased from AlPoCo in the United Kingdom and were evaluated. Some powders were also provided to SAIC, developers of the HVOF Pulsed Thermal Spray (PTS) process, a variation of thermal spraying that involves melting and rapid solidification, and thus reduces grain size.
- Slow scan rate x-ray diffraction indicated lower peak intensities and some peak broadening for the PTS coating, demonstrating that the pulsed process can refine the grain structure of the starting feedstock. Additional Al-18Co-9Ce (by weight) powders with a finer powder size (approximately 10 μm) were purchased for the PTS method since research has indicated a finer feedstock may yield an even finer coating grain size.
- Feedstock powders and processed coatings deposited were characterized by x-ray diffraction and Scanning Electron Microscopy (SEM) to identify the structure. X-ray diffraction patterns, as shown in Figure 3 indicated that feedstock powders and processed coatings were nano-crystalline in structure. The composition analysis by EDS showed that the microstructure of the Al-18Co-9Ce PTS coating consisted of

Al-16Co-10Ce matrix, Al-54.4Co-3.2Ce-3.4O and Al-26.8Ce-32.1O inclusions or constituents (by weight).

- A fine dendrite grain structure on the order of 85 nm in size was evident in areas of the coating matrix. X-ray mapping revealed that the PTS coating was relatively uniform with small amount of oxygen uptake. These results indicate that Al-18Co-9Ce system is more glass-forming and PTS coating process is able to refine the grain size of the starting powder. The main advantage of the PTS technique is the ability to deposit an amorphous or nano-crystalline coating using traditional crystalline feedstock.
- The optimal glass forming chemistries were determined by Scully and Shiflet to be Al-13Co-26Ce (by weight). Ingot materials were purchased from Arris International and atomized into amorphous/nano-crystalline feedstock powders at Valimet. SEM images indicated that Al-13Co-26Ce feedstock powders were about 10 μm in particle size and processed coatings produced via modified cold spray, as shown in Figure 4, were dense. Coatings produced via PTS using the 10μm powders varied with process parameters.
- A table of porosity and oxide measurements, demonstrating the range of both which can be obtained by varying the process, for one batch of samples is given in Table 1. Representative micrographs and diffraction patterns for a coating with low porosity and oxide versus one with higher values are given in Figure 5. PTS coatings tend to demonstrate a higher degree of amorphicity as shown in the x-ray diffraction pattern given in 5(d) as compared to the one in 5(b) where the coating has higher amounts of porosity and oxides present.
- Attempts were made by two thermal spray sources to deposit the 10μm powders using HVOF methods but powder feed issues, due to the fineness of the powder, could not be overcome. Coarser Al-13Co-26Ce feedstock powders were used since the diffraction pattern for the 45 μm shown in Figure 6 indicates similar nano-crystallinity to the 10 μm powders for the same composition. Powders were forwarded to CDNSWC and F.W. Gartner Thermal Spraying, Ltd for HVOF coating deposition. Representative coatings and x-ray diffraction patterns are shown in Figure 7. The Gartner coating appears more uniform and more amorphous. The Gartner process can be modified to produce an even more amorphous product as shown in Figure 8.
- Hardness and fatigue testing indicated that the first Al-13Co-26Ce (wt%) HVOF coatings sprayed were brittle with degraded fatigue life. A subsequent investigation brought to light the variations in sample preparation as compared to past CDNSWC methods. An evaluation of grit blasting protocols provided the fatigue results shown in Figure 9. Future HVOF and PTS coatings will be deposited on substrates grit blasted with 54 grit.
- Because the mechanical properties, especially fatigue properties, are essential for the use of this coating in aircraft applications, processing conditions as well as substrate preparation must be optimized or the composition altered to satisfy the requirements for mechanical and corrosion properties. As a result of transition funding from ONR, a parametric study is now underway to define the processing parameters for HVOF and PTS to lower hardness and enhance fatigue life. Another effective way to increase coating ductility may be to lower the Co and Ce content.

- According to the compositional guidelines developed by UVa, amorphous compositions of Al-Co-Ce alloy system with less Ce include Al-7Co-3Ce at% (Al-12.6Co-12.9Ce wt%), Al-8Co-3Ce (Al-14.3Co-12.8Ce wt%), Al-9Co-2Ce at% (Al-16.5Co-8.7Ce wt%), Al-10Co-2Ce at% (Al-18Co-9Ce wt%). Additional ingots with lower Co and Ce concentrations have been produced by Arris and atomized into powders having a range of sizes. These will be deposited via PTS and HVOF in the near future and evaluated using metallography, hardness, tensile adhesion strength tests, fatigue testing, and pre-corrosion fatigue testing. In addition, corrosion behavior and anodic protection of the AlCoCe coatings will be evaluated.
- In conclusion, there are several available routes to achieving amorphous/nano-crystalline coatings in a cost-effective manner. A summary of the methods evaluated, data and anticipated future work are given in Table 2. From a general perspective, there are two routes by which optimized amorphous or nano-crystalline coatings may be produced. One method combines the well developed HVOF technique with an amorphous/nano-crystalline powder processing technique. The other combines traditional crystalline powder production with newly developed deposition methods to refine and deposit the desired coatings.

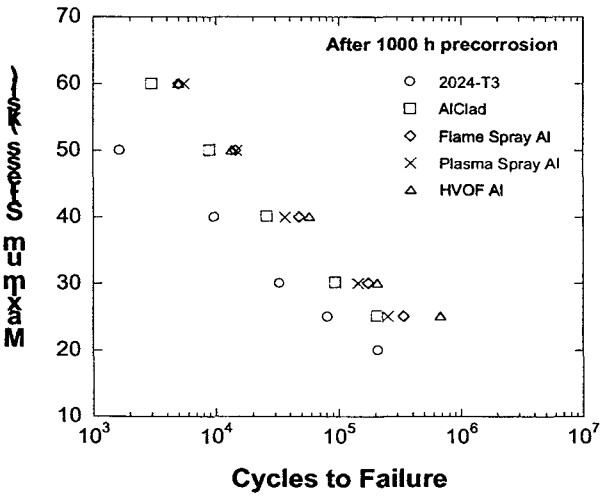

Figure 1. Pre-corroded fatigue results for Stage I.

HVOF
40 μm Al feedstock

KM
40 μm Al feedstock

HVOF
Nano-Al feedstock

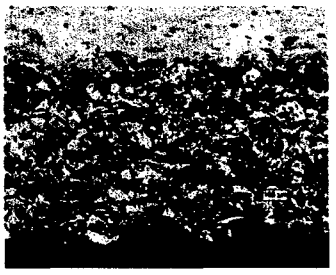

Plasma
Nano-Al feedstock

Figure 2. Optical micrographs showing the influence of different processing and different size feedstock.

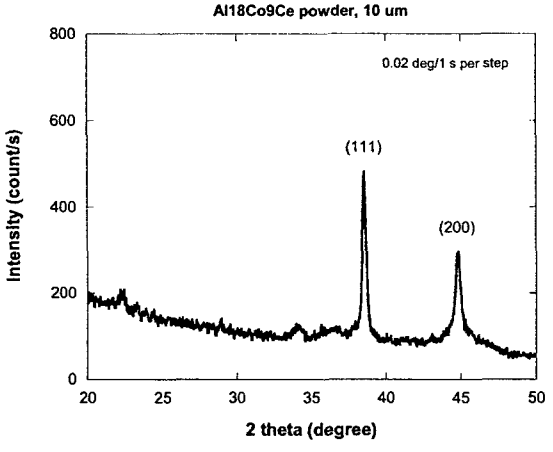

(a)

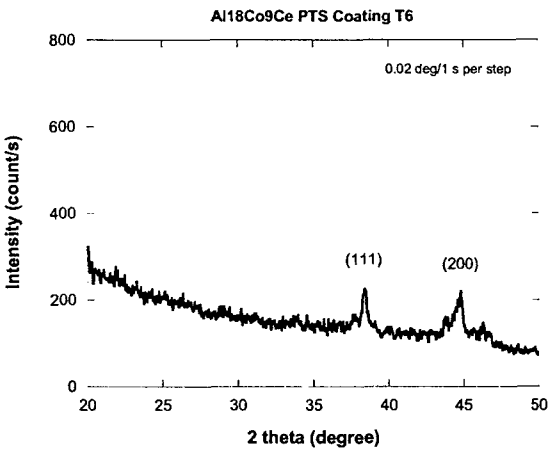

(b)

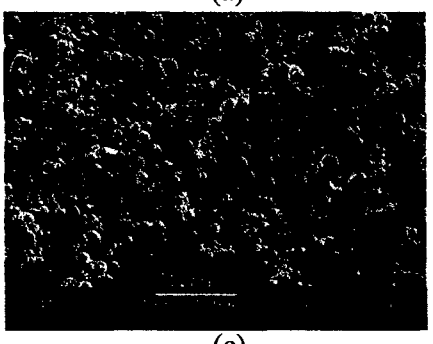

(c)

(d)

Figure 3. X-ray diffraction patterns and SEM images of Al-18Co-9Ce feedstock powders and HVOF PTS coating.

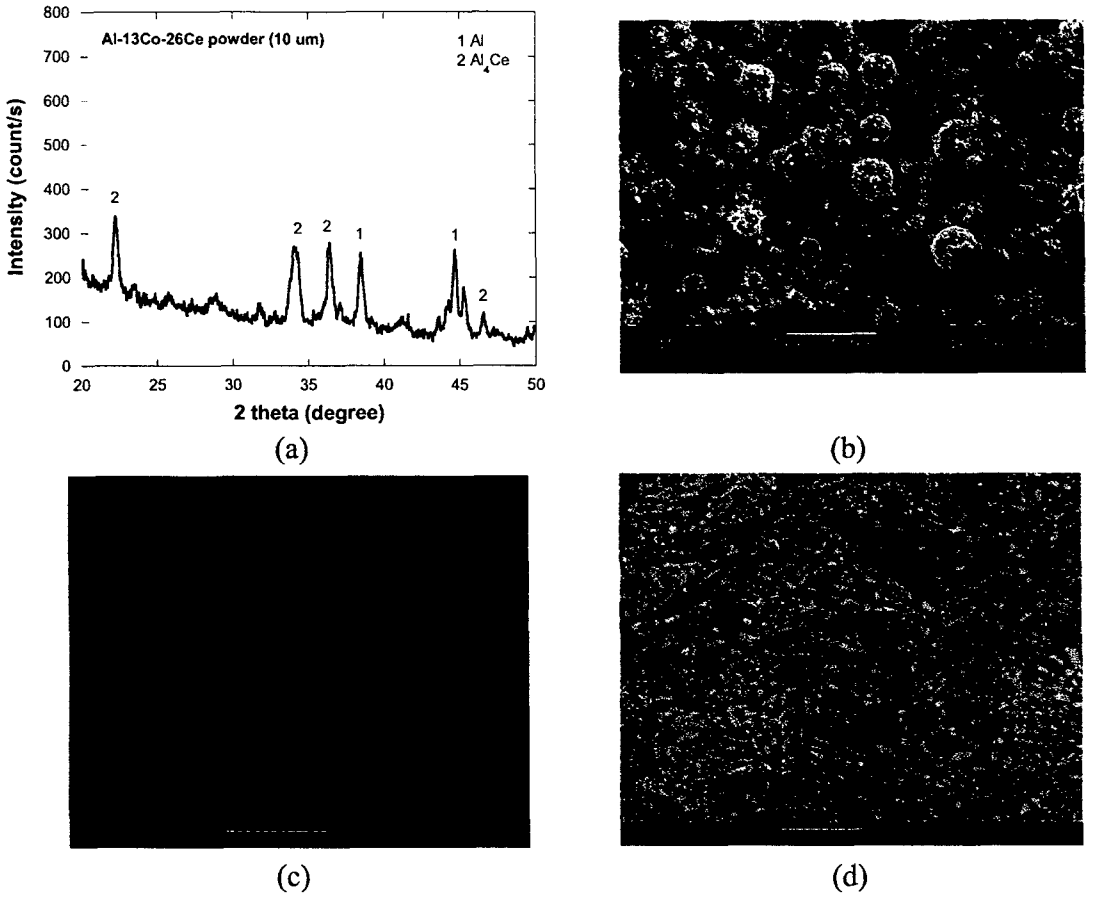

Figure 4. X-ray diffraction pattern and SEM images of Al-13Co-26Ce feedstock powders and cold spray coatings.

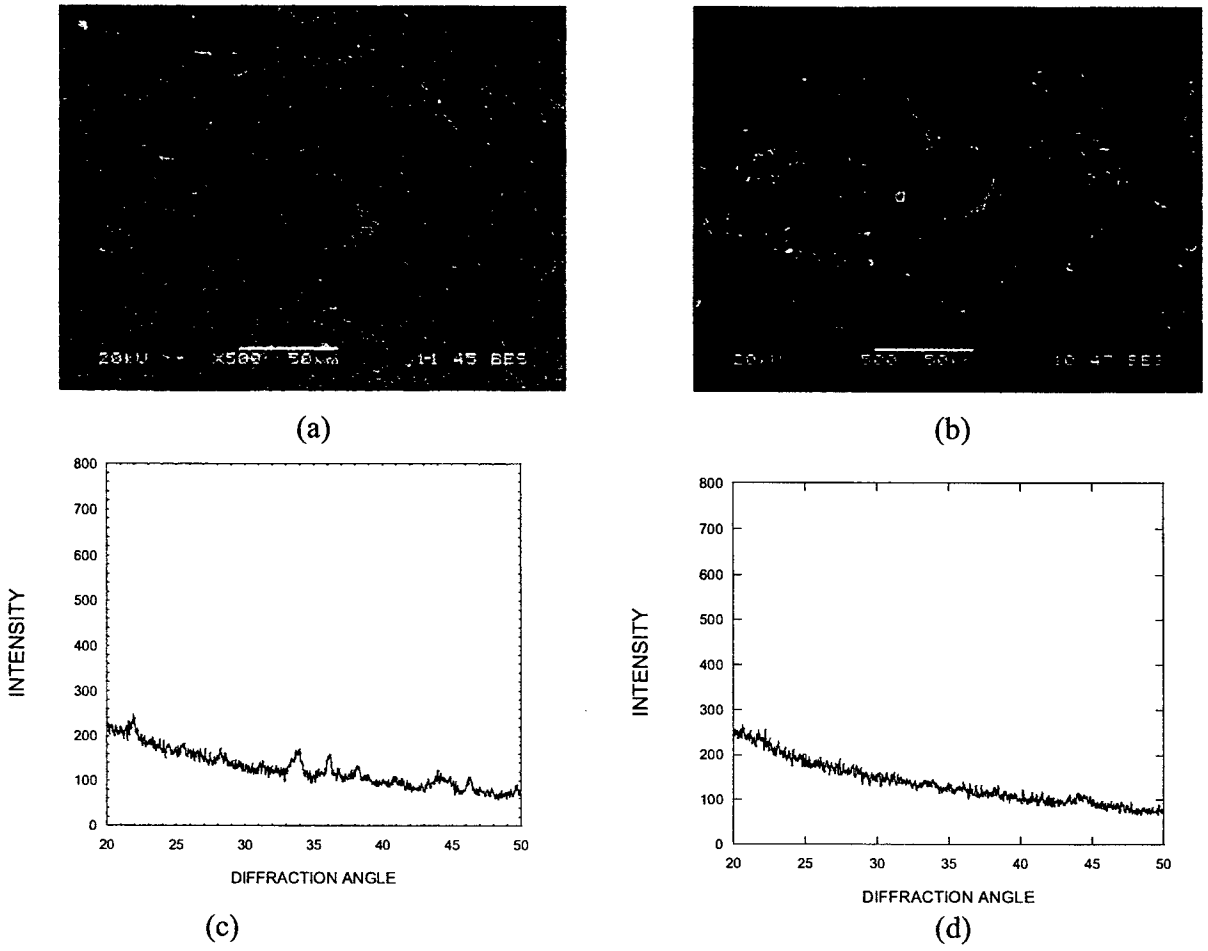

Figure 5. SEM images and x-ray diffraction patterns for PTS coatings deposited using Al-13Co-26Ce feedstock powders. Low porosity and oxide values were determined for the coating shown in (a) with its XRD pattern in (c) and high values were determined for the coating shown in (b) and (d).

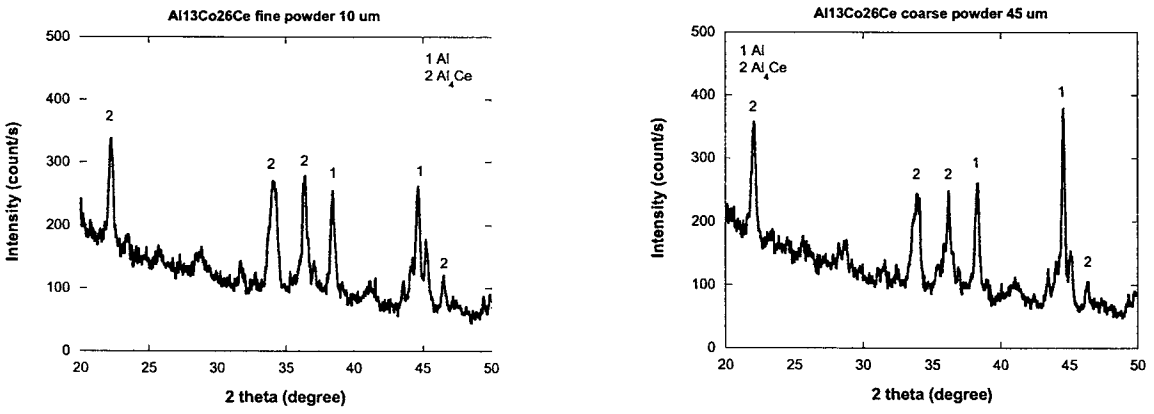

Figure 6. X-ray diffraction patterns for Al-13Co-26Ce feedstock powders.

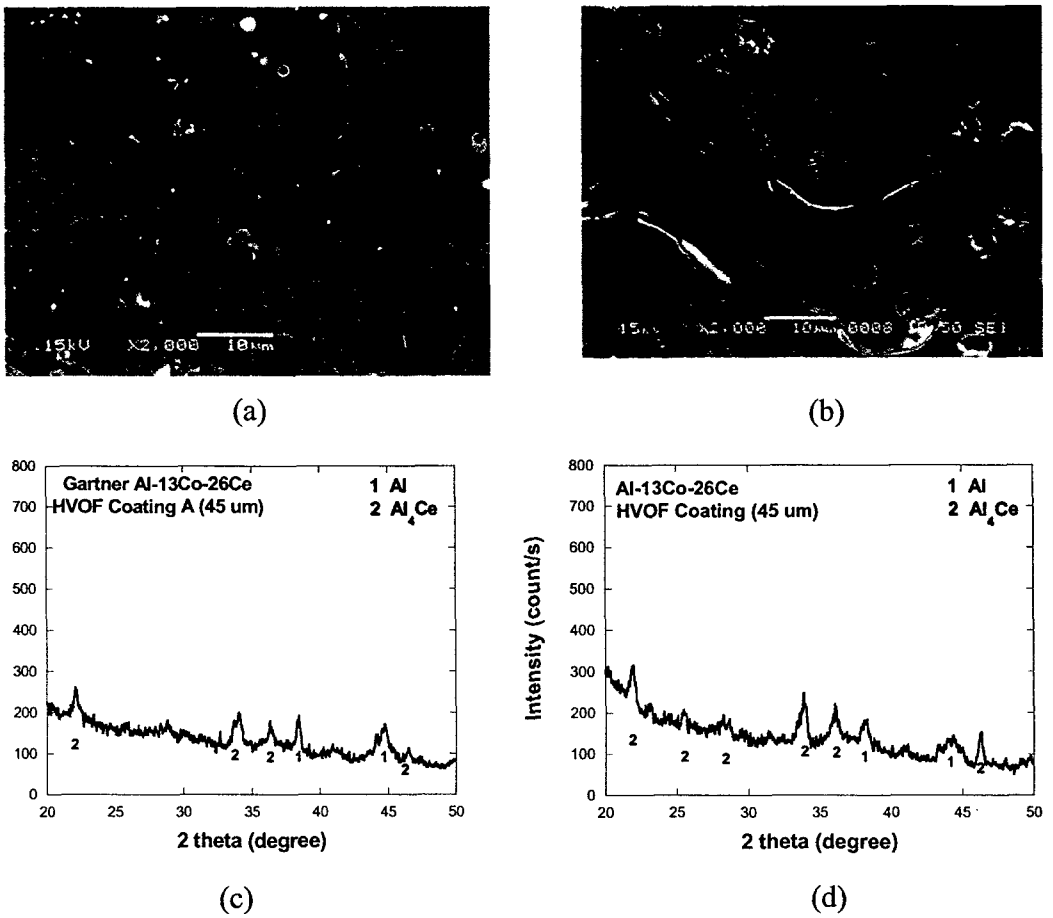

Figure 7. Representative coatings and x-ray diffraction patterns for HVOF coatings produced at F.W.Gartner (and c) and CDNSWC (b and d).

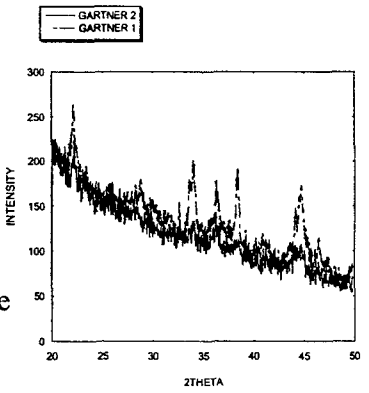

Figure 8. Subsequent Gartner coatings represented by the pattern in red have show reduced crystalline peaks as compared to earlier coatings, represented by the blue.

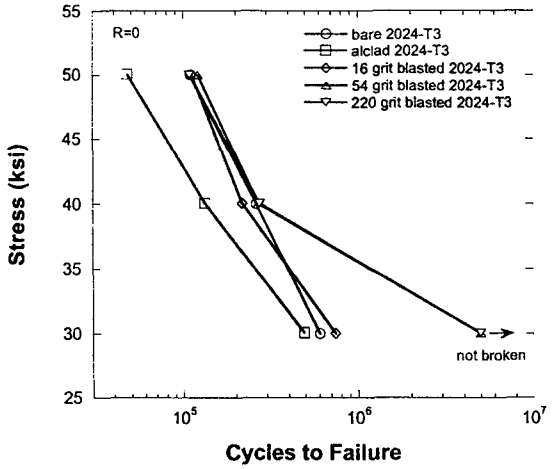

Figure 9. Effect of Alclad and grit blasting on fatigue properties of AA2024-T3.

TABLE 1. Quantitative Analysis of PTS Al-13Co-26Ce Coatings

	Microhardness Vickers 300g Average of 5 measurements	Oxygen Wt% (SEM) Average of 3 measurements	Porosity % (Optical Microscopy)	Oxide % (Optical Microscopy)	Number of samplings for porosity and oxide%
A1A	197.9	5.5	1.38	4.15	Ave of 7
A2	168.2	6.3	0.662	4.24	Ave of 4
A3	164.3	6.6	3.06	7.22	Ave of 2
A4	166.1	6.1	0.745	4.15	Ave 0f 7
A5	168.9	7.2	1.93	8.2	Ave of 4
A6	214.8	7.5	1.29	6.09	Ave of 7
A7	212.1	12.1	6.77	26.71	Ave of 5
A8	203.5	8.0	2.00	17.67	Ave of 3

TABLE 2. Coatings Sprayed/To Be Sprayed by Various Thermal Spray Methods

Powders	HVOF	PTS	Cold Spray	FS	APS
Al, 45 um	+		+	+	+
nano-Al agglomerated	+				+
AlPoCo Al-6Co-5Ce, 45 μm	+	+			
AlPoCo Al-6Co-5Ce, 45 μm cryomilled					
AlPoCo Al-18Co-9Ce, 10 μm		+			
Arris/Valimet Al-13Co-26Ce, 10 μm		+	+		
Arris/Valimet Al-13Co-26Ce, 45 μm	+				
Arris/UCD Al-17Co-16.1Ce	*	*	*		
Arris/UCD Al-12.2Co-16.6Ce	*	*	*		

- All the compositions are given by weight percentage
- The composition of Al-6Co-5Ce powder was measured while others AlCoCe powders have nominal compositions

* Future coatings under ONR program

Rick Wong
NSWC

Howard Gable, Ralph Tapphorn
Inovati

Enrique Lavernia
University of California

Daming Wang
Praxair

Chris Powers
Plasma Processes

Roy Christensen
Valimet

Boro Djordjevic
JHU

George Kim
Perpetual Technologies

Herb Herman
SUNY - Stoneybrook

Dan Branagan
NanoSteel Corp

In the search for aluminum alloy nanopowders, the following sources have been contacted:

Technanogy	Select Arc
Inframet	PolyMet
Nanostructured and Amorphous Materials	HJE Company
Aluminum Powder Company	Crucible Research
Arris Ingot	RSP-Technology
Argonide Corporation	Reade Advanced Materials
Arcos Alloys	Valimet Inc

USNA joined Cold Spray Consortium initiated by Ford Motor Company.

7. New Discoveries, Inventions, Patent Diclosures
None

8. Honors and Awards
None

References

1. Tucker, R.C., "Thermal Spray Coatings," in Surface Engineering – Volume 5 ASM Handbook, (Materials Park, OH: ASM International): pp.497.
2. Pawlowski, L., The Science and Engineering of Thermal Spray Coatings, John Wiley and Sons, Chichester, England, (1995): pp. 139-146.
3. J.W. Martin, R.D. Doherty and B. Cantor, Stability and Microstructure in Metallic Systems,86-89; 1997, Cambridge, U.K, Cambridge University Press.
4. J.W.Luster, G.R.Heath and P.A.Kammer, *Materials and Manufacturing Processes*,1996, **11(5),** 855.
5. H.J. Kim, K.M.Lim, B.G. Seong, and C.G. Park, *J. Mat. Sci.*, 2001, **36 (1)**, 49.

6. H.H. Hng, Y. Li, S.C. Ng, and C.K. Ong,, *Journal of Non-Crystalline Solids*, 1996, **208, (1-2)**, 127.
7. Johnson, *Materials Research Society Bulletin*, 1999, **24**.
8. M.R. Dorfman, *Advanced Materials & Processes*, 2002, **160(8)**, 47.
9. S. Sampath, PhD Dissertation, State University of New York – Stony Brook, Stony Brook, NY, 1989.
10. M. Moss, *Acta Met.*, 1968, **(16)**, 321.
11. V. Wilms, PhD Dissertation, State University of New York – Stony Brook, Stony Brook, NY, 1978.
12. C. Moreau, P. Cielo, M. Lamontagne, S.Dallaire, J.C. Krapez, and M. Vardelle, *Surface and Coating Technology*, 1991, **46 (2)**, 173.
13. Private communications Dr. S. Sampath, SUNY-Stony Brook, October 2002.
14. Private communications Dr. Zhang, SUNY-Stony Brook, October 2002.
15. S. Sampath, *Materials Science and Engineering*, 1993, **A167**, 1.
16. S. Sampath, *Materials Science and Engineering*, 1993, **A167**, 1.
17. B.C. Giessen, N.M. Madhava, R.J. Murphy, R. Ray and J. Surette, *Met. Trans.*, 1977, **8A**, 365.
18. K. Kumar, D. Das and R. Williams, *J. of Applied Physics*, 1980, **51(2)**, 1031.
19. S.K. Das, E.M. Norin,and R.L. Bye, *Materials Research Society Symposium Proceedings*, 1984, **28**,233.
20. V. Panchanathan, C.L.Tsai and S. Whang,, *Materials Research Society Symposium Proceedings*, 1982, **8** , 137.
21. T.P.Shmyreva and L.V. Mukhina, "Formation Behavior of New Amorphous and Composite Materials in Detonation Gun and Plasma Spraying," Proceeding of the 7th National Thermal Spray Conference, Materials Park, OH, 1995ASM International.
22. J.M. Guilemany, J.Nutting, J.R. Miguel and Z. Dong, *Scripta Met.* 1995, **33(1)**, 55.
23. M.L. Lau, H.G. Jiang, W. Nuchter and E.J. Lavernia, *Physical Status Solidi A*, 1998, **166**, 257.
24. J. He, M. Ice and E.J. Lavernia, *Met. Trans.*, 2000, **31A**, 541.
25. J. He, M. Ice and E.J. Lavernia, *Met. Trans.*, 2000, **31A**, 555.
26. F. Otsubo, H. Era, K. Kishitke, *Journal of Thermal Spray Technology*, 2000, **9(4)**, 494.
27. H. Edris, D.G. McCartney and A.J. Sturgeon, *J. of Materials Science*, 1997, **32**, 863.
28. G. Burkle, F. Banhart, F, A. Sagel, C. Wanke, G. Croopnick, and H.J. Fecht, *Materials Science Forum*, 2002, **386-388**, 571.
29. www.inovati.com

IDENTIFICATION OF ENVIRONMENTALLY COMPLIANT INHIBITORS - S.R. Taylor

I. PROJECT THRUST OVERVIEW

Once the cladding is removed, the corrosion protection provided by present day aerospace coating systems is predominantly the result of chromate-based inhibitive pigments that are incorporated into the primer resin. The chromate compounds that are used have an appropriate balance of solubility and inhibitive power, so that they may be leached at a slow enough rate so as not to leave a porous structure within the resin matrix, yet have sufficient inhibitive power to mitigate corrosion of AA2024-T3 at low molar concentration (less than 5 ppm). The properties of chromate are even more impressive when one considers that this inhibitor power is achievable on AA2024-T3, one of the most corrosion susceptible aluminum alloys. While it is widely recognized that an environmentally compliant alternative to chromate is needed, no single compound has been identified that has the same corrosion inhibition power as chromate materials. However, previous studies have shown that the combination of certain inhibitive

compounds can create synergistic effects that approach the performance of chromates on AA2024-T3. Unfortunately, there is no known method to predict these synergies and they must be identified ands characterized experimentally.

II. EFFORT REPORT

1. Objectives

- The objective of this project is to identify an environmentally compliant, synergistic combination of inhibitor compounds that can replace chromate-based pigments. Since synergism cannot be predicted, the experimental discovery of this combination is a strong candidate for high-throughput screening methods.
- Combinatorial methods for the development of chemical libraries are well established and relatively straightforward, however methods for the rapid identification of corrosion inhibitor performance are not. Thus, a secondary objective will be the identification of appropriate inhibitor performance metrics that will allow rapid screening and identification of corrosion inhibitors and synergistic combinations.
- Once suitable synergistic materials have been identified, this specific combination will examined in more detail to understand the origin of synergy for this particular pairing.

2. Summary of Activities – Status of Effort

- This last year has focused on the detailed investigation of two material combinations: $CeCl_3$ + $NaVO_3$ and $LaCl_3$ + Na_2MO_4. The Ce/VO3 combination demonstrates broad antagonism, while the La/MoO_4 combination demonstrates broad synergy. It was felt that an investigation of these pairs which are similar in chemical nature yet contrast in inhibitor performance would provide possible insight into the nature of synergy.
- The interaction of these materials with AA2024-T3 was investigated using: SEM, EDS, Raman microscopy, and electrochemical methods.
- The reaction product and supernatant were analyzed using inductively coupled plasma (ICP) in combination with a graduated ratio of materials edition to generate a Job's plot. This was done to gain insight into the stoichiometry of the reaction products.

3. Accomplishments and New Findings

- The combination of $CeCl_3$ + $NaVO_3$ has always demonstrated an antagonistic interaction according to all three high throughput screening (HTS) assays: DC bias, surface Cu assessment, and fluorometric determination of Al^{3+} concentration. The metric used in the DC bias test uses the average current between 7 and 9 hours when two AA2024-T3 wires are biased 100 mV from each other. The metric used in the surface copper measurement is the amount of elemental copper on the surface of a

AA2024-T3 wire following a 24 hour exposure to the test solution under open circuit conditions. The fluorometric technique quantifies the amount of Al ion released into solution following a 24 hour exposure of the AA2024-T3 wire to the test solution under open circuit conditions. The DC bias test energizes the electrochemical interface and is similar to linear polarization. It gives a result that is a measure of instantaneous corrosion rate. The other two HTS methods are non-energizing since they assess corrosion at open circuit conditions. They give an integral measure of corrosion similar to a weight loss measurement. Figure 1 compares the HTS results for the three different assays for three different RE-Silicate systems as a function of composition and pH. This figure reveals the high throughput capability of these methods and the cohesion of information that is obtained.

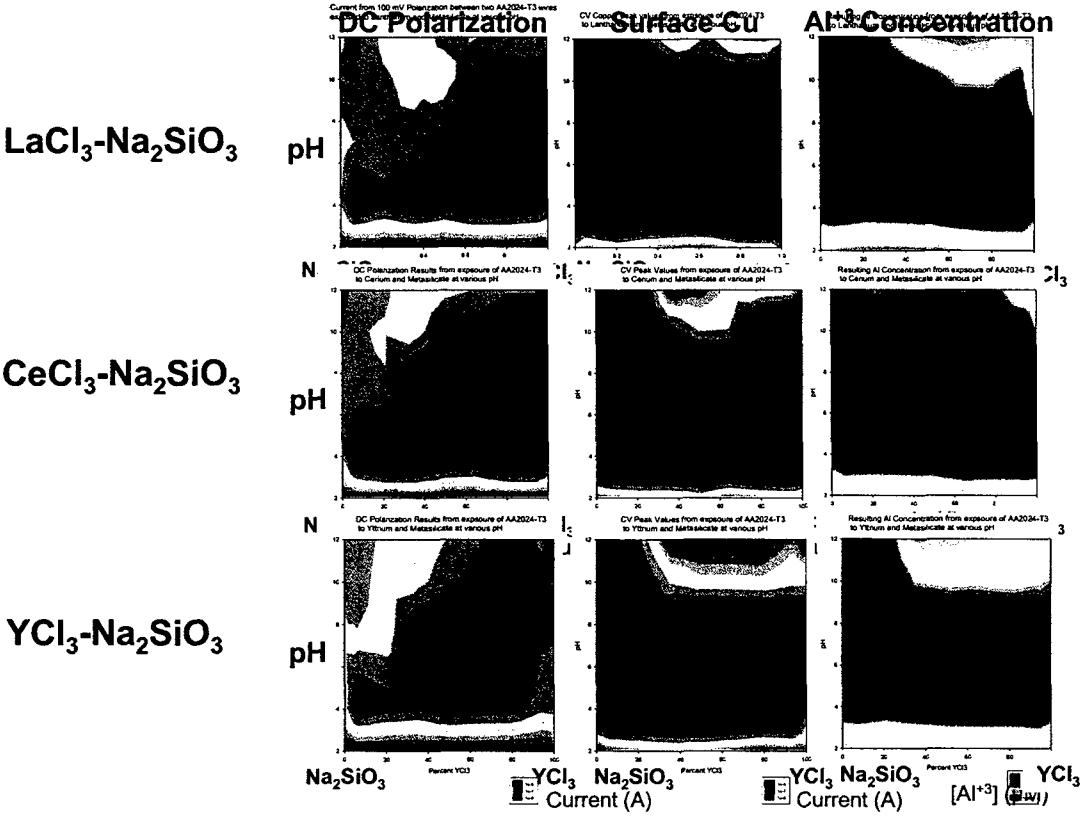

Figure 1. Composition-pH diagrams showing inhibitor performance for three rare earth-silicate systems using the three HTS assays, DC polarization, surface copper, and aluminum ion concentration.

- Other investigators within the MURI (van Ooij) have observed beneficial corrosion protection when using the combination of $CeCl_3$ + $NaVO_3$ within a coating system.
- The high throughput approaches developed for screening were further evolved to provide high throughput characterization. For example, the Multiple Microelectrode Analyzer (MMA) was used to perform 96 simultaneous polarization scans on 96 individual AA2024-T3 wires. These methods allowed the determination of the

effects of the inhibitor chemistries on the cathodic and anodic kinetics of AA204-T3 within minutes of substrate exposure to the inhibitors.

- The more rapidly initiated highly parallel polarization methods revealed a time effect of inhibitor interaction. At short times following inhibitor mixing, $CeCl_3$ + $NaVO_3$ demonstrated synergistic interaction. A few hours following mixing, the mixture of 3.4 mM $CeCl_3$ + $NaVO_3$ converted to antagonistic behavior.
- Chemical analysis of a 3.4 mM mixture of $CeCl_3$ + $NaVO_3$ in a glass beaker showed a rapid drop in constituent concentration and a significant drop in pH (ca. pH 3.5).
- As with $CeCl_3$ + $NaVO_3$, there is a polyoxometallate reaction between $LaCl_3$ and Na_2MO_4, and the effective concentration of constituents in solution is also reduced over time. However, the reaction is less susceptible to parameter variation, slower, and the resulting reaction product is more stable to pH changes.
- In the $LaCl_3$ + Na_2MO_4 system, synergy appears to be related to the heterogeneous precipitation of a pH stable reaction product. The Job's plot analysis of the reaction stoichiometry has revealed that the stoichiometry is dependent on the ratio of the reactants as well as whether chloride is present. This type of reaction variability is very typical of polyoxometallates.
- As summarized in the summary schematic of Figure 2, EDS analysis of AA2024-T3 exposed to graded ratios of $LaCl_3$ and Na_2MO_4, (total inhibitor 3.4 mM) show evidence of a bilayered lanthanum-containing and Mo-containing film on cathodic-type intermetallic particles (AlCuMg-containing and AlCuMnFeSi-containing phases). This is not observed on either end of the plot for the single inhibitor materials. Figure 3 shows the SEM micrographs and EDS spot analysis AA2024-T3 exposed to a specific La-MoO_4 chemistry for 24 hours. Further study should be directed to the actual films that form using measurement methods that are more specific to the surface (e.g., ATR-FTIR, Auger Electron Analysis). A benign self-assembled reaction product in the form of oblate ovoids and smaller spheroids could be seen distributed randomly on the surface.
- A Job's plot analysis to determine the reaction stoichiometry for mixing $LaCl_3$ and Na_2MoO_4 is shown in Figure 4. The ICP analysis of the reaction products are shown in Table 1. It can be seen that the elemental make-up of the product is not constant and depends on the ratio of A and B. The product also incorporates positive ions from the oxoanion (Na^+) as noted by reaction of materials in distilled water.

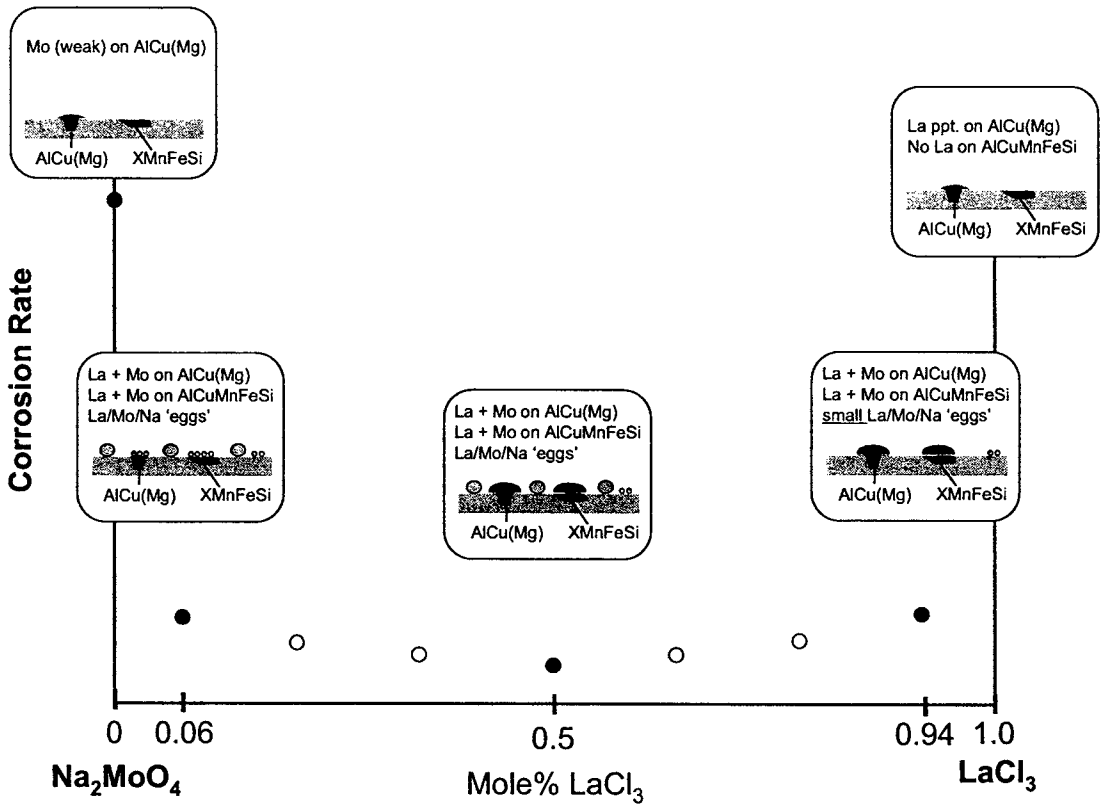

Figure 2. A schematic summary of the reaction products observed on AA2024-T3 when exposed to 3.4 mM $LaCl_3$ + Na_2MoO_4 for 24 hours. The X –axis represents the mole percent $LaCl_3$ in Na_2MoO_4, and the Y-axis is the corrosion rate as determined by all three HTS assays. Broad synergy is apparent by the reduced corrosion rates relative to either of the individual constituents. Note the bilayered-film that is associated with AlCu and AlCuMg-containing phases and the XMnFeSi-containing phases.

Table 1. Molecular formulas obtained by ICP analysis of the compounds formed at each molar ratio.

Mo molar fraction	0.6M NaCl
0.2	$[(MoO_4)_{10}La_6Na_9]Cl_7$
0.3	$[(MoO_4)_{13}La_8Na_9]Cl_7$
0.4	NA
0.5	$[(MoO_4)_{25}La_{15}Na_{10}]Cl_8$
0.6	$[(MoO_4)_{39}La_{22}Na_{13}]Cl$
0.7	$[(MoO_4)_6La_3Na_2]H$
0.8	$[(MoO_4)_{33}La_{14}Na_{34}]Cl_{10}$
0.9	$[(MoO_4)_{15}La_7Na_{10}]Cl$

4. Personnel Supported

S.R. Taylor	PI	20% effort
F. Contu	PDR Fellow	100%
S. Raman	PDR Fellow	100%
B.D. Chambers	GRA	100%
L. Fenzy	GRA (MS May '06)	100%

5. Publications

a. Referred Journals

1. S.R. Taylor and P. Moongkhamklang, "The Delineation of Local Water Interaction with Epoxy Coatings Using Fluorescence Microscopy", *Progress in Organic Coatings*, (in press).
2. F. Contu, S.R. Taylor, L. Fenzy, "An FT-IR Investigation of Epoxy Coating Interactions with Simulated Corrosion Blister Electrolytes", *Progress in Organic Coatings*, (accepted).
3. S.R. Taylor, S. Raman, F. Contu, P. Moongkhamklang, "The Use of Cationic Fluoroprobes to Characterize Ionic Pathways in Organic Coatings", *Progress in Organic Coatings*, (accepted).

4. B.D. Chambers and S.R. Taylor, "The High Throughput Assessment of Inhibitor Synergies on AA2024-T3 through Measurement of Surface Copper Enrichment", *Corrosion*, (in press).
5. B.D. Chambers, S.R. Taylor, "The High Throughput Assessment of Aluminum Alloy Corrosion Using Fluorometric Methods, Part I: Development of a Fluorometric Method to Assess Aluminum Concentration", *Corrosion Science*, (in review).
6. B.D. Chambers, S.R. Taylor, "The High Throughput Assessment of Aluminum Alloy Corrosion Using Fluorometric Methods, Part II: Rapid Evaluation of Corrosion Inhibitors and Synergistic Combinations", *Corrosion Science*, (in review).
7. B.D. Chambers and S.R. Taylor, "Multiple Electrode Methods to Massively Parallel Test Corrosion Inhibitors for AA2024-T3", NACE 2006 - San Diego, CA, Paper No.06678, National Association of Corrosion Engineers, Houston, TX (2006).
8. S.R Taylor and B.D. Chambers, "The Discovery of Non-Chromate Corrosion Inhibitors for Aerospace Alloys Using High-Throughput Screening Methods", 4th International Symposium on Aluminum Surface Science and Technology, Ed. By H. Terryn (in press).

b. Books/Book Chapters/Books Edited

None

c. Proceedings

1. B.D. Chambers and S.R. Taylor, "High Throughput Corrosion Assessment of AA2024-T3 in the Presence of Corrosion Inhibitors", in Coatings and Inhibitors, Ed. by M.W. Kendig, G.O. Ilevbare, R. Granata, and S. Kuroda, The Electrochemical Society, Pennington, NJ.

6. Interactions and Transitions

a. Participation at Professional Meetings, Conferences and Seminars

1. B.D. Chambers and S.R. Taylor, "High Throughput Corrosion Assessment of AA2024-T3 in the Presence of Corrosion Inhibitors, Fall 2005 Electrochemical Society Meeting.
2, B.D. Chambers and S.R. Taylor, "Multiple Electrode Methods to Massively Parallel Test Corrosion Inhibitors for AA2024-T3), NACE 2006. (with B.D. Chambers)
3. S.R. Taylor, B.D. Chambers, and F. Contu, "High Throughput Screening Methods for the Discovery of Non-chromate Corrosion Inhibitors", in NACE 2006 Research Topical Symposium, **(invited)**.
4. S.R. Taylor, G.J. Shiflet. J.R. Scully, R.G. Buchheit, W.J. vanOoij, C.J. Brinker, K. Sieradzki, R.E., Diaz, A.L. Moran, "Increasing the Functionality of Military Coatings Using Nano-dimensioned Materials", in Workshop on Multifunctional Materials, Keystone, CO.
5. S.R. Taylor, "The Use of Nano-dimensioned Materials for the Production of Advanced Coatings - Separating Fact and Fiction", in The Gordon Research Conference on Physics and Chemistry of Coatings and Films, New London, NH (invited).

6. S.R. Taylor, G.J. Shiflet. J.R. Scully, R.G. Buchheit, W.J. van Ooij, C.J. Brinker, K. Sieradzki, R.E. Diaz, A.L. Moran, "The Development of a Multi-functional Aerospace Coating Using Nano-Dimensioned Materials: A MURI Overview", in Tri-Service Corrosion Conference, - Orlando, FL.
7. S.R. Taylor, B.D. Chambers, and F. Contu, "New Methods for the Discovery and Delivery of Non-chromate Corrosion Inhibitors", in Tri Service Corrosion Conference, Orlando, FL.
8. S.R. Taylor, B.D. Chambers, and F. Contu, "The Discovery of Non-Chromate Corrosion Inhibitors for Aerospace Alloys Using High-Throughput Screening Methods", North Dakota State University, Dept. of Polymers and Coatings, Fargo, ND **(invited)**.
9. S.R. Taylor, B.D. Chambers, and F. Contu, "The Discovery of Non-Chromate Corrosion Inhibitors for Aerospace Alloys Using High-Throughput Screening Methods", University of Southern Mississippi, Dept. of Polymers Science and High Performance Materials, Hattiesburg, MS **(invited)**
10. S.R. Taylor, B.D. Chambers, F. Contu, "*The Hunt for Chromate Replacements:* Discovery of Promising Inhibitor Synergies Using High-Throughput Screening Methods", PPG Inc., Allison Park, PA **(invited)**.
11. S.R. Taylor, B.D. Chambers, and F. Contu, "The Discovery of Non-Chromate Corrosion Inhibitors for Aerospace Alloys Using High-Throughput Screening Methods", in 4th International Symposium on Aluminum Surface Science and Technology, Beaune, France.
12. S.R. Taylor, G.J. Shiflet, J.R. Scully, R.G. Buchheit, W.J. Van Ooij, C.J. Brinker, K. Sieradzki, R.E. Diaz, and A.L. Moran, "Increasing the Functionality of Coatings Using Nano-dimensioned Materials", (poster), in 4th International Symposium on Aluminum Surface Science and Technology, Beaune, France.
13. S.R. Taylor, "Research, Development, and Assessment of Environmentally Compliant Coatings and Inhibitors for the Protection of Military Assets" (poster), in Aging Aircraft Technical Interchange Meeting, Oklahoma City Air Logistics Center, Tinker AFB, OK.
14. S.R. Taylor, G.J. Shiflet, J.R. Scully, R.G. Buchheit, W.J. Van Ooij, C.J. Brinker, K. Sieradzki, R.E. Diaz, and A.L. Moran, "The Development of a Multi-Functional Aerospace Coating Using Nano-Engineered Materials" (poster) in Aging Aircraft Technical Interchange Meeting, Oklahoma City Air Logistics Center, Tinker AFB, OK.

c. Consultative and Advisory Activities

1. The Solar Group – Consultation regarding coatings used on mail boxes

d. Transitions - Professional Communications

1. Met with Professor Mario Geysen – Professor, Dept. of Chemistry, University of Virginia to discuss strategies for high throughput screening. (434)243-7741, geysen@virginia.edu
2. Held several conversations with Vasan Sundaram at Boeing Phantom Works to discuss applications of MURI technologies to Boeing programs. (253)773-3386.

3. Have held several meetings and conversations with Robyn McMillan, Manager of Corrosion Science, PPG Industries, Inc., (412)492-5218, rmcmillan@ppg.com to discuss transitionable technologies from MURI..
4. Have had several communications with Joerg Sander, Platform Manager Functional Coatings, Henkel Corporation, Dusseldorf, Germany, 49-211-797-9169, joerg.sander@henkel.com to discuss transitionable technologies from MURI.
5. Have had a meeting and several conversations with Bruce Hinto, Dr. Bruce Hinton DSTO, Melbourne, Victoria, 3207 AUSTRALIA. to discuss extensions of MURI research.
6. Have had multiple meetings and discussions with M.W. Kendig, Rockwell Scientific, LLC, Thousand Oaks, CA, (805)373-4241, to discuss MURI results amd transitionable technologies.

7. New Discoveries, Inventions, Patent Disclosures

1. "Novel Synergistic Combinations of Chromate-free Corrosion Inhibitors and Methods for Discovery Using High Throughput Screening", S.R. Taylor and B.D. Chambers, Provisional Patent Application No. 60/657,298.(March 2005), PCT filed March 2006.

8. Honors and Awards

Silver Medal Award – for Excellence in Research at the University of Mississippi Medical Center.

INHIBITOR ENCAPSULATION AND DELIVERY

C.J. Brinker, R.G. Buchheit, W.J. van Ooij, S.R. Taylor

I. PROJECT THRUST OVERVIEW

It is very unlikely that if an effective alternative inhibitor system for AA2024 can be identified, that it will also have an appropriate solubility for incorporation into paint. This phase of the MURI effort will examine various methods for solubility control and inhibitor delivery, which include nano-encapsulated structures (Brinker), hydrotalcite (HT) pigments (Buchheit), and encapsulation via plasma polymerization of powders (van Ooij). A new approach for the containment of corrosion inhibitors within a polymeric matrix, coordination compounds (Contu, Taylor) is also examined.

The objective is to engineer new molecular- and nano-structures that could:

(1) Supply inhibitors on-demand or as a response to specific external stimuli
(2) Impede corrosion by providing barrier properties or self-healing capabilities
(3) Provide self-sensing functionality.
(4) Sense water and aggressive ion uptake into the polymer.

6) Fractal aerogel films exhibiting 'superhydrophobic' properties for water exclusion, water collection, and self-cleaning.

- This year continued the study of the mass transport behavior in aerosol generated nanoparticles. We synthesized azobenzene-functionalized NaCl/silica particles, and measured their optically stimulated release behaviors. Also simulations were performed on the EISA during the aerosol process. As an easy means for corrosion inhibition, we developed a kind of anticorrosion sol-gel silane coating.

3. Accomplishments and New Findings

- In the last report, we prepared NaCl/silica particles by aerosol-assisted self-assembly using a vibrating orifice aerosol generator, and measured the NaCl release behavior in DI water using conductivity meter. Our group has investigated the photo-regulation of mass transport through a photoresponsive azobenzene-modified nanoporous membranes. (Liu NG, et al, *Nano Lett.* 2004). This year, we synthesized the azobenzene modified single crystal NaCl/nanoporous silica particles using the aerosol processing technique and the post-grafting synthetic method. This provides a novel model system for optically-controlled release of a target molecule with a well-understood solubility behavior. Prepared with a corrosion inhibitor or drug this approach has obvious applications in corrosion inhibition or the newly developing area of optically-targeted drug delivery. The optically switchable *trans-to-cis* conformational change of the azobenzene ligands attached on the pore surfaces controls the effective pore size, and correspondingly the releasing rate of the NaCl through the porous shells.
- Nitrogen elemental mapping, FTIR, NMR, and TGA characterization confirmed the successful synthesis of azobenzene modified single crystal NaCl/nanoporous silica particles. Figure 1 (left) shows a representative TEM image of the particle with a single crystal NaCl core and a nanoporous silica shell. To demonstrate the function of the azobenzene ligands attached on the pore surfaces, we performed the release experiment in deionized water under various conditions of illumination with UV or visible light. As shown in Figure 1 (right), the release of NaCl is very fast for the nanoparticles before azobenzene modification. The NaCl was released completely within *ca.* 7 minutes in the dark. UV exposure did not change the release rate. However, for nanoparticles after azobenzene modification, the release rate of NaCl is much slower. In the dark, the equilibration time is *ca.* 3.5 hours. Under UV exposure, the equilibration time is *ca.* 1.5 hours, indicating a faster release of NaCl than that in the dark. This is because UV light triggers the *trans-to-cis* conformational change of the azobenzene ligands, which in turn induces a dimensional decrease of *ca.* 3.4 Å. So, the effective pore size under UV irradiation is larger than that in the dark resulting in faster release.

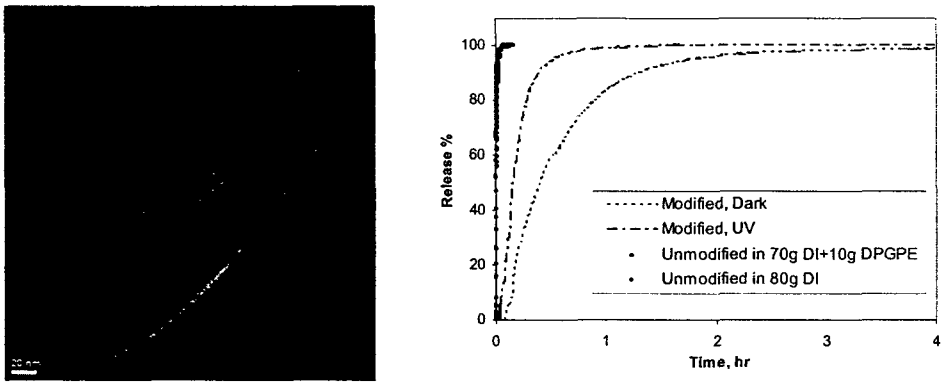

Figure 1. Left: TEM image of the azobenzene modified NaCl/porous silica particle; Right: NaCl release of unmodified and azobenzene-modified NaCl/silica particles in DI water.

- The addition of an amphiphilic additive to the external medium, such as dipropylene glycol propyl ether (DPGPE), has only a modest effect on the release rate of an unmodified particle (see Figure 1). However, the azobenzene functionalized particles show a strong effect of amphiphilic additives; the greater the addition, the slower the release. At the same level of additive, the release inhibition is in the order: dipropylene glycol propyl ether (DPGPE) > propylene glycol propyl ether (PGPE)> propylene glycol (PG) > propyl alcohol > ethanol. As shown in Figure 2, DPGPE greatly decreases the NaCl release rate from the functionalized core/shell particles. The equilibrium time for complete release of NaCl in the dark is *ca.* 150 hours for azobenzene-modified particles. Under UV irradiation, the equilibrium time for complete release of NaCl is decreased to *ca.* 90 hours. This provides an additional effective and convenient way for release control.

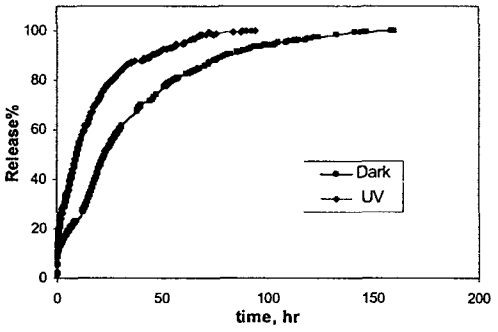

Figure 2. Photoresponsive release of azobenzene modified NaCl/silica particles in DPGPE/water solution (70g DI water +10g DPGPE).

- Simulation of aerosol evaporation is important to nanofabrication, spray drying, fuel combustion, pollution control, and medical applications. Coupled mass and heat transport and associated moving boundaries with the evaporation process remain challenging and prohibitive for quantitative description of the temporal process. A methodology has been developed recently for simulating the evolution of evaporating

droplets. The evaporation of water droplets in still air has been selected to validate the developed computer code. The effects of grid size, grid distribution, vapor phase size, and time step on the accuracy and convergence of simulation have been investigated. The simulation excellently predicted the evolution of water droplets over 700 seconds' evaporation.

- As shown in Figure 3 (left), the droplet temperature decreases quickly within the initial 20s and stabilizes at 278.9 K after 50s evaporation. It agrees well with the experimental equilibrium temperature. As shown in Figure 3 (right), the predicted droplet size decreases with time and agrees well with the experimental data. The code also simulates well the evaporation of ethanol droplets. The non-random two liquid (NRTL) model has been used to correlate the activity coefficients for ethanol-water vapor-liquid equilibria. A comparative study between the numerical simulation and quasi-steady state theory has been done. The code clearly demonstrates the evolution of composition, temperature, droplet size, and inhomogeneities for temperature and the compositions. It is inappropriate to treat it as a steady state or a quasi-state when all the properties change with time. The inhomogeneities are significant, and vapor phase temperature and composition gradients are far from those described by quasi-steady-state theory. The numerical simulation method describes accurately the effect of droplet size, droplet concentration, surrounding gas pressure, and surrounding gas temperature on the evaporation. The evolving concentration and temperature profiles are accurately calculated without using empirical scaling factors in conjunction with quasi-steady state theory. This simulation predicts well the evaporation behavior of multicomponents droplets over a short time.

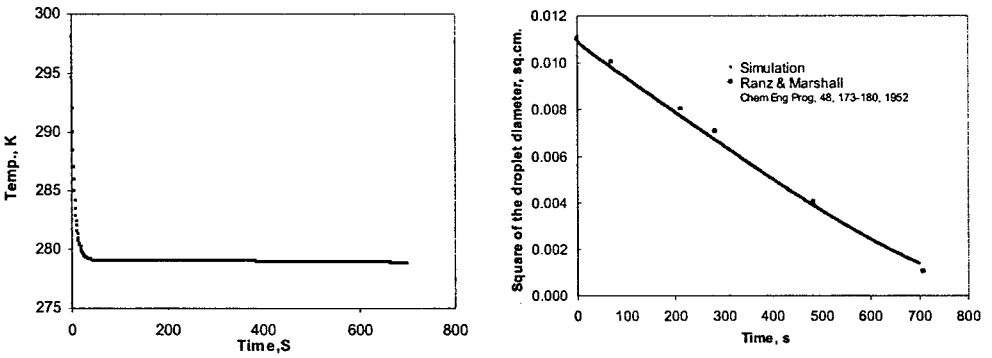

Figure 3. Left: Predicted droplet temperature depletion with evaporation time (700s); Right: Predicted droplet size depletion with evaporation time.

- To understand the EISA process, the evaporation of ethanol-water-NaCl droplet in nitrogen has been investigated by numerical simulation. Extended universal quasichemical (UNIQUAC) model combined with a Debye-Huckel term is used to describe the phase equilibrium for the moving boundary problem. Adiabatic and isothermal evaporation is a quick process. It takes 0.03~0.1s to reach equilibrium for initial 25°C, 1~2μm radius aerosol droplets of a concentration of $10^7/cm^3$. The droplets entering the heating zone can be assumed to be at equilibrium after ~1s evaporation in the drying zone, and the vapor/liquid phase compositions can be simply treated as a single-stage flash evaporation at 25°C. For 1 μm droplets, after 19 μs evaporation under 100 °C the NaCl saturation ratio reaches a value as high as 1.3

Pratik Shah	GRA	25%
George Xomeritakis	PDRA	25%
Seema Singh	PDRA	25%
Carlee Ashley	Undergrad.	20%
Adam Cook	Undergrad.	100%
Mai Nguyen	Undergrad.	50%
Ajay Bhakta	Undergrad.	20%

5. Publications

a. Refereed Journals

1. Wright, A; Gabaldon, J; Burckel, DB; Jiang, YB; Tian ZR; Liu, J; Brinker, CJ; Fan, HY, "Hierarchically organized nanoparticle mesostructure arrays formed through hydrothermal self-assembly", *Chemistry of Materials*, 2006, **18**, p.3034-3038.
2. Baca, HK; Ashley, C; Carnes, E; Lopez, D; Flemming, J; Dunphy, D; Singh, S; Chen, Z; Liu, N; Fan, HY; López, GP; Brozik, SM; Werner-Washburne, M; Brinker, CJ, "Cell-directed assembly of lipid-silica nanostructures providing extended cell viability", *Science*, July 2006, **313**, p.337-341.
3. Singh, S; Houston, J; van Swol, F; Brinker, CJ. "Drying transition of confined water". *Nature*, Aug 3 2006, **442**, p. 526. (Nature does not allow acknowledgements in *Brief Communication*)
4. Brinker, CJ; Dunphy, DR, Morphological control of surfactant-templated metal oxide films, *Current Opinion in Colloid & Interface Science*, Jun 2006, **11**, p. 126-132
5. Fan, HY; Wright, A; Gabaldon, J; Rodriguez, A; Brinker, CJ; Jiang, YB, Three-dimensionally ordered gold nanocrystal/silica superlattice thin films synthesized via sol-gel self-assembly. *Advanced Functional Materials*, May 2006, **16**, p. 891-895.
6. Jiang, XM; Brinker, CJ. Aerosol-assisted self-assembly of single-crystal core/nanoporous shell particles as model controlled release capsules. *Journal of the American Chemical Society*, April 2006, **128**, no 14, p. 4512-4513.
7. Fan, HY; Leve, E; Gabaldon, J; Wright, A; Haddad, RE; Brinker, CJ. Ordered two- and three-dimensional arrays self-assembled from water-soluble nanocrystal-micelles. *Advanced Materials*; Nov 4 2005; **17**, no.21, p.2587-2590.
8. Yang, K; Fan, HY; Malloy, KJ; Brinker, CJ; Sigmon, TW. Optical and electrical properties of self-assembled, ordered gold nanocrystal/silica thin films prepared by sol-gel processing.. *Thin Solid Films*; **491**, p.38; 2005.
9. Torquato, S; Donev, A; Evans, AG; Brinker, CJ Manufacturable extremal low-dielectric, high-stiffness porous materials.. *Journal of Applied Physics*; **97**, Art # 124103; 2005.
10. Fan, HY; Leve, EW; Scullin, C; Gabaldon, J; Tallant, D; Bunge, S; Boyle, T; Wilson, MC; Brinker, CJ. Surfactant-assisted synthesis of water-soluble and biocompatible semiconductor quantum dot micelles. *Nano Letters*; **5**, p.645; 2005.
11. Fan, HY; Chen, Z; Brinker, CJ; Clawson, J; Alam, T. Synthesis of organo-silane functionalized nanocrystal micelles and their self-assembly. *Journal of the American Chemical Society*; **127**, p.13746; 2005.

12. Doshi, DA; Dattelbaum, AM; Watkins, EB; Brinker, CJ; Swanson, BI; Shreve, AP; Parikh, AN; Majewski, J. Neutron reflectivity study of lipid membranes assembled on ordered nanocomposite and nanoporous silica thin films. *Langmuir*; **21**, p.2865; 2005.
13. Doshi, DA; Shah, PB; Singh, S; Branson, ED; Malanoski, AP; Watkins, EB; Majewski, J; van Swol, F; Brinker, CJ. Investigating the interface of superhydrophobic surfaces in contact with water. *Langmuir*; **21**, p.7805; 2005.

b. Books/Book Chapters/Books Edited

c. Proceedings/Reports

6. Interactions/Transitions

a. Participation at Professional Meetings, Conferences, and Seminars

Invited Presentations

1. Frontiers of Nanotechnology lecture series, *Bio-Inspired Self-Assembly of Porous and Composite 3D Nanostructures*, University of Virginia, Charlottesville, VA. April 10, 2006
2. Distinguished Alumnus Award Address, *Evaporation Induced Self-Assembly of Porous and Composite Nanostructures,* Rutgers University, New Brunswick, NJ. March 3, 2006
3. *Self-Assembly of Responsive Coatings for Corrosion Inhibition*, AFOSR 2005 Tri-Service Corrosion Conference, Orlando, FL. November 14-18, 2005.

Contributed Abstracts and/or Presentations at Professional Meetings

1. Chen, Z., Adams, D.P., Vasile, M.J., Liu, N., Jiang, Y.B., Xomeritakes, G., Brinker, C.J., *A Novel Design Toward Understanding and Characterizing Transport Behavior of Composite Mesoporous Silica Thin Films*, Materials Research Society Spring Meeting, April 17-21, 2006, San Francisco, CA.
2. Jiang, X., Brinker, C.J., *Self Assemblly of Responsive Core/Shell Nanostructured Particles*, Materials Research Society Spring Meeting, April 17-21, 2006, San Francisco, CA.
3. Brinker, C.J., Bunker, B., Burns, A., Liu, J., Sasaki, D., Shelnutt, J., Dattelbaum, A., Shreve, A., *Cooperative Phenomena in Molecular Nanocomposites*, 2005 DOE/BES Biomolecular Materials Program Meeting, August 25-28, 2005, Warrenton, VA.

b. Consultation and Advisory Activities

None

c. Professional Communications

- January 2004 – present
  Stuart Burchill, CEO

Industrial NanoTech, Inc.
Corporate Office
109 East 17th Street, Suite 15
Cheyenne, WY 82001
800-858-3176

This collaboration involves the development of new coatings for specialty insulation applications in high efficiency materials for architectural and manufacturing use. Mesoporous or aerogel materials tailored for specific applications, e.g. UV resistance, water repellancy, high R-value, will replace traditional ceramic particle fillers. CRADA funded July 2005.

- January 2005 – present
  David S Salloum, Ph.D.
  Emerging Technologies
  The Procter & Gamble Company
  11810 East Miami River Road
  Cincinnati, Ohio 45252
  Tel: (513) 627-0901
  Fax: (513) 277-7670

  P&G is interested in SH surfaces for a variety of consumers applications. We have supplied them SH coatings on various plastic and textile surfaces. Brinker gave lecture and demo on SH surfaces at P&G.

d. Transitions

- **Customer:** Uni-Pixel Displays, Inc., Lance Parker, (713) 398-4733
  Results: We have entered into a multiyear effort with Uni-Pixel to build prototype displays based on a UPD disruptive display concept that will utilize our ultra-low density/low refractive index coatings. We are also partnering with Lockheed-Martin Corp to build a prototype to demonstrate this technology for military and aerospace applications.
  Applications: Transparent, ultra-thin, high-resolution flat panel displays. Aircraft canopies, automobile windshields, information & status displays, entertainment devices.

  Customer: Stuart Burchill, Industrial NanoTech, Inc., 109 East 17th Street, Suite 15, Cheyenne, WY 82001, 800-858-3176
  Results: Coatings with 30 vol% aerogel fillers resulted in substantial improvements in insulating properties and excellent coatability. Organic matrix is tailored for compatibility with hydrophobic particles. 2nd year CRADA negotiations are underway.
  Applications: Highly insulating coatings for architectural and industrial applications, e.g. heating/air conditioning ducts, factory roofing, refrigerated transport units in ships and railcars, industrial storage containers.

Phase I/II STTR Program with Luna Innovations on Ultrahydrophobic Coatings awarded – PI - Dr. Bryan Koene, Senior Research Scientist, Luna Innovations (Bryan Koene, Ph.D., Phone(540)558-1699, Luna Innovations, Fax(540)951-0760, 2851 Commerce Street, Blacksburg, VA 24060, koeneb@lunainnovations.com, http://www.lunainnovations.com - This research in the area of ultrahydrophobic coatings will result in materials with superior properties for numerous applications. For example the following areas of active interest to Luna will be impacted by this research:

1. Anti Corrosion • Luna has several ongoing programs in the area of corrosion inhibiting coatings. The addition of a hydrophobic surface to these will be a great benefit to this work. If corrosive materials cannot permeate the surface in the first place, it will greatly extend the life of the coating and the underlying surfaces. • On the proposed program Luna will evaluate the effect of ultrahydrophobic coatings on the corrosion properties on aluminum substrates.
2. Chemical Protective Textiles • Luna has an effort in selectively permeable materials for chemical and biological warfare agent (CBWA) defense. The application of the hydrophobic coatings to membrane materials that possess high permeability of water will result in highly effective CBWA protective fabrics. • On the proposed program, Luna will apply ultrahydrophobic coatings to selectively permeable materials and fabrics to evaluate their effect on chemical protection.

7. New Discoveries, Inventions, Patent Disclosures

Patents

1. Fluid Light Guide Having Hydrophobic Aerogel Cladding Layer, U.S. Patent No. *6,983,093*, Issued *January 3, 2006*

Patent Applications

Patent Disclosures

1. C. Jeffrey Brinker; Pratik Shah; Eric D. Branson; Frank van Swol, "Processing and Patterning of Hydrophobic Coatings, DOE No./Sandia No. S-103,479/SD-7616
2. Helen K. Baca; C. Jeffrey Brinker; Dunphy, Darren; Brozik, Susan; Flemming, Jeb; Klavetter, Elmer, "A Cell-Based Biosensor", DOE No./Sandia No. S-102,154/SD-7431
3. Paul D. Calvert; Helen K. Baca; Eric D. Branson; C. Jeffrey Brinker; Pratik Shah, "High Resolution Ink-Jet Printing", SD-7515/S-102,263
4. Ying-bing Jiang; Joseph L Cecchi; C. Jeffrey Brinker, "Method of Making Dense, Conformal, Ultra-Thin Cap Layers for nanoporous Low-K LLD by Plasma-Assisted Atomic Layer Deposition", UNM#745

8. Honors and Awards

19. **C. Jeffrey Brinker** received the University of New Mexico Research Excellence Award in 2005
20. **C. Jeffrey Brinker** received by the Rutgers University Distinguished Alumnus Award in 2006

B. The Use of Nanoscale Phenomena in Hydrotalcites for Advanced Active Corrosion Protection and Corrosion Sensing in Opaque Coating Systems - R. G. Buchheit

1. Objectives

The overall objectives of this sub-project are to:

- Explore and demonstrate the utility of nanoscale structural and chemical phenomena in hydrotalcites and other inorganic ion exchange compounds to achieve an advanced forms of active corrosion protection and environmental awareness.
- Sense at early stages water and aggressive ion uptake in polymer coating systems.
- Explore and understand nanoscale phenomena of interested related to corrosion protection and sensing including ion exchange, and the structural memory effect of calcined hydrotalcites.

2. Summary of Activities – Status of Effort

- Explored the relationship between vanadate speciation and corrosion inhibition aluminum alloy 2024-T3 using anodic and cathodic polarization in conjunction with scanning electron microscopy and x-ray microchemical mapping.
- Developed a framework by which custom-made hydrotalcites could be tailored for different applications by interchanging cation hosts and inhibitor anion guests.
- Currently exploring the possibility of using hydrotalcites as "in-situ" chloride sensors.
- Explored the use of cerium-exchanged clay as an inhibiting and sensing pigments in organic coatings applied to Al alloys.• Explored the use of mixed cation and anion-exchanging clays as pigments that deliver synergistic mixtures of inhibitors in organic coatings.

3. Accomplishments and New Findings

- Vanadium species found in alkaline solutions (metavanadates) provide anodic and cathodic inhibition; species in acidic solution do not provide inhibition to an appreciable degree.
- Cathodic inhibition from vanadates is dependent on the presence of oxygen, while anodic inhibition occurs in both aerated and deaerated conditions.
- Hypothesized that metavanadates absorb and reduce on surface to form a thin film that slows cathodic reaction.
- Hydrotalcites with Al-Mg and Al-Li hosts were synthesized with V, Mo, P, and Si anions and screened to evaluate corrosion performance.
- EIS evaluation showed hydrotalcites with Al-Mg cation hosts containing V or Mo anions performed well, however only the V containing hydrotalcite performed well in salt spray.
- Looked at potential for synergistic inhibitor effect of Al-Mg-Mo hydrotalcite (anodic inhibitor) and Ce-bentonite (cathodic inhibitor). No real benefit was observed.
- Have made hydrotalcite sensors capable of detecting 5-6 orders of magnitude change in solution chloride concentration.
- The application of cerium exchanged bentonite as corrosion sensing pigments has been demonstrated and characterized. Release kinetic shows diffusion-controlled behavior with $t^{1/2}$ dependence.
- Cerium bentonite pigments shows modest corrosion protection and no self-healing effect, although blistering is minimized
- Promising pigments mix of zinc bentonite, cerium bentonite, and phosphate containing hydrotalcite has been identified. EIS data show comparable performance to that of strontium chromate. A yellow coating was formed on bare 2024-T3 surfaces exposed to the pigment slurry solution. Cerium and zinc have been identified as the two main components of the coating.

4. Personnel Supported

R.G. Buchheit	Investigator	3% effort
S. Mahajanam	GRA	10%
K. Ralston	GRA	100%
S. Chrisanti	GRA	100%

5. Publications

a. Refereed Journals

1. S. Chrisanti, R.G. Buchheit, "The Application of Cerium-Exchanged Clay as Corrosion Inhibiting and Sensing Pigments in Organic Coatings", in preparation.
2. S.P.V. Mahajanam, R.G. Buchheit, "Characterization of Inhibitor Release from Zn-Al-$[V_{10}O_{28}]_{6-}$ Hydrotalcite for the Corrosion Protection of AA 2024-T3," in preparation (2006).

3. S.P.V. Mahajanam, R.G. Buchheit, "Demonstration of Inhibitor Release and Corrosion Protection by Organic Coatings Containng a Zn-Al-Vanadate Hydrotalcite Pigment," in preparation (2006).
4. S.P.V. Mahajanam, R.G. Buchheit, "Exposure Testing of Organic Coatings Containing Calcined Zn-Al-Vanadate Hydrotalcite Pigments," in preparation (2006).
5. S.P.V. Mahajanam, R.G. Buchheit, "Application of Hydrotalcite as a Corrosion-Inhibiting Pigment in Exposure Testing," in preparation (2006).

b. Books/Book Chapters/Books Edited

1. R. G. Buchheit, S. P. V. Mahajanam, "Ion Exchange Compounds for Corrosion Inhibiting Pigments in Organic Coatings," ACS Symposium Series, New Developments in Coatings Technology, ACS, Philadelphia, PA (2006) accepted for publication.
2. R.G. Buchheit, "Corrosion Resistant Coatings and Paints," in Handbook of Environmental Degradation of Materials,' Myer Kutz, Ed., William Andrew Publishing, New York (2005).

c. Conference Proceedings

6. Interactions/Transitions

a. Participation/Presentations at Meetings, Conferences, Seminars, etc.

1. NACE, International Annual Meeting – San Diego, CA, March 2006. Chrisanti and Ralston presented posters. Buchheit gave an oral presentation.
2. Electrochemical Society Meeting, Los Angeles CA, October, 2005. Buchheit gave an oral presentation. Chrisanti gave a poster presentation in the Society general poster session.
3. Waterborne and Innovative Coatings Annual Symposium of the Cleveland Coatings Society, Buchheit presented an invited oral presentation.
4. ARMY Corrosion Summit, February, 2006, Clearwater Beach, FL, Buchheit gave an oral presentation.
5. Tri-Service Corrosion Meeting, November, 2005,Orlando, FL, Buchheit gave an oral presentation.

b. Consultative and Advisory Activities

c. Transitions

1. Sherwin Williams, Wai-Kwang Ho – on-going technical evaluation with Sherwin Williams. Buchheit has visited all major business units by invitation.
2. Henkel Surface Finishing Technologies, William Fristad. On-going interactions on vanadate corrosion inhibition.
3. PPG Industries, Robin MacMillan, Buchheit gave seminar at PPG Research Center.
4. Exxon-Mobile Research and Development Shuin Lin, Buchheit gave seminar at Annandale, NJ Research Laboratories.

5. Shepherd Color Company Ronald Sorice, Jeff, Simon Boocock. Shepherd Color is sponsoring research and development aimed at commercialization of hydrotalcite pigments for corrosion resistant coatings.

7. New Discoveries, Inventions, Patent Disclosures

8. Honors and Awards

1. R.G. Buchheit, John Weaver Award for Best Speaker, Waterborne and Innovative Coatings Symposium, Cleveland Coatings Society Annual Meeting. May, 2006.
2. S. Chrisanti, 1st Place Prize in the Electrochemical Society Student Poster Contest, October, 2005.

C. Insertion of Corrosion Inhibitive Species into the Polymer Matrix via Coordination Compounds – S.R. Taylor, F. Contu

1. Objectives

- One class of molecules that is of interest as a possible means for containing and delivering inhibitive species in organic coatings is the coordination compound. These are chemical species constituted by a central cation surrounded by a number of anionic organic molecules called ligands. Coordination compounds are chemical species that possess the advantages of both organic and inorganic inhibitors for use in coatings on aluminum alloys.
- The stability of coordination compounds is determined by the magnitude of the equilibrium constants (Kf) that leads to the formation of the complex.
- The application of coordination compounds as corrosion inhibitors for organically coated aluminum alloys may have several advantages compared to inorganic salts. First, ligands, such as molecules with extended delocalized π-orbitals, may facilitate the electron exchange between the central cations and the environment (anodic inhibitors) as well as the stabilization of intermediate oxidation states.
- Second, organic molecules used as ligands, offer the possibility of distributing metal cations homogeneously into an organic coating, such that chemical binding of the coordination compound to the matrix occurs, thus preventing distribution and release into the environment.
- Furthermore, release of inhibitor under demand might be an important feature of metal complexes.
- Moreover, coordination compounds absorb radiation in the UV-vis region of the electromagnetic spectrum and their spectroscopic characteristic (absorption frequency) change as a function of both the oxidation state of the central cation and the nature of the ligands. Thus, corrosion may be easily detected by local changes in the color or UV absorption spectrum of the structures undergoing failure.

Figure 1. Coordination compounds tested. Er(III) and Nd(III) are earth rare cations that, like Ce(III), could precipitate as oxides or hydroxides on active cathodic sites and act as cathodic inhibitors. Ce(IV) is a powerful oxidizer and, when released on demand, could facilitate the repassivation of the aluminum substrate. Additionally, Ce(IV), by reducing to Ce(III), would also provide a powerful cathodic inhibitor. All of the ligands are organic species that allow homogeneous distribution of the central cations within the epoxy matrix

3. Accomplishments and New Findings

- Local Electrochemical Admittance Mapping (LEAM) of AA2024-T3 alloy coated with epoxy film containing the complex Ce(III)acetylactone suggested that release-on-demand of Ce(III) occurs when its concentration in the coating is 0.1 wt%. In fact, at this concentration, the admittance peaks decrease over time and they are significantly lower than those observed at ten times more diluted concentration. This is shown in Figure 2.

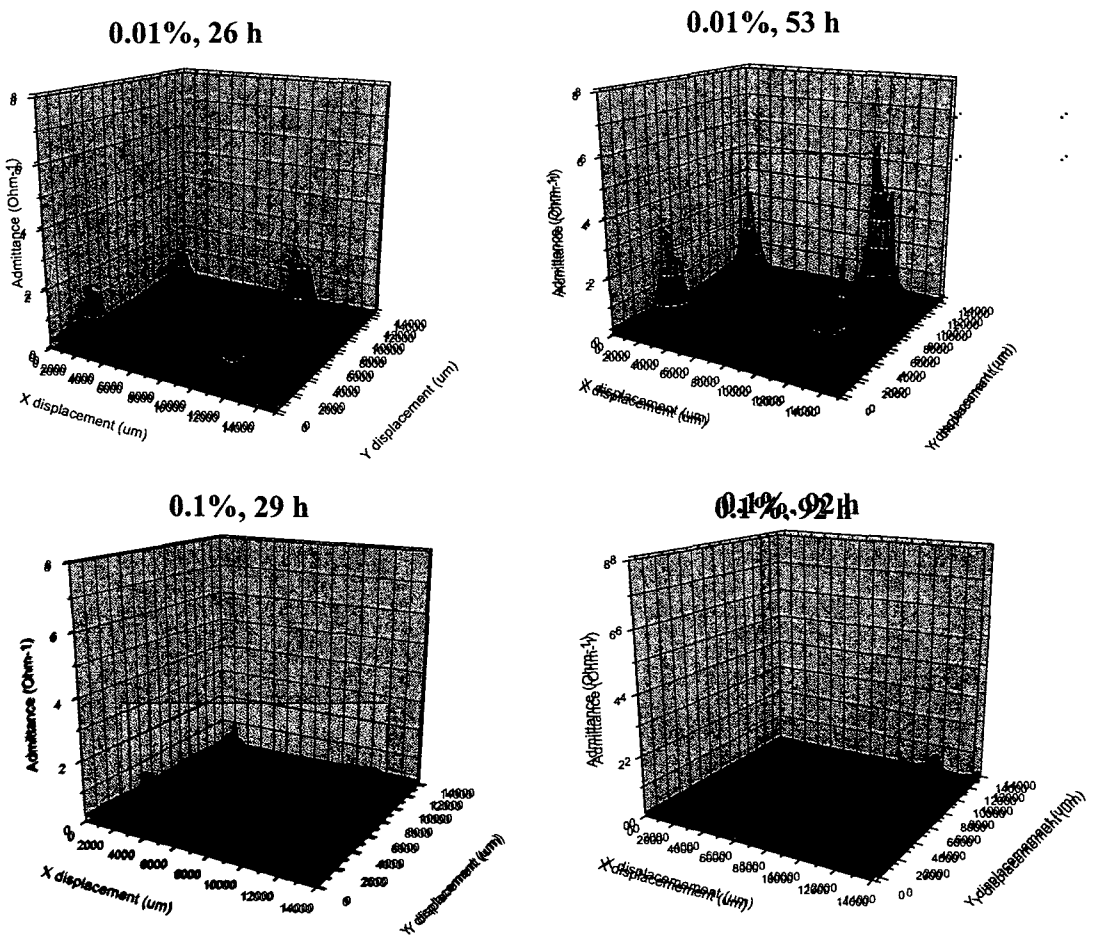

Figure 2. Preliminary evidence showing reduction in LEAM peaks over time with epoxy coatings on AA2024 panels containing higher Ce(III)acac concentrations (0.1 wt.%). Note even this "high" concentration is orders of magnitude less concentration than conventional inhibitive pigments.

Global electrochemical impedance spectroscopy was performed over time on epoxy coated AA2024-T3 panels containing coordination compounds exposed to 0.5M NaCl. These results are summarized in Figure 3.

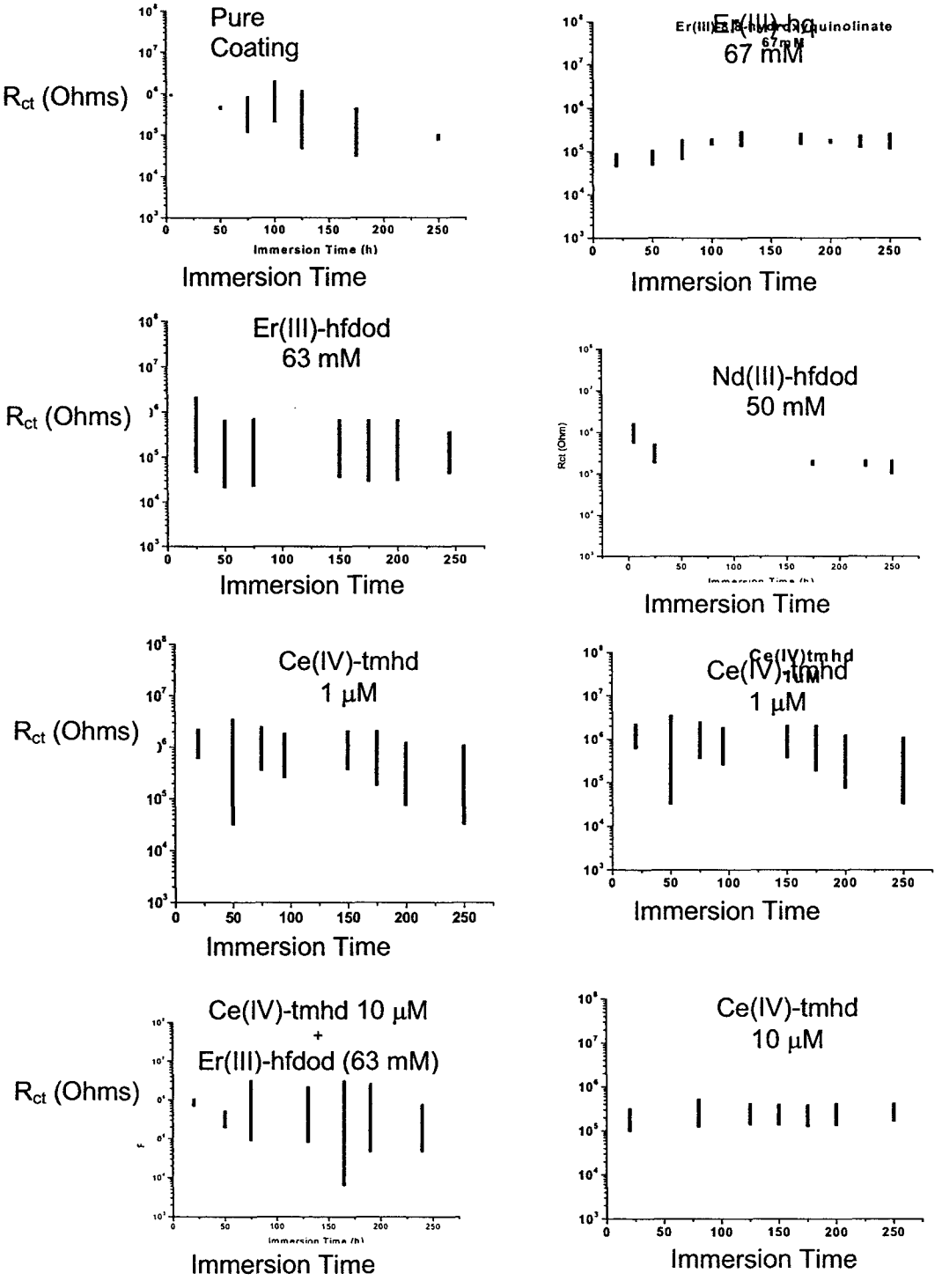

Figure 3. Charge transfer resistance (Rct) (Ohms) from global EIS data for coordination containing epoxy coatings on AA2024-T3 panels as a function of exposure time in 0.5 M

NaCl. Note the increasing or stabilizing trends observed for Eb(III) and higher concentrations of Ce(IV).

- Each bar of Figure 3 represents the range of the charge transfer resistance values (R_{ct}) ($n \geq 4$). The pure coating exhibited large bars that indicate a significant scatter in the resistance values. Additionally, a decrease in the values of the resistance is observable. In contrast, coatings containing Er(III)-hq and Ce(IV)-tmhd displayed resistance values that were very reproducible, and in the case of Er(III) containing coatings, showed an increase in the resistance values over time. This suggests release of Er(III) species which act as inhibitors. The concentration of the coordination compounds in the coating is important as illustrated by the behavior of the coating containing Ce(IV) species. Concentrations in the order of 1mM do not stabilize the performance of the pure coating, whereas 10 mM concentrations gave better stability to the films.
- Figure 4 summarizes the Rct range for the various coatings at 250 hours of exposure.

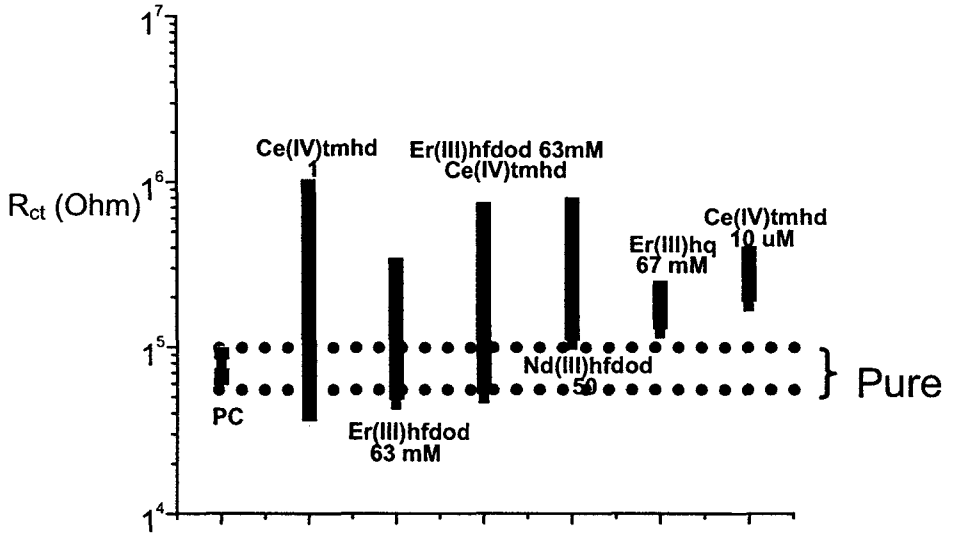

Figure 4. R_{ct} range at 250 h - 4 samples tested for each coordination compound. The range for the neat coating is shown by the dashed red lines.

- UV-Vis data of aqueous phases exposed to a xylene phase containg the coordination compounds shows evidence of cation exchange. These experiments are continuing.
- ICP analysis of acidified aqueous solutions containg cured epoxy coatings containing the coordination compounds does not show evidence of cation exchange. Either the ligands have been assimilated into the epoxy chemistry in such a way so as to lock the central cation in place, or the concentrations and times od release are insufficient so as to release a measurable level of cations. This research will continue

D. The Control of Inhibitor Solubility by Plasma Film Encapsulation - W.J. van Ooij

1. Objectives

- A superprimer coating for aluminum alloys was developed earlier in this project. It is acrylate-epoxy based and contains the following components: an acrylic resin dispersion, an epoxy resin dispersion, an isocyanate based crosslinker, a hydrophobic bis-sulfur silane and it can be loaded with a fairly high amount of chromate-free corrosion inhibitor. This superprimer composition without the inhibitor was originally termed L2. The L2 notification will be used occasionally further on.
- The objective this year was to finalize the optimization of the above described superprimer using a Taguchi approach based on L9 orthogonal arrays.
- The optimized superprimer was extensively characterized in order to understand the pot-life of the formulation, the film formation and curing chemistry of the coating.
- One of the main objectives was to understand the corrosion protection mechanism by which this superprimer coating protects the aluminum alloys AA2024-T3 and AA7075-T6. This particularly included investigating the role of the pigment in the corrosion protective mechanism of the entire system

2. Summary of Activities

- The corrosion performance of the above mentioned superprimer containing zinc phosphate (ZP) was evaluated by using electrochemical impedance spectroscopy (EIS). The EIS results of the superprimer coating with and without 30 wt.-% ZP were compared with the results of the corresponding coating containing 30 wt.-% chromate. The ZP containing coating did not show degradation within 30 days of EIS testing.
- The optimized superprimer was characterized by using SEM/EDX to determine the structure of the film and the corrosion protection mechanism of the film. The layered structure of the superprimer is shown in Figure 1.
- The metal-coating interface of the superprimer was investigated by Time-of-Flight Secondaty Ion Mass Spectroscopy (ToF-SIMS). The ToF-SIMS characterization was done by breaking the sample to remove the coating from the metal. Both the delaminated coating and the metal side of the freshly generated surfaces were investigated. Diffusion of aluminum into the superprimer was observed in the superprimer. Contrary to expectations the outmost layer of the interface was not found to be silane-rich. It consisted of primarily acrylate-based bonds.

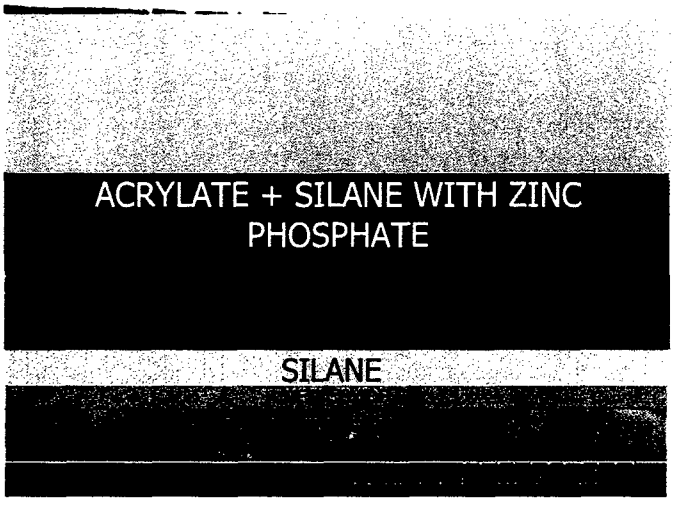

Figure 1. The superprimer on AA 7075-T6 consists of three layers, which are self-assembled upon drying of the coating.

- The water-uptake of free-standing superprimer films was compared to the electrolyte uptake of corresponding films on aluminum. The water-uptake of the free-standing films was determined by precision weighing and the electrolyte uptake of the films on metals was investigated by using EIS. The epoxy layer was found to impede water uptake from the top (Figure 1). The acrylate layer was found to have a higher rate of water uptake. Such a structure facilitates the leaching of the corrosion inhibitor only when the water is taken up by the acrylate layer, which can take place only when the coating is damaged by a scribe. Thus, the above coating successfully mimicks the "self-healing" property of the chromate-based primers.
- The leaching rate of $Zn_3(PO_4)_2$ from the coating was determined by Inductively Coupled Plasma Mass Spectroscopy (ICP-MS). The superprimer coating investigated was the one loaded with 30 wt.-% ZP. DI water was used as the media and water was in contact with the hydrophilic side of the coating. The Zn and P concentration in the water was monitored vs. time. Figure 2 shows the amount of Zn and P ions released from the coating per unit area as a function of time exposed to water.
- The curing chemistry of the superprimer coating was characterized by using Fourier Transform Infrared – Reflection Absorption (FTIR-RAIR) spectroscopy and solid-state ^{29}Si Nuclear Magnetic Resonance (NMR) spectroscopy.
- The FTIR-RAIR characterization was done by studying all possible two-component interactions in the films between the four-components of the superprimer over a 11-day period. The epoxy was seen to react with the isocyanurate-based crosslinker added to form a urethane bond due to the reaction of the -N=C=O group with the geminial -OH group of the epoxy. Further hydrolysis of the crosslinker to form Si-OH silanol bonds was observed, which condensed by reacting with one another to form a Si-O-Si network and thereby crosslinking the epoxy. Acrylate interaction with the silane in the bottom layer identified in the SEM/EDX analysis was found to be primarily hydrogen bond-based.

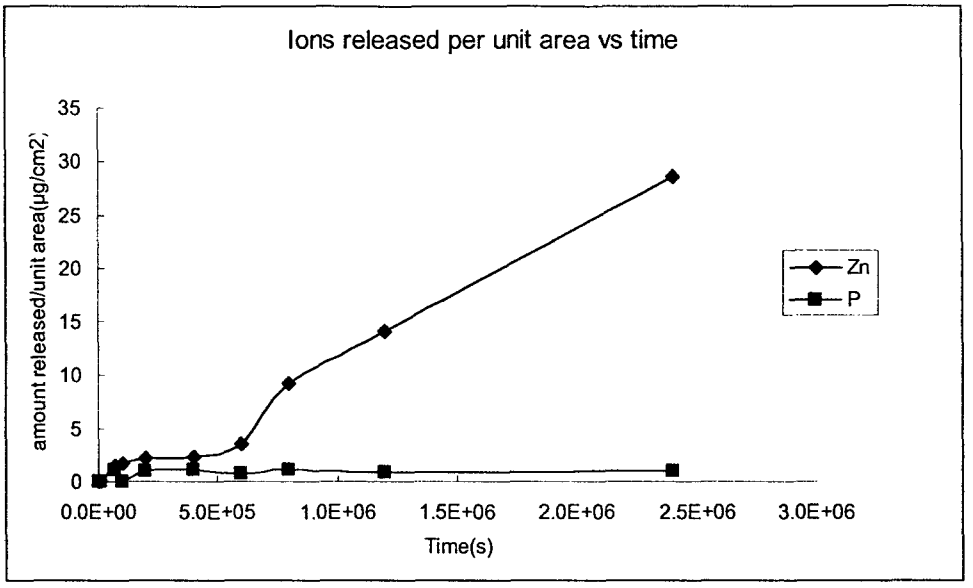

Figure 2. The Zn and P ions released from the coating per unit area as a function of time exposed to water.

- For solid-state ^{29}Si NMR analysis superprimer systems differing in the type of silane were prepared; with the first being formulated with BTSE, the second with bis-sulfur silane and the third with a combination of the both in a ratio of 2:1. These film systems were then analyzed over a period of time. According to the solid-state NMR results, BTSE-based superprimers were found to form a large number of T1 and T2 condensation products and bis-sulfur silane-based superprimers were found to form a large number of T3 condensation products.
- The pot-life chemistry of the system was studied by investigating the chemical reactions in the formulation component combinations with liquid-state ^{29}Si and ^{13}C NMR as a function of time. Based on the results, interaction of silanol groups of the hydrolyzed silane with the geminal -OH group of the epoxy was detected. Interestingly no hydrolysis products of the silane were seen in the liquid-state NMR.
- The production of the ECO-CRYL 9790 acrylic dispersion was discontinued by the manufacturer during the last year of MURI. A replacement for it needed to be sought by screening several acrylic dispersions together with suitable epoxy dispersions. This was done systematically by investigating many possible replacements pairs for the original acrylate-epoxy pair (ECO-CRYL 9790 and EPI-REZ WD510).
- The mechanical properties of the ZP containing superprimer coating have also been evaluated. Stretch tests were done to learn how the coating will perform under strains. The test coupons were made by casting the coatings on parafilm. The strength of the L2 + 30 wt.-% ZP superprimer is 2.3 MPa. It was found to fail at the strain of 20 %.
- Many inhibitors were tested for the AA2024-T3 and AA7075-T6 aluminum alloys and many inhibitors and inhibitor combinations were screened by incorporating various amounts of them into the optimized superprimer. The techniques used to evaluate the corrosion resistance of the inhibitors for aluminum have included DC polarization, extraction immersion and salt water immersion tests.

- The packability of the superprimer was investigated. This means that the components were packed into a two-pack system. The packs were aged. Every two months specified portions of the packs were mixed and the resulting coating was sprayed onto AA2024-T3. The performance of the coating was determined by different test methods.

3. Accomplishments and New Findings

- The acrylate-epoxy based superprimer was optimized and it was demonstrated that high levels of chromate-free corrosion inhibitors can be loaded in the optimized formulation of the superprimer by loading it with 30 wt.-% $Zn_3(PO_4)_2$. This chromate-free primer system performs similar to a chromate-containing primer system on aluminum. The superprimer alone on AA2024-T3 survives 2000 hrs of ASTM B-117 salt spray testing.
- Nano-sized SiO_2 and cerium silicate were found to be additional effective inhibitors (besides $Zn_3(PO_4)_2$) for the superprimer on aluminum.
- The acrylate-epoxy based superprimer was extensively characterized. The final coating was found to be a self assembled three-layer coating (Figure 1) and a corrosion-protective mechanism was proposed and evaluated for this system. The three layers in the coating consist of a silane-rich layer at metal-primer interface, a silane-rich hydrophilic acrylate layer containing the inhibitor, and a hydrophobic epoxy layer as the third layer on top of the coating.
- Promising replacements were found for the ECO-CRYL 9790 acrylic dispersion that was originally selected as an ingredient for the formulation. The combination of Rohm & Haas' Maincote AE58 acrylic resin together with Daubert's Daubond DC9010 epoxy resin was found to be a good replacement combination with lower VOC, faster curing rate and better anti-corrosion performance than the original resin combination.
- The optimized superprimer was found to be packable into a two-pack system, the performance of the resulting coatings was found to be good so far and the packs are at least stable for more than 4 months.

4. Personnel Supported

Wim J. van Ooij	PI	5% effort
Anuj Seth	GRA	100%
Lin Yang	GRA	30%
Zhangzhang Yin	GRA	100%
Paula Puomi	PDRA	50 %

5. Publications

a. Refereed Journals

1. A. Seth, W.J. van Ooij, P. Puomi, T. Metroke and A. Appblett, 'Characterization of Novel Primer Systems using liquid-state ^{29}Si and ^{13}C NMR', will be submitted to *Prog. Org. Coat.*
2. A. Seth, W.J. van Ooij, P. Puomi, Z. Yin, A. Ashirgade, S. Bafna and C. Shivane, Novel, 'One-step, Chromate-free Coatings Containing Anticorrosion Pigments for Metals – an Overview and Mechanistic Study', accepted for publication in *Prog. Org. Coat.*
3. W.J. van Ooij, D. Zhu, M. Stacy, A. Seth, T. Mugada, J. Gandhi and P. Puomi, Corrosion Protection Properties of Organofunctional Silanes – An Overview, Tsinghua *Science and Technology*, 10 (2005) 639-664

b. Books/Book Chapters/Books Edited

1. A. Seth and W.J. van Ooij, 'Optimization of One-step, Low-VOC, Chromate-free Novel Primer coatings using Taguchi Method approach', in Press (for Publication in ACS Symposium Series Book Ed. P. Zarras)

c. Proceedings

1. A. Ashirgade, P. Puomi, W.J. van Ooij, S. Bafna, A. Seth, C. Shivane and Z. Yin, 'Novel, One-step, Chromate-free Coatings Containing Anticorrosion Pigments for Metals that can be used in a Variety of Industries', paper to be published on a conference CD, Eurocorr 2006 in Maastricht, Sep 24-28, 2006.
2. P. Puomi, W.J. van Ooij, A. Seth, Z. Yin, A. Ashirgade, S. Bafna and C. Shivane Novel, 'One-step, Chromate-free Coatings Containing Anticorrosion Pigments for Metals', Extended Abstract in the Book of Abstracts of Coatings Science International, Noordwijk, The Netherlands, 26-30 June (2006) 74-78.
3. W.J. van Ooij, P. Puomi, A. Ashirgade, S. Bafna, A. Seth, C. Shivane and Z. Yin, 'Low-VOC, Chromate-free, Anti-corrosion Primers for Aluminum Alloys and HDG steel', presented at Megarust 2006, June 12-15, Norfolk, Virginia, http://www.nstcenter.com/RUST2006/presentations/thu/MR2006-22P.Puomi.pdf
4. W.J. van Ooij, A. Seth, L. Yang, Z. Yin and C. Shivane, 'Novel approaches in the development of environmentally compliant coatings for corrosion protection of metals', Proceedings of Hawaii PPF XI Conference 2005.
5. W.J. van Ooij, A. Seth, C. Shivane, A. Ashirgade, S. Bafna, L. Yang and P. Puomi, 'Superprimer: Chromate-free, low-VOC, systems eliminating chromate conversion coatings', Poster Presented in Tinker Air Force Base Conference 2005.
6. A. Seth and W.J. van Ooij, 'A Novel, low-VOC, Chromate-free, one-step primer system for the corrosion protection of metals and alloys", presented at the Fifth International Symposium on Silanes and Other Coupling agents Toronto, Canada, June 22-24, 2005 and has been accepted for publication in Silanes and Other Coupling agents Ed. K.L. Mittal.
7. L. Yang, N. Simhadari, A. Seth and W.J. van Ooij, 'Novel Corrosion Inhibitors for Silane Systems on Metals", presented at the Fifth International Symposium on Silanes

and Other Coupling agents Toronto, Canada, June 22-24, 2005 and has been accepted for publication in Silanes and Other Coupling agents Ed. K.L. Mittal

6. Interactions/Transitions

a. Participation at Professional Meetings, Conferences and Seminars

1. Fifth International Symposium on Silanes and Other Coupling agents Toronto, Canada, June 22-24, 2005 (2 papers)
2. Tinker Air Force base Conference 2005
3. Hawaii PPF XI Conference 2005
4. Megarust 2006, Norfolk, Virginia, June 12-15, 2006
5. Coatings Science International, Noordwijk, The Netherlands, 26-30 June, 2006
6. Eurocorr 2006 in Maastricht, Sep 24-28, 2006
7. 15th IFHTSE Conference in Vienna, Austria, Sep 25-29, 2006
8. 14th Asian-Pacific Corrosion Control Conference in Shanghai, China, Oct 21-24, 2006

.

b. Consultation and Advisory Activities

1. Presentation at PPG Industries Inc., Allison Park, Pittsburg, PA, about all silane-containing corrosion protective systems – including the MURI results

c. Transitions- Professional Communications

1. ECOSIL Technologies, LLC, Cincinnati, Ohio; start-up company has done lab-scale collaboration with PPG Industries Inc. on silane treatments and superprimers developed in the MURI project. Contact: Mr. Max Sorenson, 801-568-0227.
2. Discussions have been continued with Sherwin-Williams in Cleveland, Ohio, about a scale-up of the anticorrosive pigments that are being developed in this project; contact: Dr. Jugal Doshi, 216-505-7935

7. New Discoveries, Inventions, Patent Disclosures

Invention Disclosures

1. A Superprimer for Metals with Tunable Composition (with Anuj)
2. A Novel Anticorrosion Paint Pigment, $CeVO_4$ (with Lin Yang)
3. Ion-exchanged Pigment for Superprimers (with Lin)
4. A Comprehensive Superprimer Formulation (with Akshay, Chetan, Lin, John, Shekhar, Anuj)
5. A Superprimer for Concrete and Bricks (with Anuj)
6. Cerium Silicate, A New Anti-Corrosion Pigment for AI Alloys (with John Yin)

Patent Applications

1. W.J. van Ooij, A. Seth, L. Yang and D. Zhu, US Patent Application, 'Improved Superprimer', December 22, 2005

8. Honors and Awards

- Received Special Achievement Award from UC for submitting 100th invention disclosure on silane-related technologies.

STRATEGIES FOR ADDED COATING FUNCTIONALITY

K. Sieradzki and R. Diaz

I. PROJECT THRUST OVERVIEW

The main objective of this program thrust is to investigate various approaches to add certain functionalities to a coating system. We are focusing on the following issues: (1) the development of an integrated sensor system that can be easily interrogated vis-à-vis development of corrosion or mechanical damage of the protected structure, (2) development of an on-board corrosion inhibitor delivery system that can serve as a sensor/response element and (3) development of a coating that can alter its color on demand. The color-on-demand task has been added subsequent to the initial start of this MURI program.

II. EFFORT REPORT

A. Development of Large-Scale Colloidal Crystal Assemblies for Sensing – K. Sieradzki

1. Objectives

The objective is to develop a sensor with on-board inhibitor delivery and has been approached through the use of novel *photonic crystal structures*. These photonic crystals can then be incorporated into a polymer topcoat or total polymer coating system. Photonic crystals are structures in which the dielectric constant varies periodically in space. The periodicity is that of microscopic dielectric particles instead of atoms. This produces many of the same phenomena for photons (light modes) as the atomic potential produces for electrons. In analogy to the diffraction of x-rays by atomic structures, mesoscale photonic crystals diffract light in the range of ultraviolet through the visible spectrum to near infrared. Three general approaches have been employed for optical sensing of damage employing colloidal crystal structures: (1) Bragg diffraction from ordered self-assembled (111) textured films made by evaporation. (2) Ordered monolayer of polystyrene particles, forming in effect, a diffraction grating with spacing changing with deformation. (3) Ordered arrays of gold nanoparticles encased in silica yielding plasmon resonance peaks of amplitude that depend on lattice spacing. Figure 1 shows some of our most recent results based on plasmon resonance.

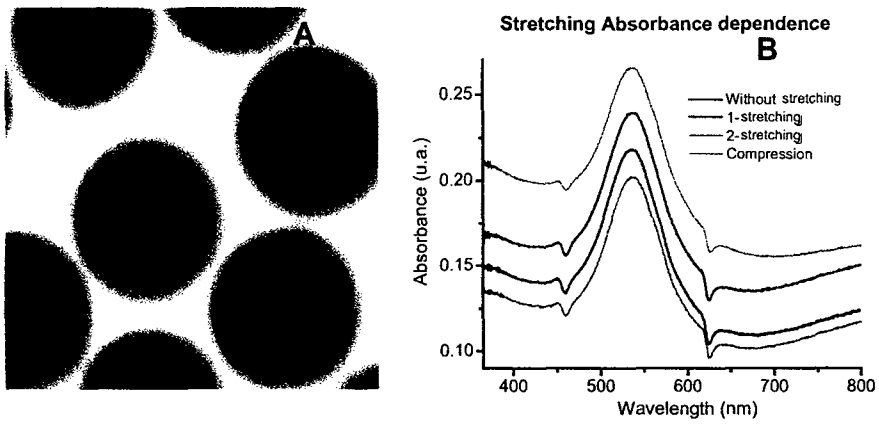

Figure 1. Silica-encased gold nanoparticles sensor. Particle diameter is 15 nm. Increasing the diameter of the silica shell, encasing the Au nanoparticles, allows us to tune the plasmon resonance. (A) TEM micrograph of the nanoparticles assembly. (B) Shift of the amplitude of the plasmon resonance peak with stretching. Black; no stretching, red and green; tensile stretching; blue in compression.

2. Summary of Activities – Status of Effort

- Development of Large-Scale Colloidal Crystal Assemblies. Three general approaches have been employed for optical sensing of damage employing colloidal crystal structures: (1) Bragg diffraction from ordered self-assembled (111) textured films made by evaporation. (2) Ordered monolayer of polystyrene particles, forming in effect, a diffraction grating with spacing changing with deformation. (3) Ordered arrays of gold nanoparticles encased in silica yielding plasmon resonance peaks of amplitude that depend on lattice spacing.
- Study of Colloidal Crystal as Strain Sensors. We used optical diffraction to study the change in interplanar spacing of colloidal crystals during straining and demonstrated that these structures can serve as sensitive strain sensors.
- Color on Demand. The approach adopted was to assess two parallel paths both experimentally and computationally. One path was to prove that microscopic all solid-state electrochromic cells can be made. The second path was to demonstrate that mechanically tunable photonic antennas can be used to generate coloration.

Colloidal Crystal as Strain Sensors.

- Colloidal crystals comprised of poly(styrene) (PS) spheres were grown on nylon substrates that subsequently were pulled in tension to examine the shift in *d*-spacing. We were limited by the wavelength resolution of our spectrometer which is ~ 0.3 nm at the position of the Bragg peaks. To our knowledge this is the first set of results demonstrating this behavior for 2-D colloidal crystals made by evaporation.

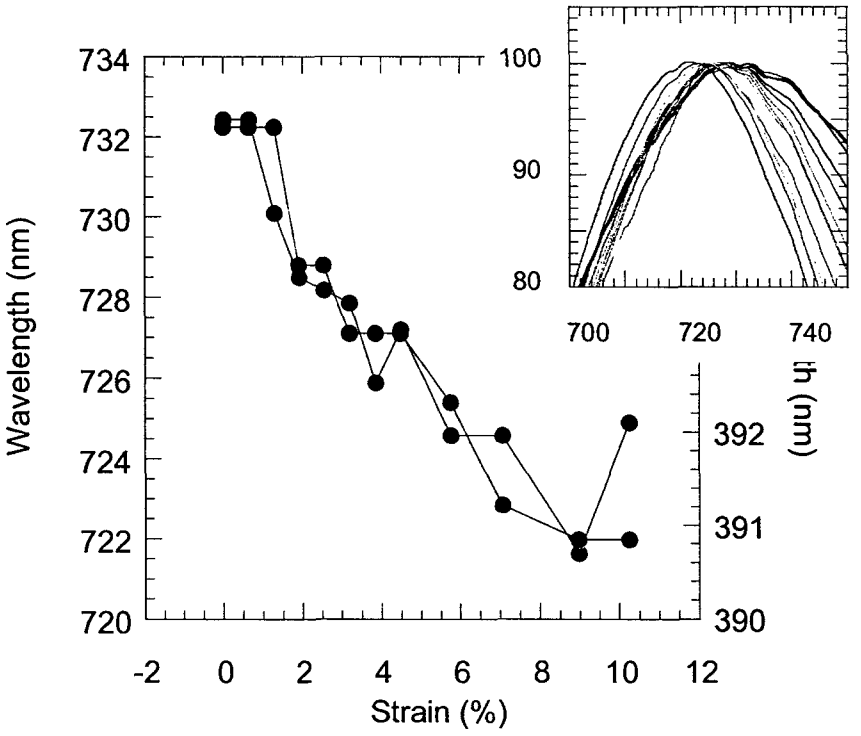

Figure 1. Results of stretching experiments of 2-D evaporated colloidal crystals grown on nylon. The crystals were composed of 300 nm particles grown from a solution containing starch to promote adhesion. Reflectance spectra showing the general shift to lower wavelengths of the Mie (red line) and Bragg (black line) peaks with increasing strain. The inset shows the Bragg diffraction peaks shifting to lower wavelengths with increasing strain.

- We have used the results in Figure 1 to determine the Posisson's ration for our colloidal crystal. Tha measured transverse strain determined from the Bragg peak positions was plotted against the applied longitudinal strain as shown in Figure 2 below which yielded a Poisson's ratio of 0.21 ± 0.03.

First proofs were made with monodisperse 270 nm SiO_2 spheres by Stöber Method

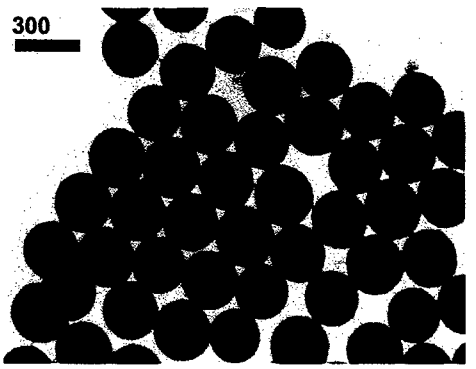

Formation SiO_2 opal

Deposition of SiO_2 spheres onto glass substrate

Slow solvent evaporation

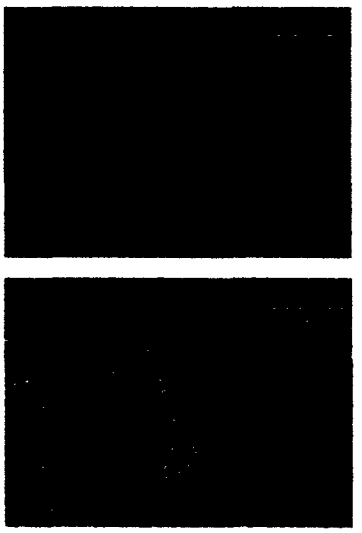

Opal SEM photographs

Opal photographs at different angles

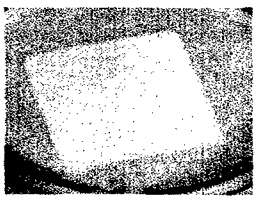

Green color

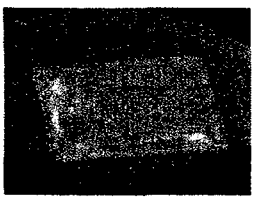

Red color

Formation inverse opal

Infiltrate SiO_2 opal with elastomer (transparent resin) and dissolution of the silica spheres with HF acid

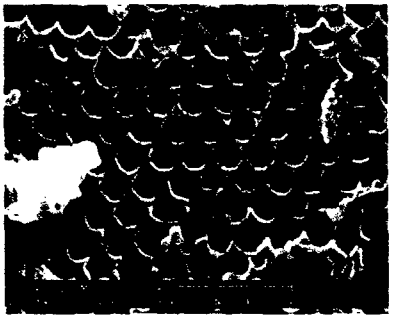

Inverse opal (without previous sinterization)

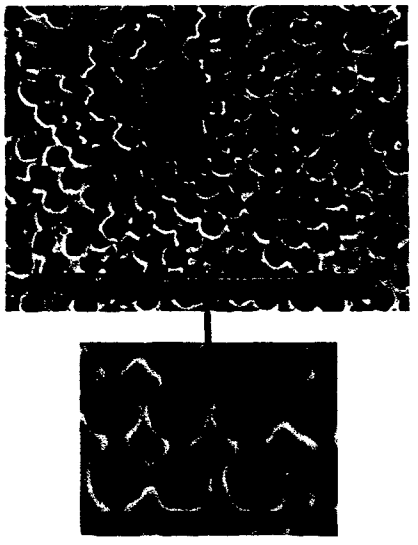

Inverse opal (with previous sinterization)

- To reduce the cracking problem of the Opal as it dried, the SiO_2 particles were coated with Polyvinylpyrrolidone. After contacting a group specializing in opals, the following ideas were proposed:
    - Try very thin opals (100nm) using the method of Colvin, which makes infiltration easier but of couse suffers from the final film being thin and fragile.
    - Opals with particle and host very close in index do not have strong contrast but do have very sharp color peaks thus it may be a viable trade-off. This we could consider an opal using PMMA spheres and an elastomer.
    - There is a concern that if we try an inverse opal the elastomer will collapse upon dissolution of the spheres.
    - Try using elastomer and TiO2 for highest contrast.
- Four elastomers from Gelest Inc. were chosen and procured:
    - Gelest ZipconeTMFA polydimethylsiloxane RTV
    - SIbridTMTI Thermoplastic Silicone-Polyimide
    - ZipconeTMTR Reflective Thermal Control Coating
    - Gelest OETM 41 1.41 refractive
- The inverse opal method turned out to be very simple. First a mono-layer of spheres is made on a substrate and the polymer deposited and cured. After peeling off the polymer layer from the substrate, the particles are dissolved using HF, yielding an

array of spherical holes. Using the strong angular selectivity of laser scattering, stretching is clearly visible.

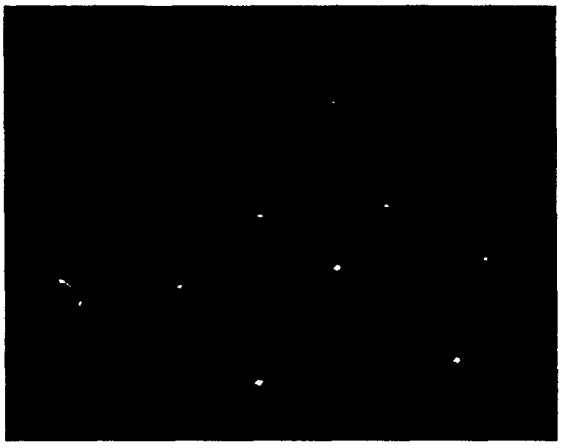

Figure 3. Diffraction of the (111) oriented Inverse opal. Note the six-fold symmetry of the spot pattern.

Figure 4. Optical diffraction from an inverse opal (an array of ordered nanometer-scale holes) embedded in an elastomer. As the elastomer is stretched the separation between the diffracted spots changes as indicated by the white marker lines in this figure.

3. Accomplishments and New Findings

As described above, our major accomplishments over the past year can be summarized by the following.

- One of our most significant accomplishments is the demonstration that colloidal crystals grown directly onto a substrate can be used as a strain sensor. In using photonic crystals as strain sensors we were able to measure the mechanical properties (Young's modulus and Poisson's ratio) of colloidal crystal assemblies.

- We were successful in using Langmuir-Blodgett self assembly methods for the production of inverse opals that had remarkable strain sensitivity. Deformation of these structures was easily interrogated using optical diffraction methods.
- Development of gold-encapsulated strain sensors base on plasmon resonance. Photonic antenna array test bed designed, process proven on Si, ready for demonstrator on BK7 glass

4. Personnel Supported

Jeffrey Thomson	GRA	25% effort
Toni Tang	GRA	25%
K.Sieradzki	Co-PI	15%

5. Publications

1. M.A. Correa-Duarte, M. Grzelczak , V. Salgueirino-Maceira V, M. Giersig , L.M. Liz-Marzan , M. Farle , K. Sierazdki , R. Diaz , "Alignment of carbon nanotubes under low magnetic fields through attachment of magnetic nanoparticles" , *J. of Phys. Chem. B*, **109,** pp.19060-19063 (2005).
2. M. Grzelczak , M.A. Correa-Duarte, V. Salgueirino-Maceira , M. Giersig , R. Diaz, L.M. Liz-Marzan, "Photoluminescence quenching control in quantum dot-carbon nanotube composite colloids using a silica-shell spacer", *Advanced Materials*, **18,** 415-420 (2006).
3. V. Salgueirino-Maceira, M.A. Correa-Duarte, M. Farle, M.A. Lopez-Quintela, K. Sieradzki, R. Diaz, "Synthesis and Characterization of Large Colloidal Cobalt Particles", *Langmuir*, **22,** pp.1455-1458 (2006).
4. V. Salgueirino-Maceira , M.A. Correa-Duarte, M. Farle, A. Lopez-Quintela, K. Sieradzki, R. Diaz, "Bifunctional gold-coated magnetic silica spheres", *Chem. of Mat.*, **18,** pp. 2701-2706 (2006).

6. Interactions/Transitions

Professional Communications

- Colloidal crystal technology has been transitioned to Luna Innovations Incorporated, 705-A Dale Ave, Charlottesville, VA 22903. There is currently a DoD Navy funded Phase I, SBIR titled, "Multifunctional Coating System for Corrosion Prevention and Structural Health Monitoring." F. Friedersdorf of Luna is principal investigator.

7. New Discoveries, Inventions, Patent Disclosures

None

8. Honors and Awards

None

B. Color-on-Demand – R.E. Diaz

1. Objectives

- The ultimate goal of this project is the creation of intelligent flakes of paint that can be incorporated in a top coat and will change color when commanded by an onboard microwave signal. The metachromatic element must possess the following features:
    - self-powered during transition, but thereafter passive
    - amplified color (to minimize the amount required)
    - triggered by a microwave signal
    - reversible
    - all implementable in mass-producible (MEMS/semiconductor) technology.

2. Summary of Activities – State of Effort

Two parallel paths were proposed toward meeting the objective.

Path #1: Amplified Galvanic Electrochromic element.

A self-assembling (via colloidal chemistry) all solid-state miniature version of the well known Gratzel nanocrystalline electrochromic and solar cells.

- Desirable features of the prior art:
    - Viologen colorant molecule being bi-stable requires power consumption only in changing state.
    - Porous nanocrystalline TiO2 electrode attains high coloration by infusing its large surface area with the colorant.
- Possible drawback of the approach is that their cell uses a liquid electrolyte.
- Novel features developed in this project
    - Colloidal chemistry assembly of the nanoporous TiO_2 substrate via self-assembly of a quasi-crystal of anatase TiO2 nanospheres.
    - Demonstrated precoating of the TiO2 nanospheres with colorant to obtain a fully coated nanoporous self-assembled electrode.

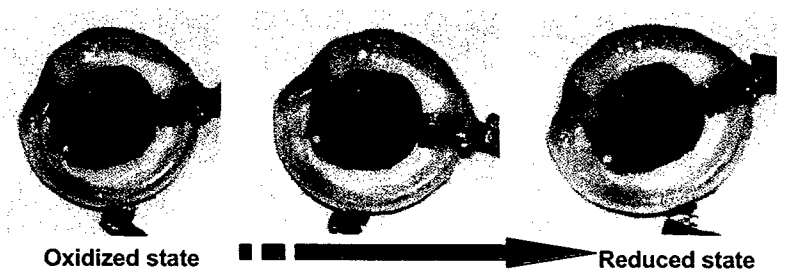

Figure 1. Demonstration of strong coloration of viologen-based ec-cell using TiO_2 nanoparticles.

- Proposed to attain amplification of the coloration by coupling the viologen to gold nanoparticles designed to undergo surface Plasmon resonance at the same wavelength.

- Two hypotheses for the lack of an amplification effect were forulated. The tested hypotheses were either: (a) The semiconducting electrode surface foils the plasmon phenomenon by dominating the electron transfer phenomena. (b) The gold nanoparticles incorporated into the electrode are too far from the majority of the dye molecules to enhance the overall absorption of the cell

- Three experiments were then performed to resolve the issue:
  - (a) Create a solution of SiO2-coated gold nanospheres and try to adsorb the dye molecules onto the spheres to observe a coloration change in the solution.
  - (b) Deposit a layer of gold nanoparticles onto a dye adsorbed TiO2 electrode in a solar cell configuration with Porphyrin Dye molecules and measure the light-induced current and voltage.
  - (c) Assuming that the problem is all one of proximity, create a monolayer of Gold nanoparticles and deposit CdTe quantum dots at various distances from this surface to determine whether or not the radiation efficiency is altered by the gold surface.

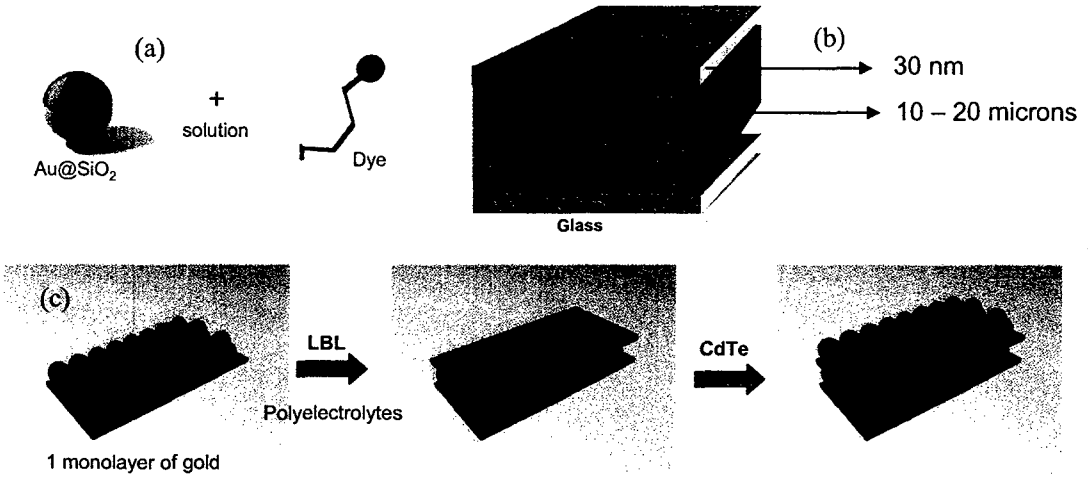

Figure 2. Three experiments performed to assess the light-absorption enhancement potential of gold nanospheres. (a) Dye-adsorbed on Au spheres (in a liquid dispersion), (b) Gold spheres deposited on Dye-adsorbed nanocrystalline TiO2 electrode, (c) CdTe quantum dots adsorbed onto a polyelectrolyte layer above Au spheres.

- Experiments (a) and (b) showed no conclusive evidence of Plasmon enhancement of the absorbance.
- Experiment (c) however demonstrated that indeed when a radiating element (in this case the CdTe quantum dots) is within 7 nm of the gold nanoparticles

(about one fiftieth of the wavelength) there is a clear increase in the luminescence. Figure 3 shows the results, where each layer of polyelectrolyte adds approximately 1nm of separation between the quantum dots and the gold film. Quenching is evident when the distance is too small, and decrease in amplification is seen when the distance is too large (10nm).

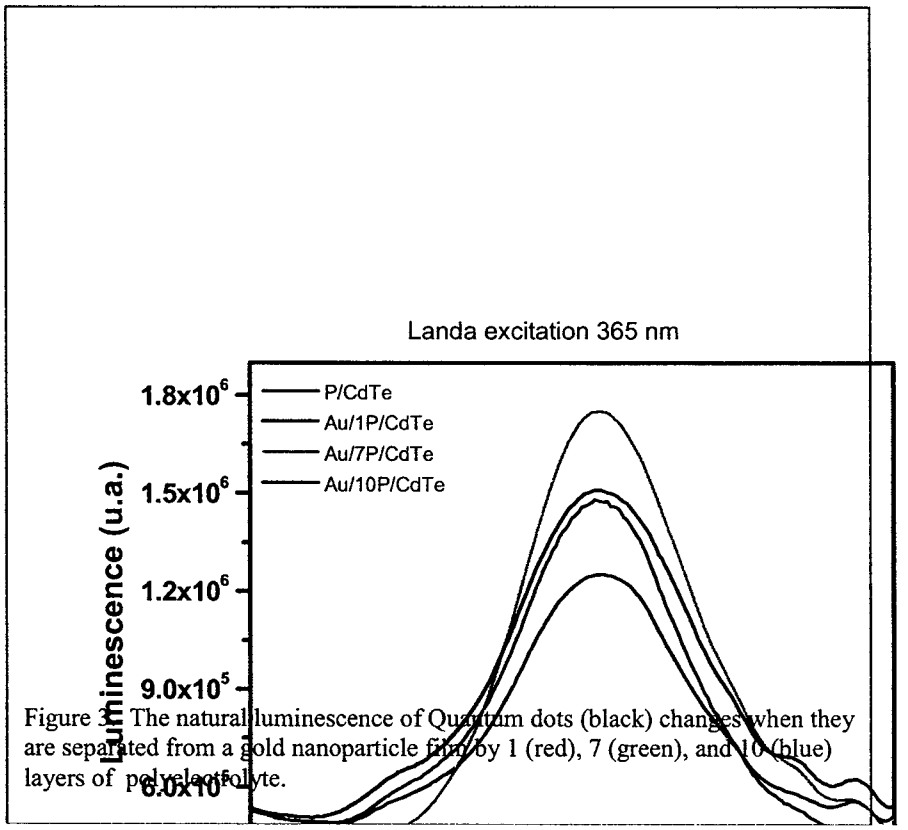

Figure 3 The natural luminescence of Quantum dots (black) changes when they are separated from a gold nanoparticle film by 1 (red), 7 (green), and 10 (blue) layers of polyelectrolyte.

- It follows that the failure in the electro-chromic cell configuration arises from the large distance between the gold nanoparticles and the dye molecules.
  - The TiO2 electrode is 10 to 20 microns thick while the gold layer is at most 30 nm thick so that only the topmost layer of dye molecules (about 1/2 of one percent of the dye molecules in the electrode) were within one quarter wavelength of the photon field of the gold layer's plasmon resonance.

- Therefore the only viable approach for the microscopic electrochromic cell of Path #1 would be to intersperse the gold nanoparticles inside the TiO2 electrode to guarantee that every dye molecule is close enough to the plasmon resonance field of the gold to derive the expected benefit.
  - This approach would require creating TiO2-coated gold nanospheres and subsequent adsorption of the dye into the surface of the TiO2. At

this point the mechanical approach of Path #2 was pursued as giving a higher chance of success.

Path #2: An all mechanical metachromic pigment.

Demonstration that a mechanically tuned photonic antenna can work as a metachromic element requiring no chemical reactions. This required:

- Computational full-physics proof that:
  - Photonic antennas can be designed to scatter or absorb pre-determined frequencies of the optical spectrum.
  - Bringing two such antennas into proximity of each other will change their resonant frequency through the mutual coupling.
- Manufacturing demonstration that such photonic antennas can be built.
- The original proposal was to use MEMS/NEMS mechanical systems to vary the distance between photonic antennas. However work by other members of the MURI team on molecular cages with adjustable pore size and molecular layers with adjustable inter-layer distance (via chemical triggers) plus the recent demonstration (including at ASU) of electrically activated biomimetic artificial muscles now makes one of these approaches the more likely vehicle for the mechanical switching of this metachromic element.
- The initial modeling effort concentrated on Perfect Electric Conductor models of the antennas to determine their tunability:
  - A pair of bowtie antennas one shorted and one open, coupled to each other by sliding one above the other in 20 nm increments demonstrated that this structure can be switched mechanically continuously between two resonant reflection bands one in the 399nm to 416nm wavelength range and the other in the 822nm to 902 nm range.
  - A narrower bandwidth folded dipole antenna was then investigated and the resulting bandwidth of scattered energy correlated to the standard RGB model of human vision.

Figure 4. A mechanically perturbed inverted folded dipole (250 nm long) is narrow-band enough to produce a scattered signal that can be varied from blue to orange

- Although these results were indicative of the possibilities, the computational work had to include the realistic properties of metals at optical frequencies. In particular, the manufacturing trials confirmed that only a noble metal photonic antenna would possess the desired strong resonance.
- Given recent developments in DNA self-assembly at ASU (Lund, K., Y. Liu, S. Lindsay and H. Yan, *Self-assembling molecular pegboard.* J. Am. Chem. Soc., 2005. **126**: p. 17606-17607.) and the affinity of that chemistry to the assembly of gold nanospheres realistic photonic antennas can be built from arrays of gold coated silver nanospheres. (See figure 5)

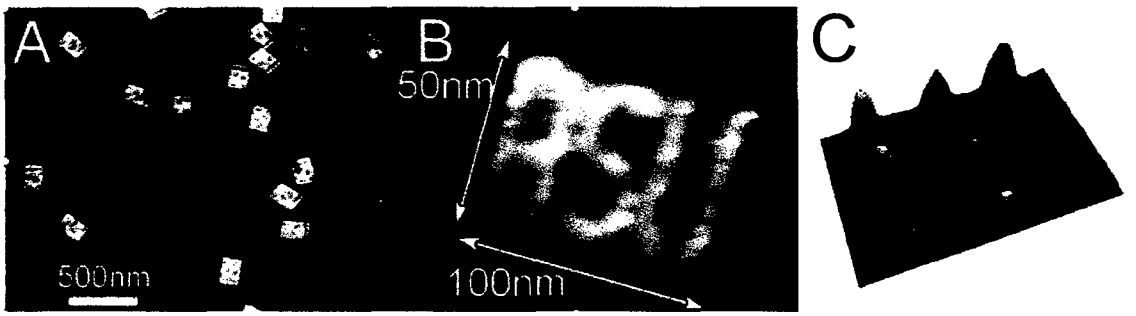

Fig. 5 (A) Raw product of folding M13 viral DNA using 'Origami' methods to make 'ASU' arrays. The yield is close to 100% in a one-step synthesis. (B) Close-up of an array. The letter pixels are made of protruding DNA loops, each one of which can act as a specific attachment and which can be placed anywhere on the array. (C) AFM scan of an array of Au nanospheres created on the DNA scaffold. (Lund, Liu, Lindsay, Yan ref.).

- The tunability of realistic Ag sphere chain antennas was demonstrated by incorporating the Drude (free-electron plasma) behavior of the noble metal into the computational electromagnetics model.
- For example a chain of three Ag spheres change peak scattering wavelength from 470nm to 500nm when the spacing between the spheres changes by 2.5 nm.

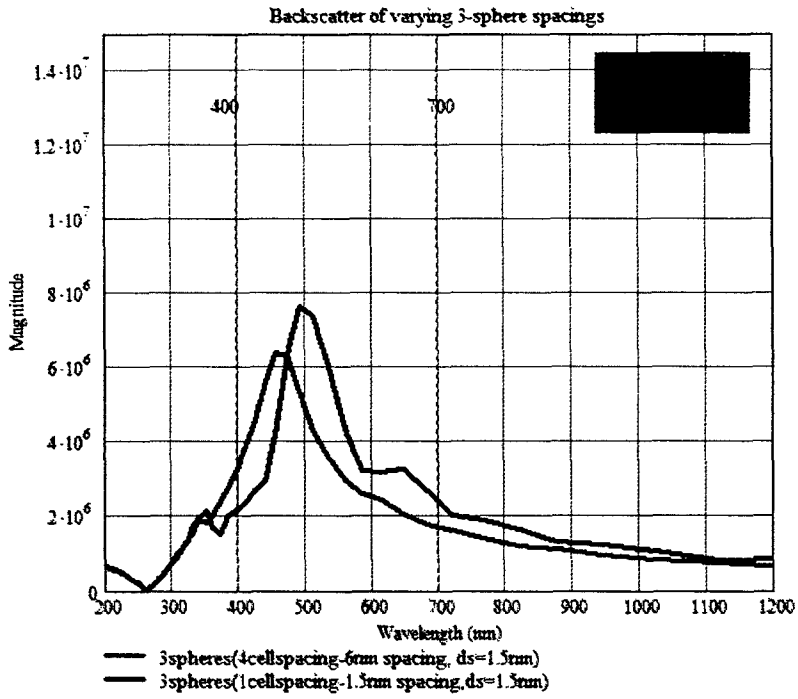

Figure 6 Computational model of a Ag three-nanosphere chain shows tunability as a function of the interparticle distance.

- The computational experiments have shown that changing the length of the sphere chain (by mechanically bringing in together two or more chains) shifts the resonant frequency across the entire optical range:

Number of spheres	1	2	3	5
Resonant Wavelength	370nm	450nm	550nm	770nm

- Therefore the final proposed metachromic element is a mechanically tuned array of Silver nanosphere chains assembled using DNA scaffold technology. The mechanical tuning is proposed to be accomplished via biomimetic artificial muscles.
- On an effort partially funded by NSF, quantum mechanical behavior was incorporated into the computational electromagnetics code to assess the fundamental nature of the radiation and absorption enhancement afforded by photonic antennas in close proximity to molecules. It was demonstrated that:
    - A photonic antenna can be designed to amplify the ambient field by concentration into hotspots by a factor of 10.
    - The radiative transition rate of a proximate2-level molecule can also be multiplied by a factor of 10.

- Thus a 100 times increase in absorption efficiency can be expected when dye molecules are coupled to resonant photonic antennas.

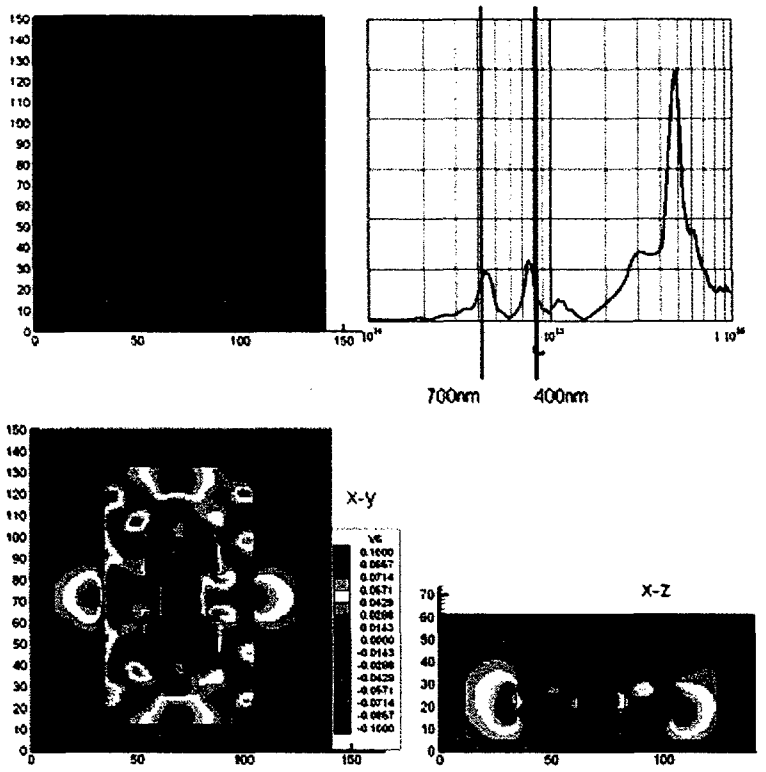

Figure 7. The final design of the Drüde symmetrical folded dipole shows two resonance peaks situated at each end of the optical spectrum. A snapshot of the x-directed E-field shows field concentration around the feeds and edges of the symmetrical folded dipole (bottom two pictures).

Results of the manufacturing trials

- The first photonic antenna array evaluated consisted of an array of Chromium Bowties manufactured in Taiwan using direct e-beam write.

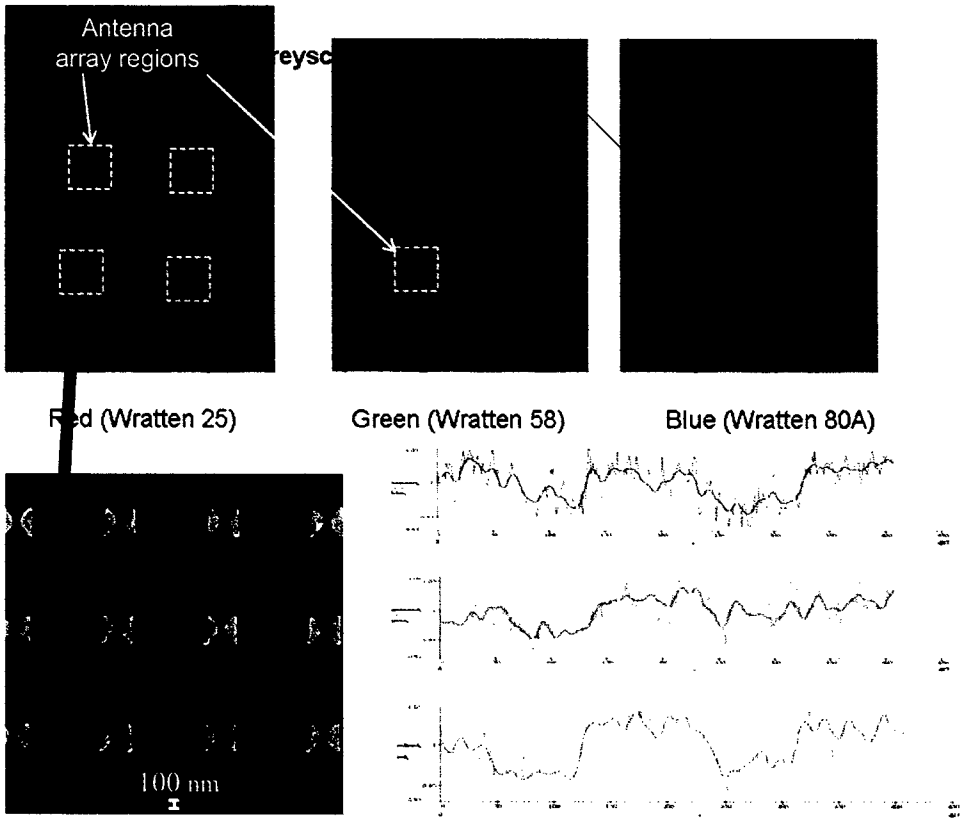

Figure 8. Microscope contrast profiles of the test wafer with bowtie arrays showed a maximum contrast with the red filter (bottom) of 12%, consistent with the antenna resonance.

- The Center for Solid State Engineering Research at ASU then developed the same technique and tried to adapt it to the creation of gold folded dipole arrays. Although successful arrays were built on Silicon, the arrays built on BK7 glass did not survive the manufacturing process.

3. Accomplishments and New Findings

Path #1 amplified galvanic electrochromic element:

- Process for the production of TiO_2 crystalline anatase nanospheres below 60nm have been obtained.
- Viologen coated TiO_2 nanospheres electrode successfully demonstrated intense coloration change in an electrochromic cell.
- Demonstrated radiation enhancement of quantum dots in immediate proximity (less than 7nm but greater then 1nm) to gold nanospheres thus demonstrating that amplified coloration is possible.

Path #2 All mechanical metachromic pigment:

- Numerical simulation demonstrated that the scattering wavelength of proximity coupled photonic antennas can be tuned across the entire optical range.
- Realistic photonic antennas were proposed and their operation confirmed using a full-physics model that incorporated the free electron plasma behavior of noble metals (Ag).
- Proposed recently demonstrated DNA scaffold assembly process as a realistic manufacturing process for a metachromic element consisting of chains of Ag nanospheres connected to artificial muscle.
- Inclusion of Quantum Mechanical transition rate phenomena into computational electromagnetics code (partially funded by NSF project) to calculate realistic amplification effects of photonic antennas on nearby fluorescent or absorbing molecules.

4. Personnel Supported

Derek Lim	GRA	50% effort

5. Publications

a. Refereed

1. Marek Grzelczak, Miguel A. Correa-Duarte, Verónica Salgueiriño-Maceira, Michael Giersig, Rodolfo Diaz, and Luis M. Liz-Marzán, "Photoluminescence Quenching Control in Quantum Dot–Carbon Nanotube Composite Colloids Using a Silica-Shell Spacer", Advanced Materials, adma.200501523.

b. Conference Proceedings

1. Lim, D., Diaz, R. E., "Classical emulation of molecular fluorescence and the modification of its quantum efficiency by nearby material structures", *Proceedings of the 9th International Conference on Electromagnetics in Advanced Applications and 11th European Electromagnetic Structures Conference*, pp. 953-955, Torino 12-16 September 2005.

6. Interactions/Transitions

Professional Communications

- Ongoing cooperation with the colloidal chemistry group at University of Vigo, Spain.

7. New Discoveries, Inventions, Patent Disclosures

None

8. Honors and Awards

None

ENHANCED ADHESION USING NANO-ENGINEERED MATERIALS

W.J. van Ooij

I. PROJECT THRUST OVERVIEW

It can not be assumed that the new coatings, coating additives, and substrates will interact in a way so as to produce optimal adhesion. To this end, it is desired to examine methods to augment adhesion of these materials. The objective of this thrust of the MURI program is to examine the abilities of silanes to act as both coupling agents and to understand the mechanism by which they enhance corrosion protection. An additional objective of the van Ooij effort is to dvelop slow-release inhibitor pigments that can possibly replace chromate pigments. (see § D of the Encapsulation and Delivery Thrust).

I. EFFORT REPORT

- ^{29}Si solid state NMR is being studied as an additional technique for the characterization of silane films – established contacts with Oklahoma State University
- **Emphasis this year was on the plasma treatment and testing of encapsulated inhibitors and less on adhesion promotion by silanes than in previous years**

1. Project Objectives

We have the following major objectives in this project:

- Improve the adhesion between nanostructured coatings and aluminum alloys, such as AA2024-T3 and AA7075-T6. Our goal is to eliminate chromate conversion coatings

and replace them with thin films of organofunctional silanes. The silane types will be varied and optimized and the adhesion mechanism investigated.

- Since chromate conversion coatings and their replacements, such as organofunctional silanes, do not contribute much to the overall corrosion protection of the coated metal, a novel system of anticorrosion pigments will be developed. They will be based on a slow-release mechanism. Based on electrochemical studies, effective inhibitors will be selected which will be surface-treated by a plasma polymerization process. This process will convert the inhibitors into slow-release materials. They will be tested for performance in standard primers for aluminum.
- A new objective was added: if good and durable adhesion could be obtained after replacement of the chromate conversion coatings by silanes, and the slow-release plasma approach showed promise, it would be attempted to combine the silane process and the inhibitor-containing primer into a one-step primer coating. Such primers would no longer require a conversion coating on the metal substrate. They will be termed 'superprimers'.

2. Summary of Activities – Status of Effort

- A 3-step treatment to replace the current chromate based technology was developed and demonstrated to work with ASTM B-117 salt spray testing which survived the test for 1000 hours and performed at par with the chromate based technology. The silanes used were bis-[trimethoxysilyl]ethane (BTSE) and vinyltriacetoxy silane (VTAS).
- This 3-step silane-based treatment with inhibitors added to it comprises a silane pretreatment loaded with cerium nitrate of the AA2024-T3 substrate to replace the chromate conversion coating. This was then coated with an epoxy coating which contained 1 wt.-% of plasma- polymerized organic and inorganic pigments of three types. This primer coat replaces the chromate pigment based, solvent based primers currently used.
- This system performed as well as the chromate-based system with just 1 wt.-% of plasma-treated pigments level.
- The conclusions of this experiment were that we were able to identify that the chromate in the conversion coating does not provide any corrosion protection and only serves the purpose of adhesion to the metal.
- The corrosion resistance in the currently used commercial system is obtained through the chromate pigments used in the system
- Plasma-treated benzotriazole (BTA) and tolyltriazole (TT) were observed to not leach out and corrosion protection of the scribe in the ASTM B117test was not obtained when panels were exposed for 1000 hours. However, plasma-treated cerium acetate protected the scribe. The BTA and TT inhibitors were observed to migrate to the interface with the metal and form a complex which enhanced adhesion of the coating.
- Based on these conclusions it was realized that the optimum corrosion inhibitor pigment such as BTA which can reach the interface and form complexes which can promote adhesion.

- Also the SUPERPRIMER idea was conceived in which the silane treatment to replace the chromate conversion coating would be integrated with the epoxy primer.
- The next few months were spent in trying various SUPERPRIMER systems which are water-based. Initially room temperature curing was not considered as a mandatory criterion for a SUPERPRIMER to be considered acceptable and good corrosion protection based on salt immersion test, DI water immersion test and Electrochemical Impedance Spectroscopy.
- Since a water-based coating was being sought all the components of the SUPERPRIMER, which are the resin and the silane system, were selected from the list of available options which were water-soluble or water-dispersed. However, since all the components were water-soluble a decent corrosion protection for long durations could initially not be obtained.
- At this stage, the idea of using water insoluble silanes was investigated by trying to dissolve them in water-dispersed resins to form the SUPERPRIMER.
- ECO-CRYL 9790 and EPI-REZ WD 510 were selected and bis-sulfur and bis-[triethoxysilyl]ethane silanes were successfully incorporated into these suspensions/dispersions. The addition resulted result in a stable SUPERPRIMER solution which had a pot life of around 5 hours.
- However, this system still was not room temperature curable and needed elevated temperatures of 110°C for curing.
- Outstanding corrosion resistance was observed in Electrochemical Impedance Spectroscopy (EIS), ASTM B117 with the system surviving 1000 hours and other tests like the Mandrel test, salt water immersion tests and DI water immersion test.
- Topcoat adhesion, however, was poor since the functionality of the system was lost due to high crosslink density in the SUPERPRIMER coating.
- Crosslinkers were then added to the SUPERPRIMER to facilitate accelerated crosslinking to facilitate a room temperature cure. This also solved the problem of poor topcoat adhesion. A useful crosslinker was Alink-25, an isocyanate.
- We now have a SUPERPRIMER system which comprises a water-dispersed resin and a water insoluble silane which cures at room temperature and results in outstanding corrosion resistance of AA2024 T3 alloy. The system thus is VOC-free and chromate-free and cures at room temperature.
- A Taguchi approach is now being used to optimize the ratio in which each component should be added to the SUPERPRIMER to optimize the performance of the current system.
- We have also incorporated the optimized pigment package in the currently room temperature cured SUPERPRIMER system. It was demonstrated that 1 wt.-% of loading of our environmentally friendly plasma-treated and untreated combination of inorganic and organic inhibitors can perform on par with the chromate conversion-coated panels. These were coated with commercially available chromate pigment-containing based primers. The pigment we used were plasma-treated cerium acetate and untreated benzotriazole. A result is shown here:

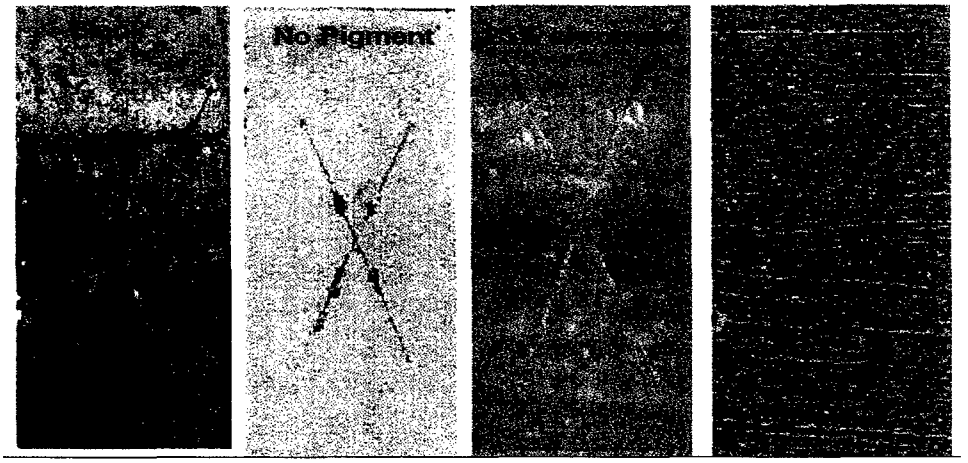

- From left to right: blank AA2023; coated with an acryate/epoxy primer; coated with a military primer (PRC Desoto MIL-PRF) which contains 25 wt.-% chromate; coated with the acrylate/epoxy primer which now contained 1 wt.-% of the inhibitor package consisting of untreated benzotriazole and plasma-treated cerium acetate. The plasma coating was made from C_6F_{14}. The test was 60 days immersion in 3% NaCl.

3. Accomplishments and New Findings

- A complete silane pretreatment based chromate-free 3-step system has been developed which performs as well as chromate-containing systems on AA2024-T3.
- A room temperature-cured SUPERPRIMER system which comprises of a water-dispersed resin and a water-insoluble silane which cures at room temperature and results in outstanding corrosion resistance of AA 2024 T3 alloy has been developed.
- A room temperature-cured SUPERPRIMER system and 1 wt.-% loading of our environmentally friendly plasma-treated and untreated combination of inorganic and organic inhibitors, respectively, has been able to perform on par in corrosion protection as compared with the chromate conversion-coated panels which were coated with commercially available chromate pigment-based primers which are contain 25 wt.-% with chromate pigments.
- The plasma-treated pigments in the SUPERPRIMER do not behave as standard pigments. As the coating ages, the pore resistance of the system increases. These effects need to be investigated.

4. Personnel Supported

See § **D** in **Inhibitor Encapsulation and Deliver Strategies**

5. Publications

See § **D** in **Inhibitor Encapsulation and Deliver Strategies**

6. Interactions and Transitions

See § D in **Inhibitor Encapsulation and Deliver Strategies**

2. Invention Disclosures

See § D in **Inhibitor Encapsulation and Deliver Strategies**

8. Honors and Awards

See § D in **Inhibitor Encapsulation and Deliver Strategies**

SYSTEM PERFORMANCE

S.R. Taylor

I. PROJECT THRUST OVERVIEW

- The production of molecularly and nano encapsulated inhibitors to be used within a coating will require verification of active corrosion protection of these materials when incorporated into a full coating system. It is well established that the performance of inhibitors in isolation does not necessarily reflect their behavior when incorporated. This phase of the investigation seeks to develop implement methods to assess the corrosion protection performance of the assembled multi-functional coating system developed under this program.

II. EFFORT REPORT

1. Objective

The objective of this research was to develop a low volume electrolyte cell and electrochemical test method that could detect and quantify the level of self-healing provided by an inhibited paint system on AA2024-T3. The results from this test procedure should be able to predict ASTM B117 salt spray performance results.

2. Summary of Activities

- A small volume (0.1 ml) glass cell in combination with EIS has been used to assess the active corrosion protection qualities of a series of coating systems provided by The Boeing Company. The low volume test cell is believed to more closely emulate the conditions experienced by an aircraft, whereby the coating and inhibitors released experience the volumes of water representative of field operation (as well as salt spray) rather than an immersion-type environment as has been used in previous testing. This cell will also allow documentation of the protective lifetime of an inhibited coating as a function of time via 'wash-out' experiments, where wash-out is achieved by exchange of the cell electrolyte containing leachate with fresh electrolyte as would occur during rain. The use of glass precludes concerns of inhibitor

absorption by a polymeric material which might contaminant subsequent experiments.

- All coating systems have now been assessed by EIS and by salt spray.

2. Accomplishments and New Findings

- This study compared 4 day Electrochemical Impedance Spectroscopy (EIS) results of aerospace coatings to salt spray (3000 hour ASTM B117) exposure data of parallel samples.
- Combinations of chromate (Alodine® 1200s) and non-chromate (Boegel®) surface pretreatments, primers, and topcoats were used to prepare coating systems on AA2024-T3 by The Boeing Company.
- Coated samples were exposed to 0.5 M NaCl in a thin layer cell (0.5 mm). After 24 hours, a pinhole defect was made through the coating system. EIS measurements were made at 0, 2, 4, 6, 8, 24, 48, 72 hours.
- The corrosion resistance, R_{corr}, was extracted from the EIS data and plotted as a function of time after defect production.
- Samples subjected to 3000 h ASTM B117 salt spray were quantified on a scale from 0 (excellent performance) to 100 (poor performance) for blistering, scribe creepage, and scribe corrosion.
- Results from the 4 day EIS test could predict 3000 hour salt spray performance in 9 out of 12 coating systems. These methods were 100% reliable for conventional coating systems that employed chromate conversion coatings and showed a 0.89 correlation between salt spray and EIS data.
- Only 3 out of 6 coating systems that had Boegel pretreatments could be predicted by the EIS damage tolerance test.
- This work demonstrated that the new, thin film electrolyte EIS test is a promising short-term method for the prediction of long-term coating system performance.

Figure 1 EIS and Salt Spray Correlation. The average of the EIS results is plotted against the corresponding average of the salt spray results. Four regions can be defined by the arbitrarily defined limits of 1 and 10 for log $\Delta Z_{0\text{-}72h}$ and salt spray score respectively. These regions are labeled 1- 4. (Next page)

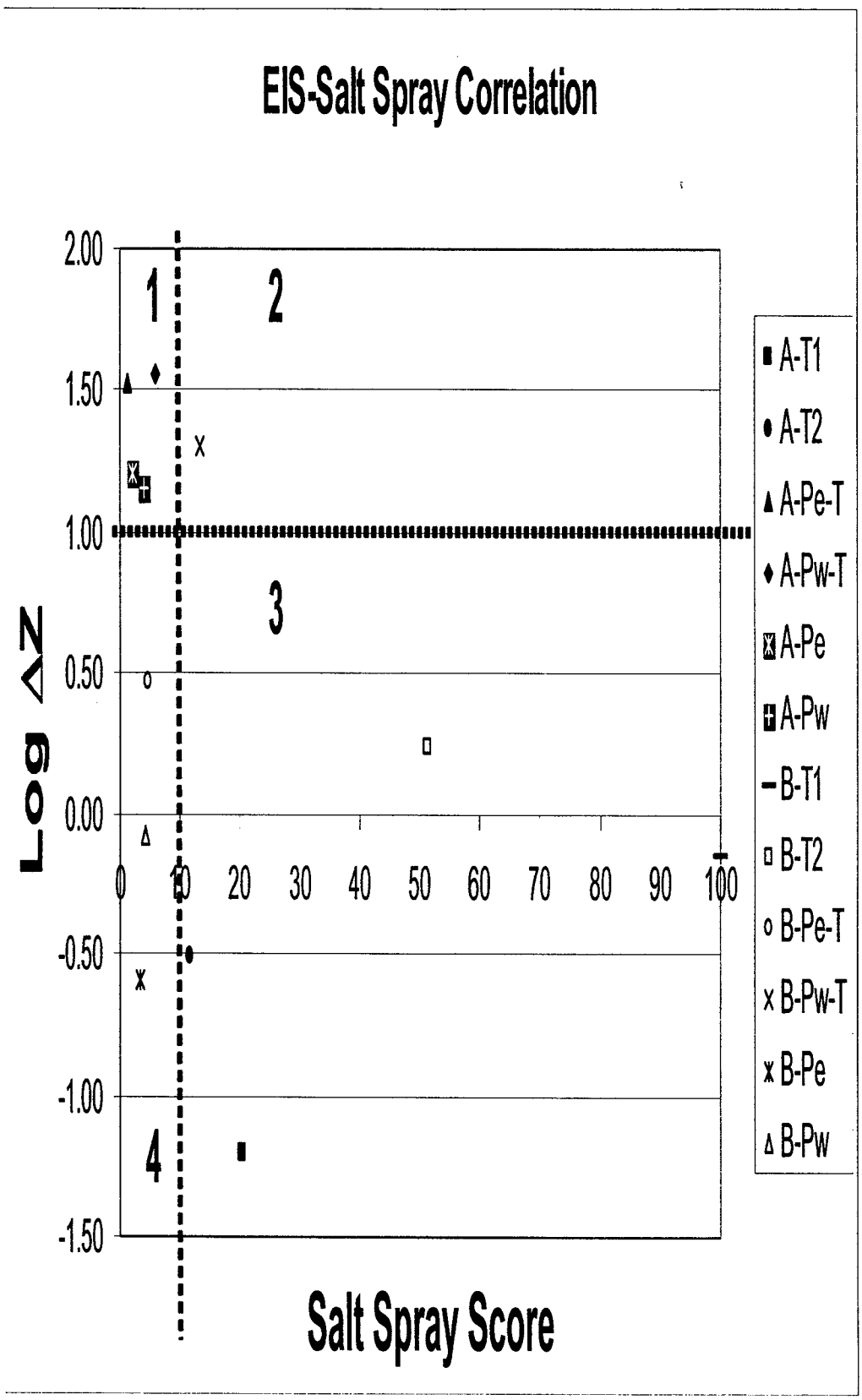
EIS-Salt Spray Correlation
2.00
1.50
1.00
0.50
0.00
-0.50
-1.00
-1.50
Log ΔZ
0
10
20
30
40
50
60
70
80
90
100
Salt Spray Score
1
2
3
4
A-T1
A-T2
A-Pe-T
A-Pw-T
A-Pe
A-Pw
B-T1
B-T2
B-Pe-T
B-Pw-T
B-Pe
B-Pw